Neuron
Article

Contributions of the 12 Neuron Classes in the Fly Lamina to Motion Vision

John C. Tuthill,[1,2,3] Aljoscha Nern,[1,2] Stephen L. Holtz,[1] Gerald M. Rubin,[1] and Michael B. Reiser[1,*]
[1]HHMI/Janelia Farm Research Campus, 19700 Helix Drive, Ashburn, VA 20147, USA
[2]These authors contributed equally to this work
[3]Present address: Department of Neurobiology, Harvard Medical School, 220 Longwood Avenue, Boston, Massachusetts 02115, USA
*Correspondence: reiserm@janelia.hhmi.org
http://dx.doi.org/10.1016/j.neuron.2013.05.024

SUMMARY

Motion detection is a fundamental neural computation performed by many sensory systems. In the fly, local motion computation is thought to occur within the first two layers of the visual system, the lamina and medulla. We constructed specific genetic driver lines for each of the 12 neuron classes in the lamina. We then depolarized and hyperpolarized each neuron type and quantified fly behavioral responses to a diverse set of motion stimuli. We found that only a small number of lamina output neurons are essential for motion detection, while most neurons serve to sculpt and enhance these feedforward pathways. Two classes of feedback neurons (C2 and C3), and lamina output neurons (L2 and L4), are required for normal detection of directional motion stimuli. Our results reveal a prominent role for feedback and lateral interactions in motion processing and demonstrate that motion-dependent behaviors rely on contributions from nearly all lamina neuron classes.

INTRODUCTION

Fly motion detection is a key model system for studying fundamental principles of neural computation. Flies exhibit robust visual behaviors (Heisenberg and Wolf, 1984), and neurons in the fly visual system are highly sensitive to visual motion stimuli (Hausen, 1982). A mathematical model for visual motion detection, the Hassenstein-Reichardt elementary motion detector (HR-EMD; Hassenstein and Reichardt, 1956), successfully reconciles a wide range of behavioral and electrophysiological phenomena measured in flies (Egelhaaf and Borst, 1989; Götz, 1964; Haag et al., 2004; Hausen and Wehrhahn, 1989). The basic operation of the HR-EMD is a multiplication of two input signals after one of them has been temporally delayed (Figure 1B; Reichardt, 1961). The "correlation-type" structure of the HR-EMD is highly similar to models for motion detection in the vertebrate retina (Borst and Euler, 2011) and may represent a common neural computation across sensory systems (Carver et al., 2008).

In spite of the success of the EMD model, its cellular implementation remains unknown. There is evidence that EMD motion computation is implemented locally, between neighboring retinotopic subunits of the fly eye (Buchner, 1976, 1984) and that local motion signals are then spatially integrated within motion-sensitive tangential neurons in downstream circuits (Figure 1B; Krapp et al., 1998; Single and Borst, 1998; Single et al., 1997). However, it is unclear if the computational nodes of the HR-EMD, the delay filter and the multiplier, correspond to individual cell types, or if motion detection is computed in a more distributed manner, with distinct contributions from many different neurons. It is also possible that there are multiple circuits dedicated to motion computation; different neuron types could extract specific visual features, as in vertebrate retinal ganglion cells (Gollisch and Meister, 2010), and compute motion independently within parallel channels. Indeed, several recent studies suggest that fly motion vision may be segregated into parallel, functionally distinct channels (Clark et al., 2011; Eichner et al., 2011; Joesch et al., 2010; Katsov and Clandinin, 2008; Rister et al., 2007).

The fly visual system consists of four ganglia called the lamina, medulla, lobula, and lobula plate (Figure 1A), which together are referred to as the optic lobes. As the first synaptic relay between the photoreceptors and motion-sensitive tangential neurons in the lobula plate, it has been hypothesized that the early stages of motion computation may occur in the lamina (Coombe et al., 1989; Douglass and Strausfeld, 1995). The lamina is organized into an array of ~750 retinotopic "cartridges," each of which corresponds to a discrete sample of the visual world, ~5° in *Drosophila* (Braitenberg, 1967; Buchner, 1971; Kirschfeld, 1967). The anatomy and connectivity of lamina neurons is known in exquisite detail, owing to detailed Golgi studies (Fischbach and Dittrich, 1989) and electron microscopy (EM) reconstructions (Meinertzhagen and O'Neil, 1991; Rivera-Alba et al., 2011). Six light-sensitive photoreceptors, R1–R6, project their axons into each lamina cartridge. Two other photoreceptor neurons, R7 and R8, pass through the lamina and synapse in specific layers of the medulla.

Besides the photoreceptor axons, the lamina also contains processes of 12 other neuronal cell types (Figures 1C and 1D). These lamina-associated neurons include five lamina output neurons, six putative feedback neurons, and one lamina intrinsic cell (Fischbach and Dittrich, 1989). Eight of these neuron classes are columnar—there is one cell per retinotopic column (Figure 1C). The columnar neurons include the feedforward lamina monopolar cells, L1–L5 (Figure 1C, red), which send axonal processes into the medulla. The largest of the monopolar cells, L1,

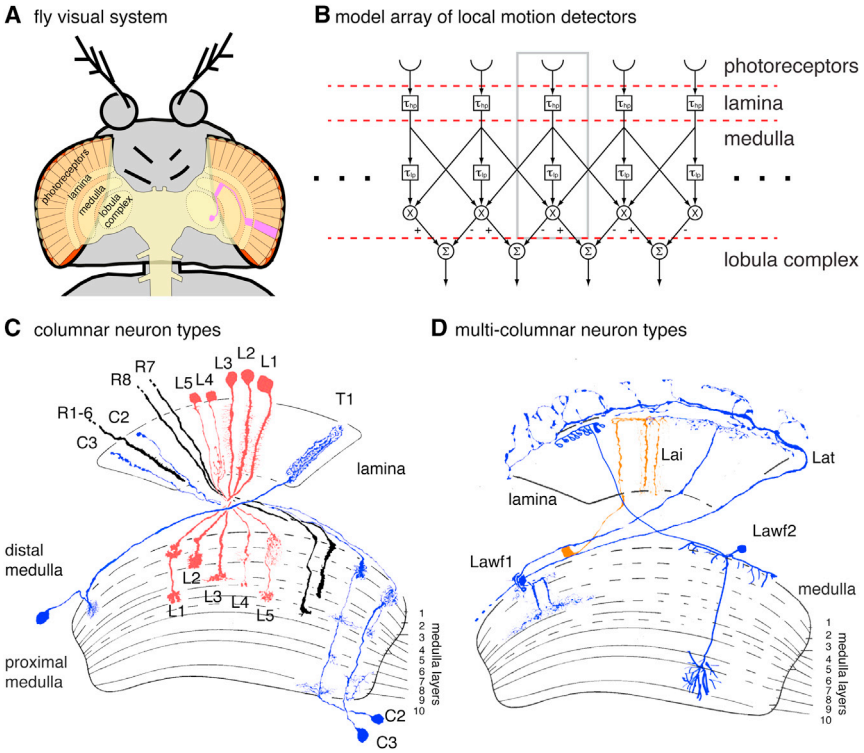

Figure 1. Overview of the Fly Visual System and Its Proposed Role in Local Motion Computation

(A) In the early visual system of *Drosophila*, input from photoreceptor neurons in the retina is initially processed in the optic lobes, which consist of a series of optic ganglia called the lamina, medulla, and lobula complex (comprising the lobula and lobula plate). Optic lobe neuropils are organized as arrays of retinotopic columns. One series of columns is highlighted in pink.

(B) A schematic of an array of HR-EMDs, the classical computational model for local motion detection in the optic lobes. In this typical implementation, visual input passes from photoreceptors and is temporally filtered in the lamina. Motion detection is then performed by mirror-symmetric subunits, each multiplying the incoming signal with a time-delayed version from neighboring columns. This computation is commonly believed to occur within the medulla. The gray rectangle outlines a single columnar unit within the model, which corresponds to a single anatomical column within the lamina and medulla.

(C) The columnar neurons with synaptic connections in the lamina. Lamina output neurons L1–L5 are shown in red and putative feedback neurons from the medulla (C2, C3, T1) in blue. Photoreceptor neurons are also illustrated (gray). These neurons are present in all lamina columns, and single example profiles are shown arrayed across the lamina and medulla. This figure is adapted from Golgi drawings by Fischbach and Dittrich (1989).

(D) The multicolumnar neurons with processes in the lamina. These neurons are present with less than one cell per column, but as a population their arbors cover the entire visual field. Lamina intrinsic neurons (Lai; orange) are confined to the lamina. Lamina wide-field neurons (Lawf1, Lawf2; blue) provide feedback from the medulla to the distal lamina. Lamina tangential neurons (Lat; blue) arborize even more distal in the region of lamina neuron cell bodies. Lat cell bodies (data not shown) are located between the optic lobe and central brain near the accessory medulla. Lat cells also arborize in the ipsilateral central brain and the accessory medulla (data not shown). Like (C), this figure is adapted from Fischbach and Dittrich (1989), except for Lawf2, which was drawn based on single-cell labeling data obtained in this study (see Figure 2J).

L2, and L3, receive direct synaptic input from the R1–R6 photoreceptors, but L4 and L5 do not (Meinertzhagen and O'Neil, 1991; Rivera-Alba et al., 2011). In addition to these five lamina output neurons, three putative feedback neurons, T1, C2, and C3, are also columnar (Figure 1C, blue). These neurons have cell bodies in the medulla and send their axons back to the lamina. EM studies have shown that C2 and C3 are presynaptic on several cell types in the lamina (Meinertzhagen and O'Neil, 1991; Rivera-Alba et al., 2011). By contrast, no synaptic targets are currently known for T1 neurons.

Four other lamina-associated neuron classes are multicolumnar: there is less than one neuron per lamina column, and the arbors of each neuron span multiple columns (Figure 1D). With the exception of the lamina intrinsic amacrine neurons (Lai), which are confined to the lamina, the anatomy of these multicolumnar neurons suggests that they function as feedback neurons. Wide-field feedback from the medulla to the lamina is provided by two types of lamina wide-field neurons (Lawf1 and Lawf2). Lawf2, which was identified in the course of the present study and was also recently reported elsewhere (Hasegawa et al., 2011), can be clearly distinguished from Lawf1 by its layer specificity in the medulla (Figure 1D). Finally, lamina tangential neurons (Lat), approximately four cells per optic lobe, project from the ipsilateral central brain to the distal surface of the lamina. These neurons do not innervate the medulla proper but have arborizations in the accessory medulla, a small medulla-associated neuropil thought to function in the control of circadian rhythms (Helfrich-Förster et al., 2007).

Several studies have investigated the functional roles of the large monopolar cells, L1 and L2. L1 and L2 are together required for motion detection. Simultaneously silencing both neuron types eliminates behavioral (Clark et al., 2011; Rister et al., 2007) and electrophysiological (Joesch et al., 2010) responses to motion, while silencing each cell type individually has been reported to cause differential responses to progressive and regressive motion at low contrasts (Rister et al., 2007), contrast-inverting edges (Clark et al., 2011), and motion stimuli defined by brightness increments and decrements (Joesch et al., 2010). Electrophysiological recordings (Laughlin and Hardie, 1978; Zheng et al., 2006) and calcium imaging studies (Clark et al., 2011) have found that the physiological responses of L1 and L2 are largely similar. Both are nonspiking neurons that respond to luminance increases with a transient hyperpolarization and luminance decreases with a transient depolarization. Neither L1 nor L2 is selective for moving stimuli. Overall, these data suggest that L1 and L2 provide input to

motion circuits but are not directly involved in elementary motion computation.

In comparison to L1 and L2, little is known about the contributions of the other ten lamina-associated neuron types. This is primarily because the small size of these neurons has, except for a few examples in larger flies (Douglass and Strausfeld, 1995), prevented electrophysiological recording. Specific GAL4 driver lines for these remaining neuron types have also not been available for behavioral genetics studies. In this Article, we use intersectional genetic strategies to build a collection of driver lines that target each of the 12 lamina-associated neuron types. We then genetically silence and activate each lamina neuron type and evaluate the consequences on behavioral responses to a panel of visual stimuli. Our results provide evidence that most lamina-associated neurons contribute to motion processing and that the HR-EMD model describes the emergent properties of a complex circuit, rather than discrete arithmetic operations implemented by a small number of individual neuron types.

RESULTS

Construction of Specific GAL4 Driver Lines for Individual Lamina Neuron Types

We first surveyed a large collection of imaged GAL4 lines (Jenett et al., 2012; Pfeiffer et al., 2008) for expression in the *Drosophila* lamina and further examined expression patterns of selected lines by reimaging at higher resolution or with single-cell labeling techniques. Individual lamina neuron types could be identified in this screen by their distinct stereotyped morphology using both the overall expression pattern and single-cell labeling (Figure 2). Our screen revealed multiple drivers for each of the lamina-associated neuron types. However, similar to available GAL4 lines, such as lines widely used in the study of L1 and L2 function (Figure S1 available online; Clark et al., 2011; Gao et al., 2008; Joesch et al., 2010; Katsov and Clandinin, 2008; Rister et al., 2007), most of these driver lines had expression in other cell types of the optic lobes, central brain, or ventral nerve cord. We therefore used the intersectional Split-GAL4 method (Luan et al., 2006; Pfeiffer et al., 2010) to further refine expression patterns. In this method, two parts of the GAL4 transcription factor, the activation domain (AD) and DNA-binding domain (DBD), are expressed in the two patterns to be intersected. Functional GAL4 is only reconstituted in cells that express both the AD and DBD, ideally resulting in a specific driver targeting only the cell population of interest.

Taking advantage of the modular nature of the enhancer-GAL4 collection (Jenett et al., 2012; Pfeiffer et al., 2008), we generated multiple AD and DBD drivers with predicted expression in each lamina cell type. We then assayed the expression patterns of more than 100 AD/DBD combinations and selected suitable lines for further use. For 10 of the 12 types of lamina neurons, we identified at least two Split-GAL4 driver lines with high specificity (Table S1). Figure 2 shows the expression patterns for one line of each cell type, as well as example images of single labeled cells that summarize the critical identifying anatomical features (images of the additional Split-GAL4 lines and ventral nerve cord expression of all lines are available on the authors' website: http://www.janelia.org/lab/reiser-lab). We confirmed the cell-type expression of these lines by imaging UAS-EGFP-Kir2.1 expression patterns (Figure S3A). For L1, the identified lines showed variable levels of incomplete expression (Figures 2A′ and 2A″) and only one such line was examined (we note that the UAS-EGFP-Kir2.1 expression pattern appeared more complete, Figure S3A). We detail the completeness of expression within each line in Table S1. We also tested one lamina tangential (Lat) line and lines that drove expression in two important cell-type combinations (L1/L2 and C2/C3). The advantage of using two highly specific drivers in functional studies is that the common phenotypic effects of driving neural effectors with different Split-GAL4 combinations can be confidently attributed to perturbation of the lamina-associated neurons.

Manipulating Lamina Neurons Affects Visual Behavior

During flight, flies rely on vision to maintain course control, avoid collisions, and orient toward objects (Heisenberg and Wolf, 1984). Quantifying flight steering is a sensitive way to measure visually evoked behaviors (Götz, 1964; Heisenberg and Wolf, 1984). For this reason, we examined visual behavior in tethered flying flies positioned within a cylindrical LED arena (Figure 3A; Reiser and Dickinson, 2008). In the flight arena, we used an optical wing-beat analyzer (Götz, 1987) to measure yaw steering responses to an extensive set of open- and closed-loop visual stimuli (Figures 3A, 3B, and S2). We tested several classic visual stimuli, such as large-field (optomotor) gratings of varying spatial frequency, velocity, and contrast (Duistermars et al., 2007a; Götz, 1964), small-field stripe patterns that oscillated at high and low frequencies (Duistermars et al., 2007b; Reichardt and Wenking, 1969), and motion stimuli that mimicked the optic flow patterns encountered by flies during flight (Theobald et al., 2010). We also designed novel stimuli to test specific hypotheses about lamina function, such as selectivity for progressive (front-to-back) versus regressive (back-to-front) motion (Duistermars et al., 2012; Rister et al., 2007), rotation versus expansion (Duistermars et al., 2007a; Katsov and Clandinin, 2008), and ON versus OFF motion signals (Clark et al., 2011; Joesch et al., 2010). Finally, we adapted several psychophysical techniques used to study early vision in other systems, such as reverse-phi motion (Anstis and Rogers, 1975; Tuthill et al., 2011) and contrast nulling (Cavanagh and Anstis, 1991; Chichilnisky et al., 1993; Smear et al., 2007). All of these stimuli were interleaved within a single protocol that required ~40 min of sustained flight behavior. A complete description of the visual stimuli used in this study is included in Figure S2 and described in the Supplemental Experimental Procedures.

In order to test the functional role of each lamina-associated neuron type in peripheral visual processing, we genetically expressed an inwardly rectifying K+ channel, Kir2.1, which suppresses synaptic activity by hyperpolarizing the resting potential (Baines et al., 2001). Consistent with previous findings (Clark et al., 2011; Joesch et al., 2010; Rister et al., 2007), expression of Kir2.1 in both L1 and L2 abolished fly turning responses to visual motion stimuli, such as the rotation of a wide-field grating and the oscillation of a dark stripe (Figures 3B and 3C). Because the Kir2.1 channel was tagged with GFP, we were able to confirm the expression in the Split-GAL4 lines by confocal microscopy (Figures S3A and S3B). We also verified that Kir2.1 expression effectively silenced light-evoked electrical activity

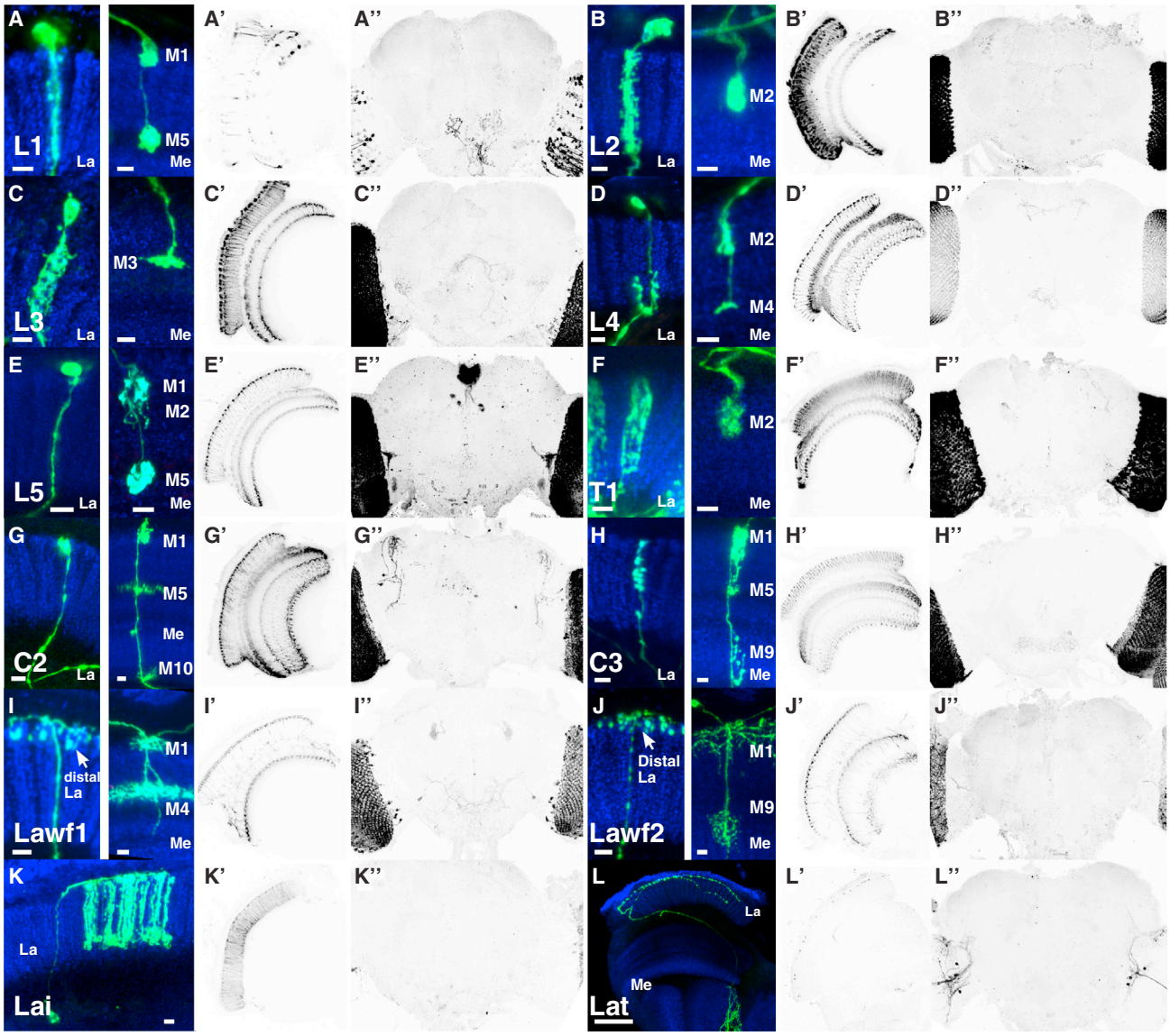

Figure 2. Each of the 12 Neuron Classes in the Fly Lamina Was Targeted Using the Split-GAL4 Technique

Shown for each cell type are the following: single cell images illustrating defining features of each neuron class (A–L), a confocal section through an optic lobe of one Split-GAL4 driver (A′–L′), and a maximum intensity projection of expression in the central brain of the same Split-GAL4 line (A″–L″). Expression patterns were visualized by confocal microscopy using UAS-driven expression of a membrane-targeted GFP and anti-GFP antibody staining (detailed in Supplemental Experimental Procedures). Blue labeling in single cell images shows a presynaptic marker (Brp; Nc82 antibody staining). Layer positions of terminals in the medulla are indicated as M1, M2, etc. in (A)–(L). For example, L1 has medulla terminals in layers M1 and M5 and L2 in layer M2. Each of the lamina-associated neurons can be unambiguously identified by these anatomical features. Specific drivers used for each image are listed in Table S1. Ventral nerve cord expression patterns and images of the remaining Split-GAL4 lines are available on the authors' website. Scale bars represent 50 μm in (A′), (A″), and (L), and 5 μm in all others.

through targeted whole-cell patch-clamp recordings from Lawf2 neurons (Figure S3C). In a complementary set of experiments, we genetically expressed the temperature-gated cation channel dTrpA1 (Hamada et al., 2008), which depolarizes *Drosophila* neurons (Pulver et al., 2009).

We compared the behavioral responses of experimental Split-GAL4 lines crossed to UAS-Kir2.1 to the responses of four control lines (each an individual Split-GAL4 half crossed to UAS-Kir2.1). The behavioral responses of these control lines were indistinguishable and were pooled. For most cell types, we tested more than one Split-GAL4 line and then employed a statistical analysis to control for false discovery rate (Benjamini and Hochberg, 1995). For each cell type and for each stimulus condition, we report as significant only those cases in which both of the Split-GAL4 lines that target each cell type pass our statistical criterion (see Supplemental Experimental Procedures for details). Although statistical tests were always performed on individual Split-GAL4 lines, we display behavioral response data

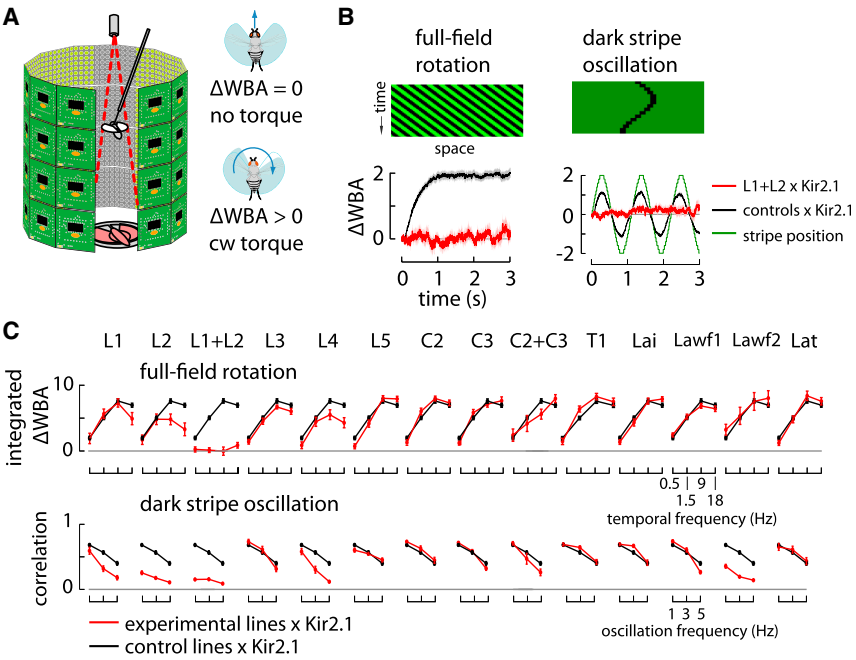

Figure 3. Silencing or Activating Specific Lamina Neurons Alters Fly Visual Behavior in a Virtual Reality Flight Simulator

(A) A flying fly is suspended within an LED arena in which the amplitude of each wing beat is tracked by an optical detector. The difference between the two wing-beat amplitudes (ΔWBA) is proportional to yaw torque. For example, when the amplitude of the left wing beat is greater than the right, the fly is attempting to steer to the right with clockwise torque.

(B) Example flight steering responses (mean ± SEM) to rotation of a full-field stimulus (90°/s corresponding to a temporal frequency of 3 Hz, left) and oscillation of a dark stripe (started at the center of the arena and oscillated between ±37.5° at 0.9 Hz, right). Silencing both L1 and L2 neurons with Kir2.1 abolishes behavioral responses to full-field and small-field motion stimuli. The space-time diagrams illustrate the luminance patterns displayed to the fly in the arena.

(C) Behavioral tuning curves for two motion stimuli across all experimental genotypes. The results for each experimental line (or average of two lines), crossed to Kir2.1, are shown in red, while the results for the control flies are shown in black (see text for details). Top: mean integrated steering responses (±SEM) to a full-field rotation stimulus (30° spatial period) at four temporal frequencies. Bottom: fly responses to oscillation of a dark stripe at three frequencies. Tuning curves show the mean correlation (±SEM) between the stimulus position and the ΔWBA.

in Figures 3, 4, 5, 6, and 7 as the average of all lines tested for each cell type.

We found that silencing most lamina neurons had subtle effects on basic visual behaviors, such as the wide-field optomotor responses and small-field stripe tracking (Figure 3C). However, testing fly responses to many unique visual stimuli revealed that some cell types contribute to motion detection under specific stimulus conditions. The difference between wild-type responses to all of the stimuli we tested and the responses of flies in which we have manipulated each lamina cell type are summarized with color-coded levels of statistical significance in Figure 4A. In this results matrix, each row represents the targeted neuron class, while each column is a separate visual stimulus condition (visual stimuli are detailed in Figure S2 and Supplemental Experimental Procedures). The color and intensity of each cell indicates whether Kir2.1 expression significantly affected fly behavior. The behavioral results summarized in Figure 4 are elaborated for a few cell types in Figures S5 and S7; the complete data set is available on the authors' website (http://www.janelia.org/lab/reiser-lab).

The strongest phenotypes we observed were for the primary lamina output neurons, L1 and L2 (top three rows of Figure 4A). Silencing either of these cell types significantly affected fly responses to many different behavioral conditions, supporting the hypothesis that these neurons are the primary feedforward inputs to downstream motion circuits. A previous report has suggested that L1 and L2 support detection of motion generated by luminance increments and decrements, respectively (Joesch et al., 2010). We found that silencing L2 neurons significantly altered fly responses to a decreasing luminance gradient but did not affect tracking of moving dark edges (ON and OFF motion stimuli in Figures 4A and S5B). Silencing L1 neurons did not affect fly response to either of these stimuli (Figures 4A and S5A), but more subtle deficits for L1 inactivation were seen in further experiments (Figure S6).

Apart from L1 and L2, the phenotypic effects were much sparser for secondary lamina output neurons and lamina-associated feedback neurons. Silencing most neuron types specifically affected fly responses to a small number of visual behaviors (bottom nine rows of Figure 4A), indicating specialized roles for these neurons. These behavioral phenotypes were largely consistent across different Split-GAL4 combinations (Figure S4), strongly suggesting that behavioral effects were due to Kir2.1 expression in lamina neurons rather than off-target consequences of our genetic manipulations. This is corroborated by the fact that silencing some neuron classes, such as L5, had no measurable effect on the behaviors we tested. Likewise, some visual behaviors, such as orientation toward a lateral flickering stripe, were entirely unaffected by silencing any of the 12 neuronal types. It is possible that such behaviors are mediated in part by input from the R7 and R8 photoreceptors that bypass the lamina and terminate in the medulla.

We also tested a subset of behaviors while depolarizing neurons by heat activation of dTrpA1. Surprisingly, dTrpA1 expression in the primary lamina output neurons, L1 and L2, did not dramatically impair visual motion detection (Figure 4B). However, in several instances, when expressed in other neurons, dTrpA1 expression altered fly behavior in unexpected ways. For example, depolarizing T1 neurons dramatically reduced the flight steering responses to most visual stimuli tested (Figure 4B). T1 cells are a mysterious type of columnar neurons that, based on EM reconstructions, appear to be exclusively postsynaptic

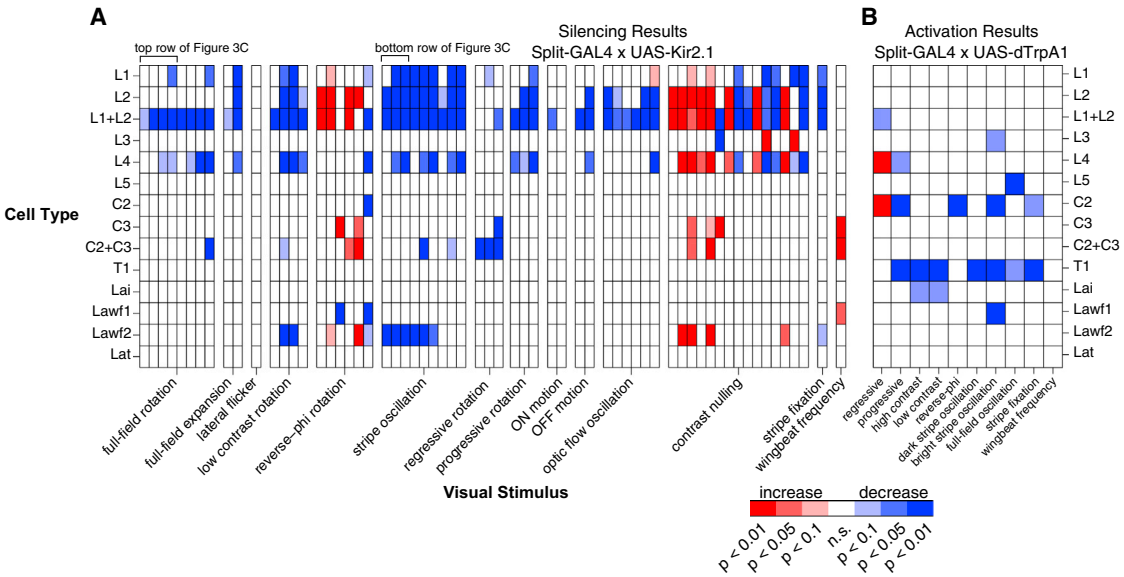

Figure 4. Summary of Behavioral Results for All Lamina Neurons

(A) The results of silencing each class of neurons are summarized as a heatmap, where each node represents the summary p value for the comparison between the experimental and control genotypes. The visual stimuli corresponding to each column are shown in Figure S2. Red (and blue) indicates a numerical increase (and decrease) in the test metric as determined by the signed difference between the mean of the test metric for each cell type and the mean of the control set. The p values corresponding to each line are shown in Figure S4 and have been aggregated for each cell type here. See Supplemental Experimental Procedures for details of the statistical procedure.

(B) Heatmap summary of all stimuli and lines tested using dTrpA1. Each cell represents the summary p value for comparisons between experimental and control genotypes (GAL4AD; GAL4DBD/UAS-dTrpA1 at 21°C and GAL4AD; UAS-dTrpA1 at 28°C). Specific Split-GAL4 lines tested are listed in Table S1.

in both the lamina (Meinertzhagen and O'Neil, 1991; Rivera-Alba et al., 2011) and the medulla (Takemura et al., 2008). Our data suggest that T1 neurons interact extensively with other lamina cell types, perhaps through gap junctions not resolvable by electron microscopy and that tonic depolarization of these cells is sufficient to disrupt basic visual behaviors.

Overall, we observed at least one phenotype for each lamina neuron type except for the lamina tangential cell (Lat). In several cases (L5, T1, Lai), neuronal silencing had no measurable effect on the behaviors we tested (Figure 4A), while activation using dTrpA1 significantly affected behavior (Figure 4B). For the remainder of the paper, we will focus on behavioral phenotypes related to specific aspects of spatial and temporal processing.

Role of Lamina Neurons in Directionally Selective Steering

The optic flow a fly experiences as it flies forward is predominately progressive, moving from front-to-back across both eyes (Figure 5A). When presented with either progressive or regressive motion restricted to a single eye, tethered flying flies respond by turning in the direction of stimulus motion (Götz, 1968), although responses to regressive motion are weaker (Duistermars et al., 2012; Heisenberg, 1972; Tammero et al., 2004). In comparison, freely walking flies respond more robustly to regressively moving objects (Zabala et al., 2012). Despite behavioral evidence that the visual system differentiates regressive from progressive motion, the neuronal origin of these asymmetries is unknown. Such asymmetries could arise from nonuniform spatial integration of local motion signals in the lobula plate (Krapp et al., 1998; Single and Borst, 1998; Single et al., 1997) or from nonlinear binocular interactions of lobula plate tangential neurons (Farrow et al., 2006; Krapp et al., 2001). It has also been proposed that directional asymmetries originate earlier in the visual system, perhaps in the lamina (Katsov and Clandinin, 2008; Rister et al., 2007). Our experiments identified four columnar lamina neurons that contribute to processing asymmetric motion signals moving either progressively or regressively across the eye (Figures 5A and 5B).

L4 neurons are unique among the lamina output neurons in that they interact with neighboring retinotopic columns within the lamina (Figure 5B). Within each lamina cartridge, L4 receives synaptic input from L2. In addition, each L4 neuron sends collaterals into posterior lamina cartridges (Strausfeld and Campos-Ortega, 1973), which synapse on both L2 and L4 neurons (Meinertzhagen and O'Neil, 1991; Rivera-Alba et al., 2011). In the medulla, L4 axons provide input to retinotopically posterior columns (Takemura et al., 2011). Based on this anatomical organization, it was proposed that the L2/L4 circuit mediates the detection of progressive motion (Braitenberg and Debbage, 1974; Takemura et al., 2011; Zhu et al., 2009).

Consistent with this prediction, we found that silencing L4 neurons impaired fly responses to monocular progressive but not regressive motion (Figure 5I). Silencing L2 neurons, the primary presynaptic input to L4, also altered fly responses to progressive but not regressive motion (Figure 5J), consistent with a previous report (Rister et al., 2007). Surprisingly, acute depolarization of

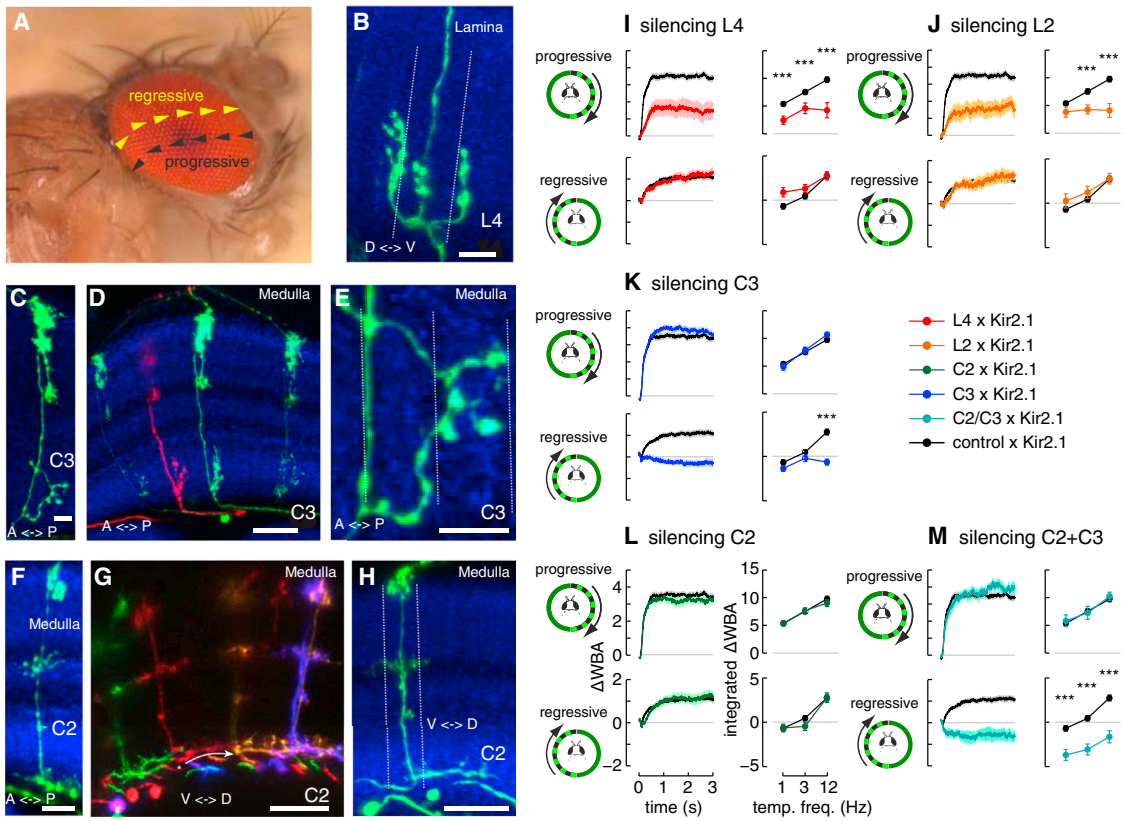

Figure 5. Silencing Four of the 12 Lamina-Associated Neuron Types Results in Directionally Asymmetric Changes to Fly Visual Perception

(A) Flies respond differently to visual motion presented in either the regressive (back-to-front) or progressive (front-to-back) directions.

(B) L4 branches in the proximal lamina possess a characteristic, column-crossing arborizations. Dotted lines indicate approximate positions of column boundaries based on anti-Brp (Nc82) antibody staining (blue).

(C–E) C3 neurons have multicolumnar directional branches in the proximal medulla.

(C) Medulla arborizations of a single C3 neuron.

(D) Stereotyped orientation of C3 branches. Multiple examples of C3 neurons in the same medulla visualized by multicolor stochastic labeling (details in Supplemental Experimental Procedures). Note that arbors in the proximal medulla consistently point in the posterior direction.

(E) C3 arbors in M9 are multicolumnar as shown by a higher-magnification view of branches of the individual C3 neuron in (C).

(F–H) C2 neurons are also multicolumnar and often have directional processes (for more examples, see Figure S3D).

(F) A single cell flip-out of a C2 neuron shows C2 arborizations in different medulla layers.

(G) Multicolor stochastic labeling of multiple C2 neurons in the same optic lobe showing similar oriented processes (along the DV axis) in M10. White arrow indicates approximate direction and length of one of these oriented processes.

(H) A single C2 cell viewed along the DV axis shows a pronounced asymmetry in layer M10. Dotted lines indicate approximate positions of column boundaries. Scale bars represent 5 μm in (B), (C), and (E), 10 μm in (F), and 20 μm (D), (G), and (H).

(I–M) Fly responses to monocularly restricted progressive motion are significantly reduced by Kir2.1 expression in L4 (I) and L2 (J), but not C2 (K) or C3 (L). Conversely, silencing C3 (L) or both C2 and C3 (M) reduced fly responses to regressive motion. All steering responses (mean ± SEM) to a lateral optomotor stimulus ($\lambda = 30°$) rotating progressively at 360°/s (12 Hz). Right: mean integrated turn responses to progressive motion at three speeds ($n \geq 10$ flies per genotype; ***$p < 0.01$, **$p < 0.05$; t tests on maximum p values, corrected for multiple comparisons; see Supplemental Experimental Procedures for details).

L4 neurons by dTrpA1 expression decreased fly responses to progressive motion and increased responses to regressive motion stimuli (Figures 4B and S7A). These results demonstrate that silencing L4 neurons alters detection of progressive motion across the eye and that silencing its primary lamina input, L2, has a similar effect.

In addition to affecting progressive motion responses, silencing L2 and L4 produced several other behavioral phenotypes. Kir2.1 expression in L2 neurons dramatically affected most motion behaviors tested (Figures 4A and S5B), consistent with its role as one of the primary feedforward inputs to downstream motion circuits (Clark et al., 2011; Joesch et al., 2010; Rister et al., 2007). Silencing L4 neurons also decreased full-field optomotor responses at low contrasts and very fast stimulus speeds and impaired the ability of flies to track rapidly oscillating patterns (Figure S7A).

In contrast to L2 and L4, we found that the columnar, centrifugal neurons C2 and C3 play an important role in shaping behavioral responses to regressive motion stimuli. C2 and C3 are GABAergic neurons (Fei et al., 2010; Kolodziejczyk et al., 2008) that arborize in multiple layers of the proximal and distal medulla and send axons into the lamina, where they are primarily

presynaptic on several neuron types, including L1, L2, and Lai neurons (Meinertzhagen and O'Neil, 1991; Rivera-Alba et al., 2011). In the distal medulla, C2 and C3 both receive presynaptic input from L1 and form synapses on L2; C2 is also presynaptic to L1 (Takemura et al., 2008).

In addition to the distal medulla, C3 neurons arborize in the proximal medulla, primarily in layer M9 (Figures 1C and 2H). Examination of the C3 terminals in the medulla revealed that putative dendritic arbors in layer M9 showed a stereotyped orientation, with processes extending posteriorly from the branch point off the main axon (Figures 5C and 5D). This directionality was highly stereotyped (33/33 neurons from 3 brains). Closer examination revealed that these arbors extend into neighboring columns (Figure 5E), reminiscent of the multicolumnar projections of L4 in lamina (Figure 5B; Strausfeld and Campos-Ortega, 1973) and medulla (Takemura et al., 2011). This organization suggests that C3 neurons receive synaptic input from posterior medulla columns and provide output to more anterior lamina and medulla columns. Such an asymmetric circuit could enhance the detection of regressive motion by amplifying signals translating from posterior to anterior across the eye. Consistent with this hypothesis, we found that silencing C3 neurons abolished steering responses to regressive motion stimuli moving at high speeds (Figure 5K, bottom row) but did not affect responses to progressive motion (Figure 5K, top row) or basic optomotor stimuli (Figure S7C).

C2 neurons also had multicolumnar, presumably dendritic, arborizations in the medulla (Figures 5F–5H). Most of the C2 arbors in layer M10, while variable in their detailed shapes, were strongly asymmetric (18/20 neurons from 19 brains), extending preferentially in a dorsal direction relative to the main neurite (Figures 5G, 5H, and S3D). This multicolumnar profile of C2 neurons suggests that they may also be involved in integrating signals from neighboring columns. Silencing C2 neurons resulted in decreased fly responses to slow regressive motion (3 Hz) in only one of the two Split-GAL4 lines we tested (Figures 5L and S7B). However, depolarizing C2 neurons with dTrpA1 increased steering responses to regressive motion and decreased responses to progressive motion (Figures 4B and S7B).

In addition to examining the effect of silencing C2 and C3 neurons individually, we tested a Split-GAL4 line that targeted both centrifugal neurons. Remarkably, silencing both C2 and C3 neurons together dramatically shifted fly responses to all regressive motion stimuli, such that clockwise regressive motion caused flies to turn counterclockwise (Figure 5M, bottom row). However, behavioral responses to progressive motion were unaffected (Figure 5M, top row).

During forward flight, rapid feedback from the centrifugal neurons could actively enhance the coding of luminance signals moving regressively across the eye. Although the LMCs are not themselves sensitive to motion (Clark et al., 2011; Laughlin and Hardie, 1978; Reiff et al., 2010), C2 and C3 may contribute to asymmetric filtering of luminance signals via synapses within the lamina (Meinertzhagen and O'Neil, 1991; Rivera-Alba et al., 2011), through presynaptic inhibition at the LMC terminals in the proximal medulla (Takemura et al. 2008, 2011) or by providing input to unidentified downstream neurons in the medulla. The parallels between the phenotypes of C2 and C3 suggest that they perform overlapping functional roles, perhaps each with distinct temporal and spatial properties.

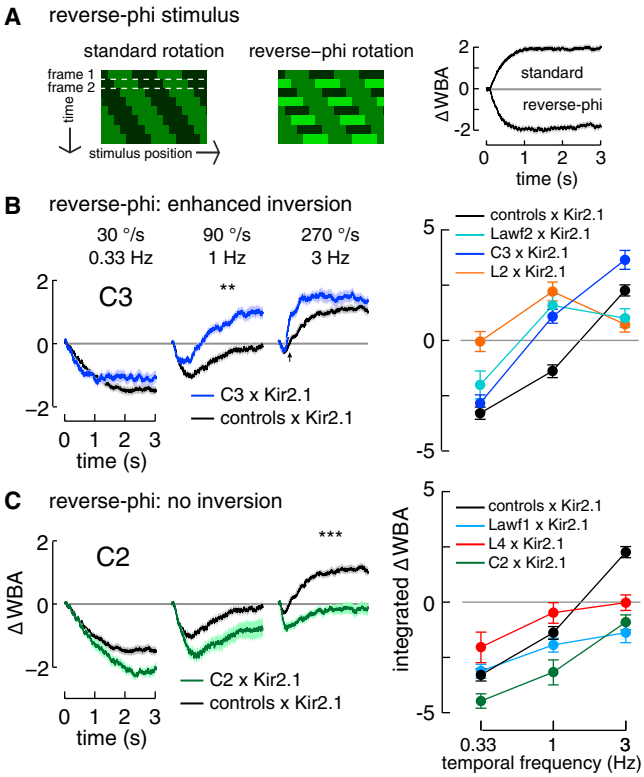

Figure 6. Lamina Neurons Differentially Contribute to Temporal Visual Processing

(A) Left: space-time depictions of reverse-phi and standard motion stimuli. Right: example steering responses to clockwise rotation of standard and reverse-phi motion stimuli ($\lambda = 30°$, 12 Hz).

(B) Left: silencing C3 neurons increases the rate of the reverse-phi inversion. Time series are flight steering responses (mean ± SEM) to rotation of a reverse-phi motion stimulus (90° spatial period) at three speeds. Right: mean integrated turn amplitude (±SEM) for cases in which silencing a class of lamina neurons increased reverse-phi inversion. The arrowhead marks the start of the reverse-phi inversion (see primary text).

(C) Same as in (B), except for cell types that eliminate the reverse-phi inversion.

Role of Lamina Neurons in Temporal Processing

To investigate how lamina neurons shape the temporal properties of fly vision, we compared tuning curves to standard and reverse-phi motion stimuli. Reverse-phi is a visual illusion that combines a contrast reversal with motion (Anstis and Rogers, 1975). Many species, including humans (Anstis and Rogers, 1975), perceive an illusory reversal in the direction of a reverse-phi motion stimulus. Flies typically turn in the direction opposite that of a reverse-phi motion pattern (Figure 6A)—they exhibit a "reverse-optomotor response" (Tuthill et al., 2011). However, very fast reverse-phi motion stimuli trigger transient reverse-optomotor steering, followed by compensatory turning in the opposite direction (Figure 6B, arrowhead). The timing and amplitude of these responses depend on the flicker rate of the reverse-phi stimulus and were predicted to arise from adaptation in peripheral circuits (Tuthill et al., 2011).

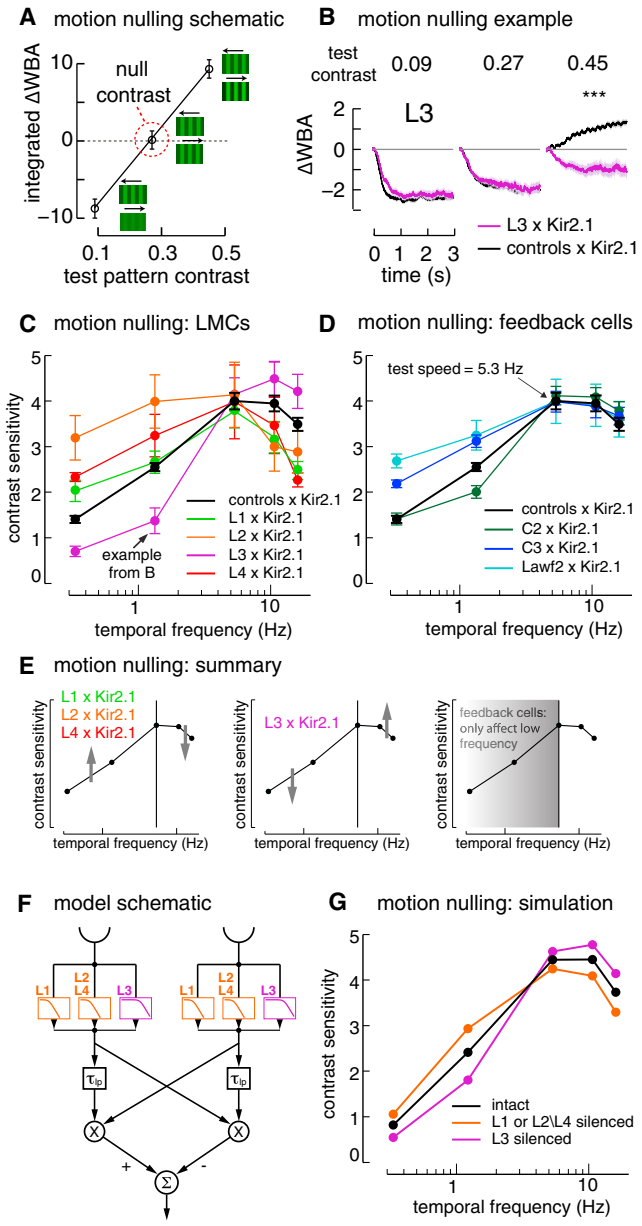

Figure 7. Motion Nulling Reveals Contributions of Lamina Neurons to Contrast Sensitivity as a Function of Stimulus Speed

(A) Nulling stimuli consist of two superimposed square-wave gratings (45° spatial period): a constant reference stimulus and a test stimulus whose contrast is varied across trials. At low test contrast, flies follow the reference stimulus (ΔWBA < 0); at high test contrast, flies follow the test stimulus (ΔWBA > 0). The null contrast is the contrast of the test stimulus needed to cancel, or "null," the reference stimulus.

(B) Example of a motion nulling phenotype: silencing L3 neurons alters fly contrast sensitivity at low speeds. The reference stimulus has a relative contrast of 0.27 and rotates counterclockwise at 4 Hz, while the test stimulus rotates clockwise at 1.33 Hz and the contrast is varied across trials. Control flies follow the high-contrast test stimulus on the last trial, while flies with L3 silenced follow the reference stimulus.

(C) Tuning curves of contrast sensitivity (1/null contrast) measured over a range of test stimulus temporal frequencies. Silencing four of the lamina monopolar cells, L1–L4, alters contrast sensitivity tuning at both high and low frequencies.

We found that silencing several lamina cell types specifically altered the amplitude and timing of behavioral responses to reverse-phi motion (Figures 6B and 6C). One phenotypic class, which included the cell types C3, L2, and Lawf2, exhibited an enhancement of the reverse-optomotor inversion at high speeds. For example, silencing C3 neurons dramatically increased the speed and magnitude of the reverse-phi inversion (Figure 6B). Silencing the other type of centrifugal neurons, C2, had the opposite effect, increasing the magnitude of reverse-optomotor responses and decreasing the rate of the steering inversion (Figure 6C). Silencing L4 and Lawf1 neurons also abolished the inversion of reverse-optomotor responses (Figure 6C). These disparate phenotypes suggest that several different lamina neuron types differentially influence the time course of visual adaptation. We note that related feedback neuron pairs (C2/C3 and Lawf1/Lawf2) appear to exert opposing effects.

Both behavioral responses and the activity of motion-sensitive neurons are known to depend on the temporal frequency of the motion stimulus (Borst et al., 2010). To closely explore temporal tuning of motion circuits, we employed a psychophysical technique known as motion nulling (Chichilnisky et al., 1993; Smear et al., 2007), in which two motion gratings are superimposed—a reference pattern moving in one direction and a test pattern moving in the opposite direction. We tested the ability of flies to distinguish between high- and low-contrast motion stimuli by varying the velocity and contrast of the test pattern across trials. We quantified contrast sensitivity as a function of stimulus velocity by determining the "null contrast" at each test speed (Figure 7A). The null contrast level of control flies varied as a function of the test pattern velocity, providing a measure of contrast sensitivity across stimulus speeds (black line, Figure 7B). Because the reference pattern remained constant (and at a speed close to *Drosophila*'s temporal frequency optimum), peak contrast sensitivity occurred when the reference and test pattern were moving at the same speed (5.33 Hz).

(D) Same as in (F) but for feedback neurons that contribute significantly to contrast sensitivity tuning. The neuron classes shown here represent all of the individual cell types for which the null contrast of at least two temporal frequencies is significant at the $p < 0.1$ level or lower (details in Supplemental Experimental Procedures).

(E) Summary of the changes in temporal tuning: inactivating L1, L2, and L4 leads to enhanced contrast sensitivity at lower frequencies and reduced sensitivity at higher frequencies, L3 inactivation leads to the opposite phenotype, and the feedback cells only affect the flies' contrast sensitivity at lower frequencies.

(F) A model for lamina processing with parallel inputs to an HR-EMD, representing the L1, L2/L4, and L3 pathways. L1 and L2/L4 preprocessing were modeled as fast pathways (with identical low-pass filters with time constants of $\tau = 4$ ms), while the L3 input was modeled as a much slower pathway (low-pass filter with $\tau = 80$ ms). The remainder of the model is a standard HR-EMD (with the delay implemented as a low-pass filter with $\tau = 18$ ms; see Supplemental Experimental Procedures for details of the simulation).

(G) Simulated responses of this model to the identical stimuli used in the motion nulling behavioral experiments capture the general changes in temporal tuning seen in (C). Removing either L1 or L2/L4 pathway input resulted in enhanced contrast sensitivity to low-frequency stimuli and a reduction in the high-frequency sensitivity, while removing the L3 input lead to the opposite phenotype.

Silencing four of the five lamina output neuron types (the feedforward pathway) had a strong effect on the shape of contrast sensitivity tuning curves. For example, silencing L3 neurons increased the tendency of flies to follow high-velocity, low-contrast patterns (Figure 7B), which extended the height of the contrast sensitivity tuning function (Figure 7C). In comparison, silencing L1, L2, and L4 resulted in a compression of the contrast sensitivity tuning functions (Figure 7C).

Silencing three of the four types of feedback neurons, C2, C3, and Lawf2, affected the ability of flies to distinguish small contrast differences at low test speeds, while behavior at higher test speeds remained normal. Interestingly, manipulating lamina output neurons reveals an imbalance (when compared to the control response) between contrast discrimination at high and low speeds (Figures 7C and 7E). In other words, amplified sensitivity in one speed range was accompanied by decreased sensitivity at other speeds. To explore this apparent trade-off and to identify mechanisms that could recapitulate these inactivation results, we simulated lamina processing as the input to a classic HR-EMD (Figure 7C). We observed this imbalanced response with simulations in which the L1 and L2/L4 pathways were tuned differently than the L3 pathway. Specifically, we set the L1 and L2/L4 pathways to be identical and significantly faster than L3 (Figure 7F). When we simulated this model (detailed in Supplemental Experimental Procedures) for the stimulus conditions used in the behavioral experiments of Figure 7C, we found a general agreement between the shape of the temporal tuning curves, as well as the effects of inactivating the faster (L1 or L2/L4) or slower (L3) input pathways.

In contrast to lamina output neurons, manipulation of lamina-associated feedback neurons specifically altered contrast sensitivity at low speeds (Figures 7D and 7E). This distinction is consistent with basic principles from control theory that stable closed-loop systems require low-frequency, bandwidth-limited feedback signals (Csete and Doyle, 2002).

DISCUSSION

In this study, we combined psychophysical measurements with targeted genetic manipulations in order to understand how lamina-associated neurons in *Drosophila* shape visual perception. By testing a wide range of visual behaviors, we identified distinct behavioral phenotypes for 11 out of the 12 neuron types that innervate the lamina (Figures 4A and 4B). Overall, our results suggest that the critical elements of motion detection probably reside downstream of the lamina but that lamina neurons play an important role in shaping the input signals to motion circuits.

We were surprised to find that silencing several lamina neuron classes altered fly responses to asymmetric motion stimuli (i.e., progressive versus regressive). Models for fly motion detection typically assume that visual circuits are organized symmetrically across the eye. However, for four cell types, L2, L4, C2, and C3, we found behavioral phenotypes that depended on the direction of stimulus motion. L4, C2, and C3 are the only columnar lamina-associated neurons that extend across multiple retinotopic columns in the medulla, and L2 provides the primary inputs into L4. These extensions are consistently asymmetric with respect to the coordinates of the eye, suggesting a mechanistic correlation between anatomy and function. For example, we found that C3 arbors in layer M9 of the medulla innervate more posterior columns, consistent with our finding that silencing C3 neurons produced striking deficits in the perception of regressive motion. One possibility is that feedback from more posterior columns onto more anterior columns would augment the response of the more anterior column to an edge moving regressively. Responses to edge stimuli moving in the opposite direction progressively would not be affected. C2 and C3 also make connections in the medulla, where they could affect processing in downstream circuits. Distinguishing between these hypotheses will require physiological recordings from C2 and C3 neurons, or recordings from LMC neurons while manipulating centrifugal neuron feedback. Similarly, recording from L2 neurons while silencing L4 neurons will provide insight into how L4 contributes to progressive motion processing.

Our data suggest that several features previously attributed to visual motion computation may result from processing in peripheral premotion circuits. For example, an important prediction of the HR-EMD model is that the time constant of the delay line shapes the temporal tuning of fly motion detection and thus the shape of the optomotor response curve (Figures 1B and 3C; Reichardt, 1961). However, we found that silencing some lamina neurons (L1, L2, and L4) specifically decreased the tendency of flies to follow very fast motion stimuli, while silencing L3 had the opposite effect, increasing fly responses to fast motion stimuli (Figure 7C). Consistent with our behavioral and simulation results, L3 neurons in larger flies have a higher input resistance than L1 or L2 (Hardie and Weckström, 1990), which could result in attenuation of high-frequency signals in L3 (although this attenuation may also occur in neurons downstream of L3).

The simulation results of Figures 7F and 7G strongly suggest that processing by individual cell types (and subsequent downstream pathways) contribute to the aggregate tuning of motion vision. Specifically, the temporal frequency optimum of the elaborated HR-EMD (Figure 7F) is no longer determined strictly by the time constant of the delay line but is affected by the time constants of the input pathways as well (and would be further influenced by the dynamics of feedback pathways if included in the model). This simulation illustrates one example of a potentially general principal of the fly lamina: anatomically related cell types carry out similar functions but with distinct temporal properties. The two classes of reverse-optomotor phenotypes (Figure 6) suggest that L2 and L4, C2 and C3, and Lawf1 and Lawf2 may in each case represent two "arms" of a balanced network. The duplication of function with temporal specializations that we propose need not be independent (as in our model of Figure 7F) from the recently described bifurcation into pathways specialized for the detection of luminance increments and decrements (Joesch et al., 2013). Overall the diverse range of phenotypes related to motion responses at different speeds (Figures 6 and 7) suggests that many lamina cell types contribute to shaping the temporal tuning of early visual processing. By structuring the inputs to downstream motion circuits, lamina neurons appear to play an important role in shaping the tuning of visual behaviors, such as the optomotor response, that have previously been

compactly described by the HR-EMD model. These observations provide one possible explanation for the apparent mismatch between the minimal complexity of motion detection models and the elaborate diversity of lamina and medulla neuron classes.

Our data also do not support the hypothesis that specific lamina neurons serve as dedicated pathways for encoding global stimulus features, such as patterns of optic flow. Rather, a small number of neuron types, mainly L1 and L2, are essential for basic motion detection, while the majority of lamina neuron types serve to dynamically sculpt and enhance these feedforward signals. For example, we discovered that four classes of feedback neurons, the centrifugal neurons C2 and C3 and the wide-field neurons Lawf1 and Lawf2, play an intimate role in visual motion processing. These feedback projections from the medulla could mediate adaptation, gain control, or behavioral state modulation of the lamina neurons that provide input to motion circuits.

Our results suggest that lateral interactions between retinotopic columns and feedback from downstream neurons both play an important role in shaping visual motion detection. These pathways may serve to enhance the coding capacity of motion pathways through adaptation mechanisms previously identified in the lamina, such as predictive gain control (Srinivasan et al., 1982) and lateral inhibition (Laughlin et al., 1987). For example, the reduced sensitivity to low-contrast and fast-motion stimuli we observed in L4 silencing experiments (Figures 4A and S7A) could result from decreased lateral interactions within the lamina and a consequent decrease in coding efficiency. Similarly, feedback from the centrifugal neurons C2 and C3 could enhance detection of unexpected regressive motion signals (Zabala et al., 2012) by integrating signals from neighboring posterior columns in the medulla.

We found that specific spatial and temporal features of fly motion perception can be separated using targeted genetic manipulations of lamina neurons. This suggests that the HR-EMD model may be implemented in a more distributed manner than previously thought, possibly involving parallel circuits that rely on contributions from many neuronal cell types in the lamina and medulla. Several recent studies have reached similar conclusions, for example, proposing that parallel motion circuits exist for detecting ON- and OFF-type edges (Clark et al., 2011; Joesch et al., 2010, 2013). Although we did not find evidence for lamina neurons providing strong rectification into ON and OFF input channels, this is most likely due to differences in behavioral assays and not differences in GAL4 lines or neural effectors (Figure S6). It is also possible that some visual stimuli used in this study activated multiple, parallel motion circuits, which could mask the effects of silencing a single neuron class. This could be tested in the future by silencing other specific combinations of closely related lamina neurons, such as L2 and L4 or L1 and L3.

Previous studies of the lamina have used different neural effectors, in particular a temperature-sensitive dynamin mutant ($Shibire^{ts}$) (Kitamoto, 2001), to silence neurons (Clark et al., 2011; Joesch et al., 2010; Rister et al., 2007). We chose to use the Kir2.1 channel because its expression permitted sustained flight behavior for long periods (enabling the comparative study of many visual stimuli), which is not possible at the higher temperatures required for $Shibire^{ts}$. Because the Kir2.1 channel is tagged with GFP, we were also able to verify its expression and efficacy (Figure S3). One caveat of this approach is that Kir2.1 expression hyperpolarizes the resting potential, which could affect neighboring neurons through electrical gap junctions. Because gap junctions in the fly nervous system are not detectable by electron microscopy, their frequency and distribution in the visual system are not well understood (Meinertzhagen and O'Neil, 1991; Rivera-Alba et al., 2011). However, there is some evidence for their existence in the lamina, for example between L1 and L2 (Joesch et al., 2010). Two pieces of evidence indicate that the Kir2.1 expression in our experiments did not affect multiple cell types. First, we observed unique and specific phenotypes for most of the cell types examined. Second, for those cases in which we silenced neuron pairs (L1/L2 and C2/C3), we observed stronger phenotypes when we manipulated both cells compared to the component neurons. Nonetheless, it is still possible that Kir2.1 expression enhances the deficits we report by affecting electrically coupled neurons, and future experiments using improved neural effectors will be required to test this possibility.

A common approach to probe the functional role of neuronal cell types is to selectively silence or activate small subsets of neurons and then examine the resultant effects on behavior. Though this approach is widely used in *Drosophila* and other genetic model organisms, its utility has been limited by two main experimental challenges. First, highly specific genetic driver lines have been unavailable for most cell populations. This has made it difficult to confidently attribute observed behavioral phenotypes to the manipulation of individual cell types. Second, the behavioral assays applied have often been too limited to reveal potential functions for most of the neuronal classes examined. Our results for the fly lamina show that it is possible to use intersectional genetic techniques to systematically target all the neuronal cell types in a brain region of interest. Furthermore, we show that diverse quantitative behavioral assays can reveal functional roles for nearly all examined neuronal classes. With the recent availability of a large collection of defined GAL4 driver lines (Jenett et al., 2012), this approach can now be readily applied to other parts of the *Drosophila* brain.

EXPERIMENTAL PROCEDURES

Split-GAL4 transgenes were selected based on GAL4-line expression patterns (Jenett et al., 2012), constructed as previously described in Pfeiffer et al. (2010) and listed in Table S1. Expression patterns of Split-GAL4 lines were assessed by anti-GFP antibody staining and confocal imaging of 5- to 10-day-old female flies expressing one of two different UAS reporters. A "flip-out"-based approach (Struhl and Basler, 1993) was used for stochastic single-cell labeling.

For all tethered flight experiments, we used female *Drosophila* (3–5 days old), which were heterozygous for both GAL4 and UAS transgenes (effectors backcrossed into Dickinson Laboratory [DL] or Canton-S [CS] wild-type backgrounds). Each fly was tethered to a tungsten wire with UV-cured glue and suspended within an electronic visual flight simulator consisting of a 32 × 88 cylindrical array of green LEDs (Reiser and Dickinson, 2008). The amplitude and frequency of the fly's wing beats were monitored with an optical wingbeat analyzer, allowing us to present visual stimuli in either open- or closed-loop mode (Götz, 1987). All visual stimuli are described in the Supplemental Experimental Procedures and depicted in Figure S2. Each 3 s open-loop

stimulus condition was followed by 3.5 s of closed-loop "stripe fixation" to ensure that flies were actively steering at the onset of each trial. Within an experiment, each set of conditions was presented as random blocks repeated three times. Trials in which the fly stopped flying were repeated at the end of each block. These data were averaged on a per fly basis to produce a mean turning response for each stimulus condition. Further details of the all methods used are provided in the Supplemental Experimental Procedures.

SUPPLEMENTAL INFORMATION

Supplemental Information includes seven figures, one table, and Supplemental Experimental Procedures and can be found with this article online at http://dx.doi.org/10.1016/j.neuron.2013.05.024.

ACKNOWLEDGMENTS

We thank Barret Pfeiffer, Heather Dionne, and Chris Murphy for molecular biology of Split-GAL4 constructs, Teri Ngo and Ming Wu for assistance with Split-GAL4 screening, the Janelia Fly Core for assistance with *Drosophila* care, the Janelia Fly Light Project for providing images of the primary GAL4 lines and of C2 single neurons, the Janelia Fly Light Scientific Computing Team for image processing software, Matt Smear and Stephen Huston for assistance with stimulus design, Damon Clark for discussions of L1- and L2-inactivation phenotypes, and Magnus Karlsson and Jinyang Liu for continued development and support of the visual display system. The Iso-D1 and the two L1 stocks used in Figure S6 were a gift from Tom Clandinin. We also thank Larry Zipursky, Alla Karpova, Stefan Pulver, Vivek Jayaraman, Anthony Leonardo, and members of the Reiser, Jayaraman, Card, and Rubin laboratories. This project was supported by HHMI.

Accepted: May 10, 2013
Published: June 20, 2013

REFERENCES

Anstis, S.M., and Rogers, B.J. (1975). Illusory reversal of visual depth and movement during changes of contrast. Vision Res. *15*, 957–961.

Baines, R.A., Uhler, J.P., Thompson, A., Sweeney, S.T., and Bate, M. (2001). Altered electrical properties in Drosophila neurons developing without synaptic transmission. J. Neurosci. *21*, 1523–1531.

Benjamini, Y., and Hochberg, Y. (1995). Controlling the false discovery rate: a practical and powerful approach to multiple testing. J. R. Stat. Soc. Ser. B-Methodol. *57*, 289–300.

Borst, A., and Euler, T. (2011). Seeing things in motion: models, circuits, and mechanisms. Neuron *71*, 974–994.

Borst, A., Haag, J., and Reiff, D.F. (2010). Fly motion vision. Annu. Rev. Neurosci. *33*, 49–70.

Braitenberg, V. (1967). Patterns of projection in the visual system of the fly. I. Retina-lamina projections. Exp. Brain Res. *3*, 271–298.

Braitenberg, V., and Debbage, P. (1974). A regular net of reciprocal synapses in the visual system of the fly, *Musca domestica*. J. Comp. Physiol. A Neuroethol. Sens. Neural Behav. Physiol. *90*, 25–31.

Buchner, E. (1971). Dunkelanregung des stationären Flugs der Fruchtfliege *Drosophila*. PhD thesis, Univeristy of Tübingen, Tübingen, Germany.

Buchner, E. (1976). Elementary movement detectors in an insect visual system. Biol. Cybern. *24*, 85–101.

Buchner, E. (1984). Behavioural analysis of spatial vision in insects. In Photoreception and Vision in Invertebrates, M. Ali, ed. (New York: Plenum), pp. 561–619.

Carver, S., Roth, E., Cowan, N.J., and Fortune, E.S. (2008). Synaptic plasticity can produce and enhance direction selectivity. PLoS Comput. Biol. *4*, e32.

Cavanagh, P., and Anstis, S. (1991). The contribution of color to motion in normal and color-deficient observers. Vision Res. *31*, 2109–2148.

Chichilnisky, E.J., Heeger, D., and Wandell, B.A. (1993). Functional segregation of color and motion perception examined in motion nulling. Vision Res. *33*, 2113–2125.

Clark, D.A., Bursztyn, L., Horowitz, M.A., Schnitzer, M.J., and Clandinin, T.R. (2011). Defining the computational structure of the motion detector in Drosophila. Neuron *70*, 1165–1177.

Coombe, P.E., Srinivasan, M.V., and Guy, R.G. (1989). Are the large monopolar cells of the insect lamina on the optomotor pathway? J. Comp. Physiol. A Neuroethol. Sens. Neural Behav. Physiol. *166*, 23–35.

Csete, M.E., and Doyle, J.C. (2002). Reverse engineering of biological complexity. Science *295*, 1664–1669.

Douglass, J.K., and Strausfeld, N.J. (1995). Visual motion detection circuits in flies: peripheral motion computation by identified small-field retinotopic neurons. J. Neurosci. *15*, 5596–5611.

Duistermars, B.J., Chow, D.M., Condro, M., and Frye, M.A. (2007a). The spatial, temporal and contrast properties of expansion and rotation flight optomotor responses in Drosophila. J. Exp. Biol. *210*, 3218–3227.

Duistermars, B.J., Reiser, M.B., Zhu, Y., and Frye, M.A. (2007b). Dynamic properties of large-field and small-field optomotor flight responses in Drosophila. J. Comp. Physiol. A Neuroethol. Sens. Neural Behav. Physiol. *193*, 787–799.

Duistermars, B.J., Care, R.A., and Frye, M.A. (2012). Binocular interactions underlying the classic optomotor responses of flying flies. Front. Behav. Neurosci. *6*, 6.

Egelhaaf, M., and Borst, A. (1989). Transient and steady-state response properties of movement detectors. J. Opt. Soc. Am. A *6*, 116–127.

Eichner, H., Joesch, M., Schnell, B., Reiff, D.F., and Borst, A. (2011). Internal structure of the fly elementary motion detector. Neuron *70*, 1155–1164.

Farrow, K., Haag, J., and Borst, A. (2006). Nonlinear, binocular interactions underlying flow field selectivity of a motion-sensitive neuron. Nat. Neurosci. *9*, 1312–1320.

Fei, H., Chow, D.M., Chen, A., Romero-Calderón, R., Ong, W.S., Ackerson, L.C., Maidment, N.T., Simpson, J.H., Frye, M.A., and Krantz, D.E. (2010). Mutation of the Drosophila vesicular GABA transporter disrupts visual figure detection. J. Exp. Biol. *213*, 1717–1730.

Fischbach, K.F., and Dittrich, A.P. (1989). The optic lobe of Drosophila melanogaster. I. A Golgi analysis of wild-type structure. Cell Tissue Res. *258*, 441–475.

Gao, S., Takemura, S.Y., Ting, C.Y., Huang, S., Lu, Z., Luan, H., Rister, J., Thum, A.S., Yang, M., Hong, S.T., et al. (2008). The neural substrate of spectral preference in Drosophila. Neuron *60*, 328–342.

Gollisch, T., and Meister, M. (2010). Eye smarter than scientists believed: neural computations in circuits of the retina. Neuron *65*, 150–164.

Götz, K.G. (1964). Optomotorische Untersuchung des visuellen Systems einiger Augenmutanten der Fruchtfliege *Drosophila*. Kybernetik *2*, 77–92.

Götz, K.G. (1968). Flight control in Drosophila by visual perception of motion. Kybernetik *4*, 199–208.

Götz, K.G. (1987). Course-control, metabolism and wing interference during ultralong tethered flight in Drosophila melanogaster. J. Exp. Biol. *128*, 35–46.

Haag, J., Denk, W., and Borst, A. (2004). Fly motion vision is based on Reichardt detectors regardless of the signal-to-noise ratio. Proc. Natl. Acad. Sci. USA *101*, 16333–16338.

Hamada, F.N., Rosenzweig, M., Kang, K., Pulver, S.R., Ghezzi, A., Jegla, T.J., and Garrity, P.A. (2008). An internal thermal sensor controlling temperature preference in Drosophila. Nature *454*, 217–220.

Hardie, R.C., and Weckström, M. (1990). Three classes of potassium channels in large monopolar cells of the blowfly *Calliphora vicina*. J. Comp. Physiol. A Neuroethol. Sens. Neural Behav. Physiol. *167*, 723–736.

Hasegawa, E., Kitada, Y., Kaido, M., Takayama, R., Awasaki, T., Tabata, T., and Sato, M. (2011). Concentric zones, cell migration and neuronal circuits in the Drosophila visual center. Development *138*, 983–993.

Hassenstein, V.B., and Reichardt, W. (1956). Systemtheoretische Analyse der Zeit-, Reihenfolgen und Vorzeichenauswertung bei der Bewegungsperzeption des Rüsselkäfers Chlorophanus. Z Naturforsch *11b*, 513–524.

Hausen, K. (1982). Motion sensitive interneurons in the optomotor system of the fly. II. The horizontal cells: receptive-field organization and response characteristics. Biol. Cybern. *46*, 67–79.

Hausen, K., and Wehrhahn, C. (1989). Neural circuits mediating visual flight control in flies. I. Quantitative comparison of neural and behavioral response characteristics. J. Neurosci. *9*, 3828–3836.

Heisenberg, M. (1972). Comparative behavioral studies on 2 visual mutants of Drosophila. J. Comp. Physiol. A Neuroethol. Sens. Neural Behav. Physiol. *80*, 119–136.

Heisenberg, M., and Wolf, R. (1984). Vision in Drosophila: Genetics of Microbehavior (Berlin: Springer-Verlag).

Helfrich-Förster, C., Shafer, O.T., Wülbeck, C., Grieshaber, E., Rieger, D., and Taghert, P. (2007). Development and morphology of the clock-gene-expressing lateral neurons of Drosophila melanogaster. J. Comp. Neurol. *500*, 47–70.

Jenett, A., Rubin, G.M., Ngo, T.T., Shepherd, D., Murphy, C., Dionne, H., Pfeiffer, B.D., Cavallaro, A., Hall, D., Jeter, J., et al. (2012). A GAL4-driver line resource for Drosophila neurobiology. Cell Rep *2*, 991–1001.

Joesch, M., Schnell, B., Raghu, S.V., Reiff, D.F., and Borst, A. (2010). ON and OFF pathways in Drosophila motion vision. Nature *468*, 300–304.

Joesch, M., Weber, F., Eichner, H., and Borst, A. (2013). Functional specialization of parallel motion detection circuits in the fly. J. Neurosci. *33*, 902–905.

Katsov, A.Y., and Clandinin, T.R. (2008). Motion processing streams in Drosophila are behaviorally specialized. Neuron *59*, 322–335.

Kirschfeld, K. (1967). Die Projektion der optischen Umwelt auf das Raster der Rhabdomere im Komplexauge von MUSCA. Exp. Brain Res. *3*, 248–270.

Kitamoto, T. (2001). Conditional modification of behavior in Drosophila by targeted expression of a temperature-sensitive shibire allele in defined neurons. J. Neurobiol. *47*, 81–92.

Kolodziejczyk, A., Sun, X., Meinertzhagen, I.A., and Nässel, D.R. (2008). Glutamate, GABA and acetylcholine signaling components in the lamina of the Drosophila visual system. PLoS ONE *3*, e2110.

Krapp, H.G., Hengstenberg, B., and Hengstenberg, R. (1998). Dendritic structure and receptive-field organization of optic flow processing interneurons in the fly. J. Neurophysiol. *79*, 1902–1917.

Krapp, H.G., Hengstenberg, R., and Egelhaaf, M. (2001). Binocular contributions to optic flow processing in the fly visual system. J. Neurophysiol. *85*, 724–734.

Laughlin, S.B., and Hardie, R.C. (1978). Common strategies for light adaptation in the peripheral visual systems of fly and dragonfly. J. Comp. Physiol. A Neuroethol. Sens. Neural Behav. Physiol. *128*, 319–340.

Laughlin, S.B., Howard, J., and Blakeslee, B. (1987). Synaptic limitations to contrast coding in the retina of the blowfly Calliphora. Proc. R. Soc. Lond. B Biol. Sci. *231*, 437–467.

Luan, H., Peabody, N.C., Vinson, C.R., and White, B.H. (2006). Refined spatial manipulation of neuronal function by combinatorial restriction of transgene expression. Neuron *52*, 425–436.

Meinertzhagen, I.A., and O'Neil, S.D. (1991). Synaptic organization of columnar elements in the lamina of the wild type in *Drosophila melanogaster*. J. Comp. Neurol. *305*, 232–263.

Pfeiffer, B.D., Jenett, A., Hammonds, A.S., Ngo, T.T., Misra, S., Murphy, C., Scully, A., Carlson, J.W., Wan, K.H., Laverty, T.R., et al. (2008). Tools for neuroanatomy and neurogenetics in Drosophila. Proc. Natl. Acad. Sci. USA *105*, 9715–9720.

Pfeiffer, B.D., Ngo, T.T., Hibbard, K.L., Murphy, C., Jenett, A., Truman, J.W., and Rubin, G.M. (2010). Refinement of tools for targeted gene expression in Drosophila. Genetics *186*, 735–755.

Pulver, S.R., Pashkovski, S.L., Hornstein, N.J., Garrity, P.A., and Griffith, L.C. (2009). Temporal dynamics of neuronal activation by Channelrhodopsin-2 and TRPA1 determine behavioral output in Drosophila larvae. J. Neurophysiol. *101*, 3075–3088.

Reichardt, W. (1961). Autocorrelation, a principle for the evaluation of sensory information by the central nervous system. In Sensory Communication, W.A. Rosenblith, ed. (New York: John Wiley), pp. 303–317.

Reichardt, W., and Wenking, H. (1969). Optical detection and fixation of objects by fixed flying flies. Naturwissenschaften *56*, 424–425.

Reiff, D.F., Plett, J., Mank, M., Griesbeck, O., and Borst, A. (2010). Visualizing retinotopic half-wave rectified input to the motion detection circuitry of Drosophila. Nat. Neurosci. *13*, 973–978.

Reiser, M.B., and Dickinson, M.H. (2008). A modular display system for insect behavioral neuroscience. J. Neurosci. Methods *167*, 127–139.

Rister, J., Pauls, D., Schnell, B., Ting, C.Y., Lee, C.H., Sinakevitch, I., Morante, J., Strausfeld, N.J., Ito, K., and Heisenberg, M. (2007). Dissection of the peripheral motion channel in the visual system of Drosophila melanogaster. Neuron *56*, 155–170.

Rivera-Alba, M., Vitaladevuni, S.N., Mishchenko, Y., Lu, Z., Takemura, S.Y., Scheffer, L., Meinertzhagen, I.A., Chklovskii, D.B., and de Polavieja, G.G. (2011). Wiring economy and volume exclusion determine neuronal placement in the Drosophila brain. Curr. Biol. *21*, 2000–2005.

Single, S., and Borst, A. (1998). Dendritic integration and its role in computing image velocity. Science *281*, 1848–1850.

Single, S., Haag, J., and Borst, A. (1997). Dendritic computation of direction selectivity and gain control in visual interneurons. J. Neurosci. *17*, 6023–6030.

Smear, M.C., Tao, H.W., Staub, W., Orger, M.B., Gosse, N.J., Liu, Y., Takahashi, K., Poo, M.M., and Baier, H. (2007). Vesicular glutamate transport at a central synapse limits the acuity of visual perception in zebrafish. Neuron *53*, 65–77.

Srinivasan, M.V., Laughlin, S.B., and Dubs, A. (1982). Predictive coding: a fresh view of inhibition in the retina. Proc. R. Soc. Lond. B Biol. Sci. *216*, 427–459.

Strausfeld, N.J., and Campos-Ortega, J.A. (1973). The L4 monopolar neurone: a substrate for lateral interaction in the visual system of the fly Musca domestica (L.). Brain Res. *59*, 97–117.

Struhl, G., and Basler, K. (1993). Organizing activity of wingless protein in Drosophila. Cell *72*, 527–540.

Takemura, S.Y., Lu, Z., and Meinertzhagen, I.A. (2008). Synaptic circuits of the Drosophila optic lobe: the input terminals to the medulla. J. Comp. Neurol. *509*, 493–513.

Takemura, S.Y., Karuppudurai, T., Ting, C.Y., Lu, Z., Lee, C.H., and Meinertzhagen, I.A. (2011). Cholinergic circuits integrate neighboring visual signals in a Drosophila motion detection pathway. Curr. Biol. *21*, 2077–2084.

Tammero, L.F., Frye, M.A., and Dickinson, M.H. (2004). Spatial organization of visuomotor reflexes in Drosophila. J. Exp. Biol. *207*, 113–122.

Theobald, J.C., Ringach, D.L., and Frye, M.A. (2010). Dynamics of optomotor responses in Drosophila to perturbations in optic flow. J. Exp. Biol. *213*, 1366–1375.

Tuthill, J.C., Chiappe, M.E., and Reiser, M.B. (2011). Neural correlates of illusory motion perception in Drosophila. Proc. Natl. Acad. Sci. USA *108*, 9685–9690.

Zabala, F., Polidoro, P., Robie, A., Branson, K., Perona, P., and Dickinson, M.H. (2012). A simple strategy for detecting moving objects during locomotion revealed by animal-robot interactions. Curr. Biol. *22*, 1344–1350.

Zheng, L., de Polavieja, G.G., Wolfram, V., Asyali, M.H., Hardie, R.C., and Juusola, M. (2006). Feedback network controls photoreceptor output at the layer of first visual synapses in Drosophila. J. Gen. Physiol. *127*, 495–510.

Zhu, Y., Nern, A., Zipursky, S.L., and Frye, M.A. (2009). Peripheral visual circuits functionally segregate motion and phototaxis behaviors in the fly. Curr. Biol. *19*, 613–619.

Neuron, Volume *79*

Supplemental Information

Contributions of the 12 Neuron Classes in the Fly Lamina to Motion Vision

John C. Tuthill, Aljoscha Nern, Stephen L. Holtz, Gerald M. Rubin, and Michael B. Reiser

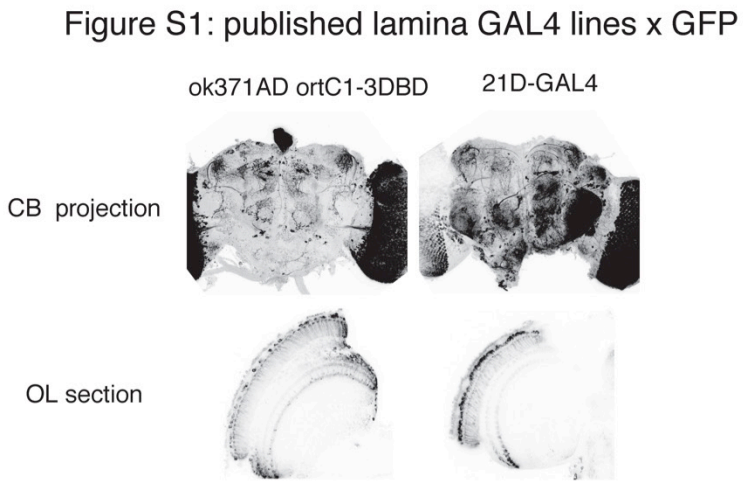

Figure S1, related to Figure 2. Images of GFP expression in previously used lamina lines. GFP expression in brains of 5-10 day old female flies of the indicated GAL4 or Split-GAL4 lines crossed to pJFRC12-10XUAS-IVS-myr::GFP was visualized by indirect immunofluorescence with anti-GFP antibodies. The labeling and imaging protocol was the same as that used for the Split-GAL4 lines described in this study. A maximum intensity projection of a confocal stack through the central brain and a single confocal section through the optic lobes are shown. Note broad expression in the brain. The optic lobe patterns also include more than one cell type.

Figure S2: visual stimuli

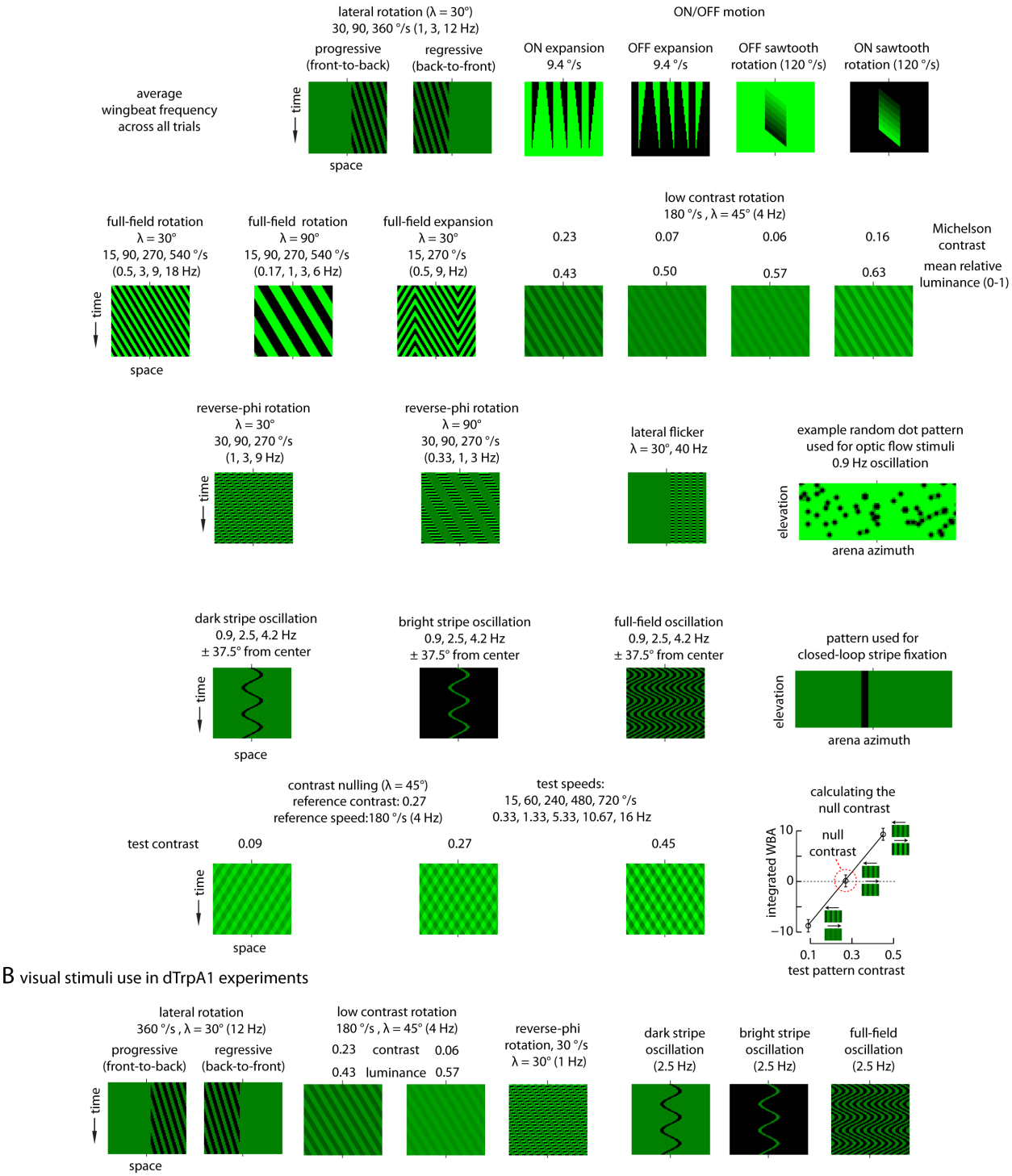

Figure S2, related to Figure 4. Visual stimuli used in all behavioral experiments. (A) Visual stimuli used in silencing experiments using Kir2.1, results summarized in Figure 4A and S4. (B) Stimuli used in activation experiments using dTrpA1, results summarized in Figure 4B.. The intensity range of the green LEDs was 0 to 72 cdm^{-2}, and relative luminance values are scaled linearly within this range (from 0 to 1). The temporal frequency of the grating stimuli is defined as the ratio of the angular velocity and the spatial wavelength, and is listed alongside the angular velocity of the stimuli in units of Hz. See Supplemental Experimental Procedures for further details of each visual stimulus condition.

Figure S3: Kir2.1 expression images and controls

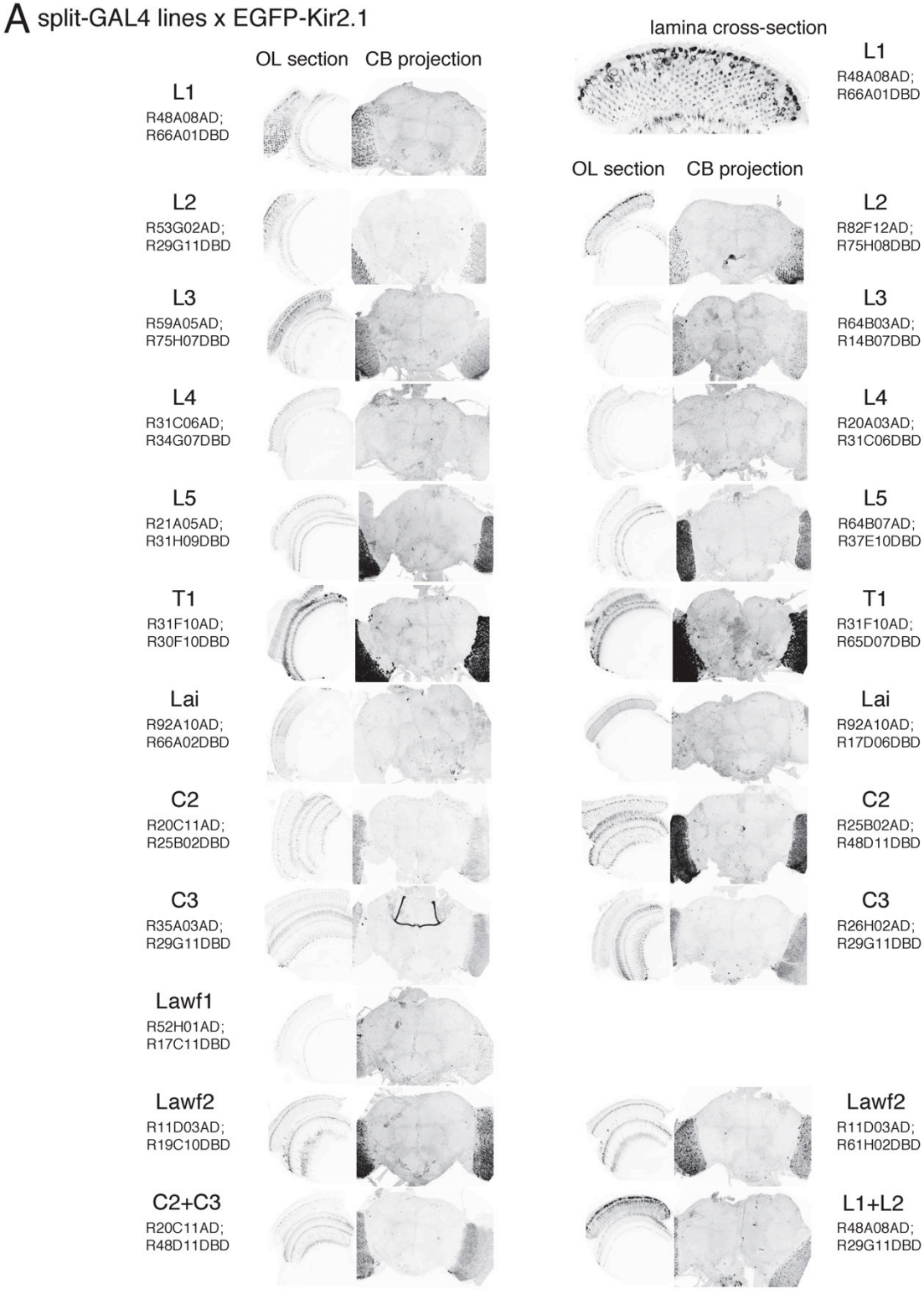

Figure S3 (continued)

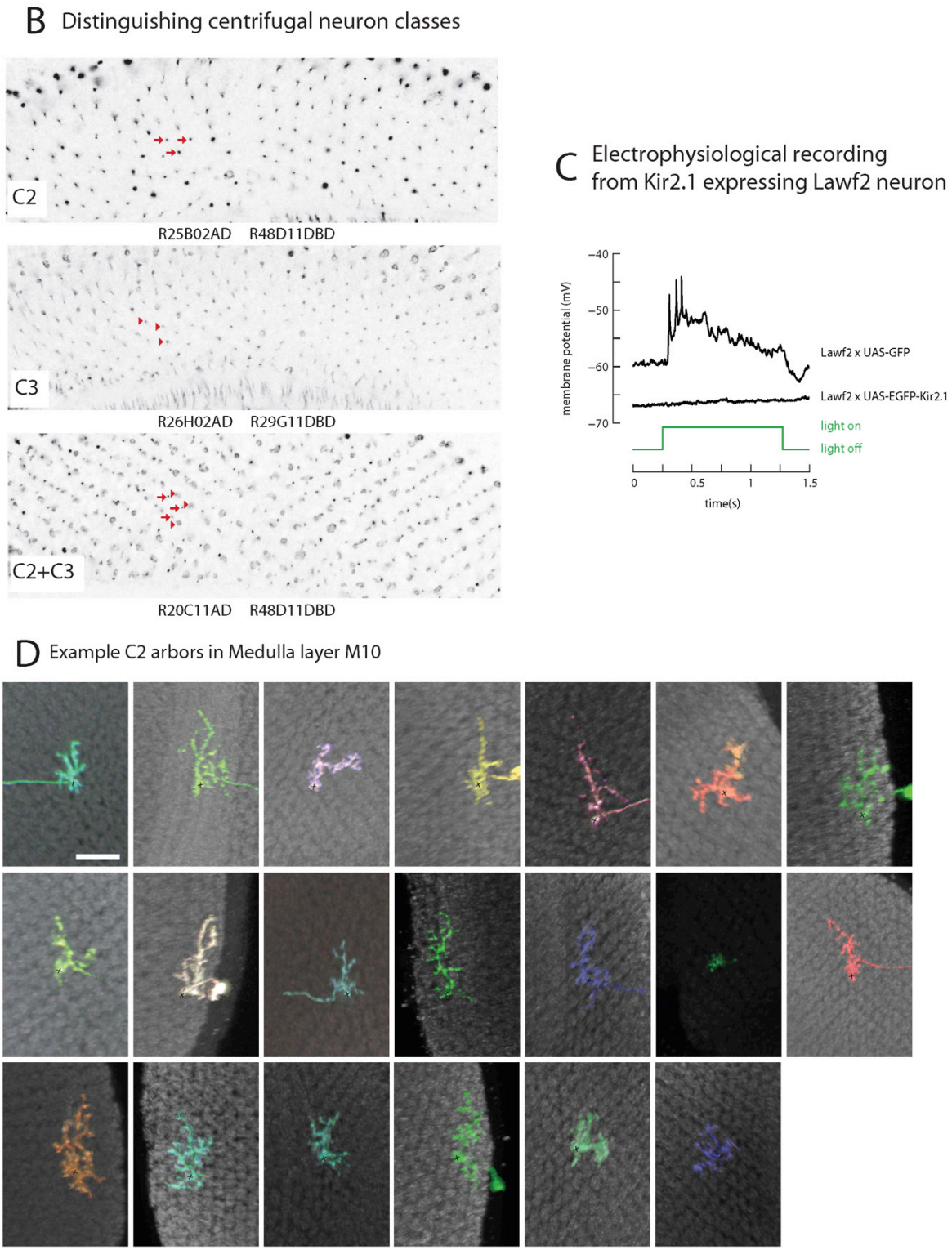

Figure S3, related to Figure 2. (A) Split-GAL4 driven expression of UAS-EGFP-Kir2.1. Images are of brains of 5-10 day old female flies labeled by antibody staining against GFP. Single confocal sections through the optic lobes (OL) and maximum intensity projection of confocal stacks through the central brain (CB) are shown. For the L1 line, an optical cross-section through the lamina illustrates that most (>90%), though not all L1 neurons show expression. (B) UAS-EGFP-Kir2.1 expression in C2, C3, and C2+C3 Split-GAL4 lines. Single confocal cross-sections through the lamina are shown. Each lamina cartridge contains one C2 and one C3 axon, one or both of which are labeled depending on the driver lines. Arrowheads point to examples of C2, arrows to examples of C3 axons. (C) Kir2.1 expression silences Lawf2 neurons. Whole-cell patch clamp recordings were targeted to Lawf2 neurons expressing UAS-MCD8-GFP (top) and UAS-EGFP-Kir2.1 (bottom). Example traces show current clamp recordings of Lawf2 neurons expressing Kir2.1 to a brief light flash. In 4 cells recorded in 2 flies expressing Kir2.1, no light-evoked responses were observed. Expression of Kir2.1 also hyperpolarized the resting potential, and decreased the average input resistance of Lawf2 neurons (0.500 ± 0.159 GΩ vs. 1.09 ± 0.064 GΩ). See Tuthill et al. (in review) for details about whole-cell patch clamp electrophysiology. (D) Variability and asymmetry of arbors of C2 neurons in layer M10 (related to Figure 5F,G,H). Reoriented views (see Supplemental Experimental Procedures) of 20 individual C2 neurons (from 19 fly brains) showing the branches in layer M10 with an anti-Brp (mAb Nc82) labeled (in grey) reference pattern. In each image the position of the main C2 neurite is marked (small black x). Each image is oriented so that dorsal is approximately up. Scale bar represents 10 μm.

Figure S4: complete P-value matrix for lines x Kir2.1

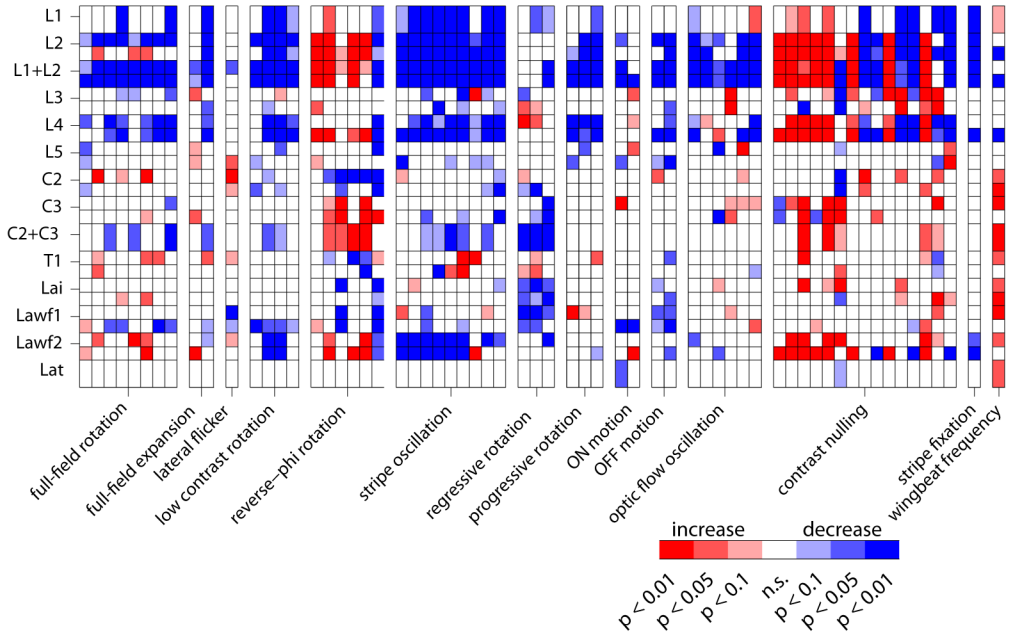

Figure S4, related to Figure 4. Heatmap of all neuron/behavior combinations. This table is similar to Figure 4A, except that each individual genotype is shown and p-values are not corrected for multiple comparisons. Each node in the matrix represents the p-value of unpaired t-tests between a single Split-GAL4 line and the 4 pooled control genotypes. The order of GAL4 lines displayed in this figure corresponds to the order of the genotypes listed in Table S1.

Figure S5A: Lamina Monopolar Cell 1 (L1)

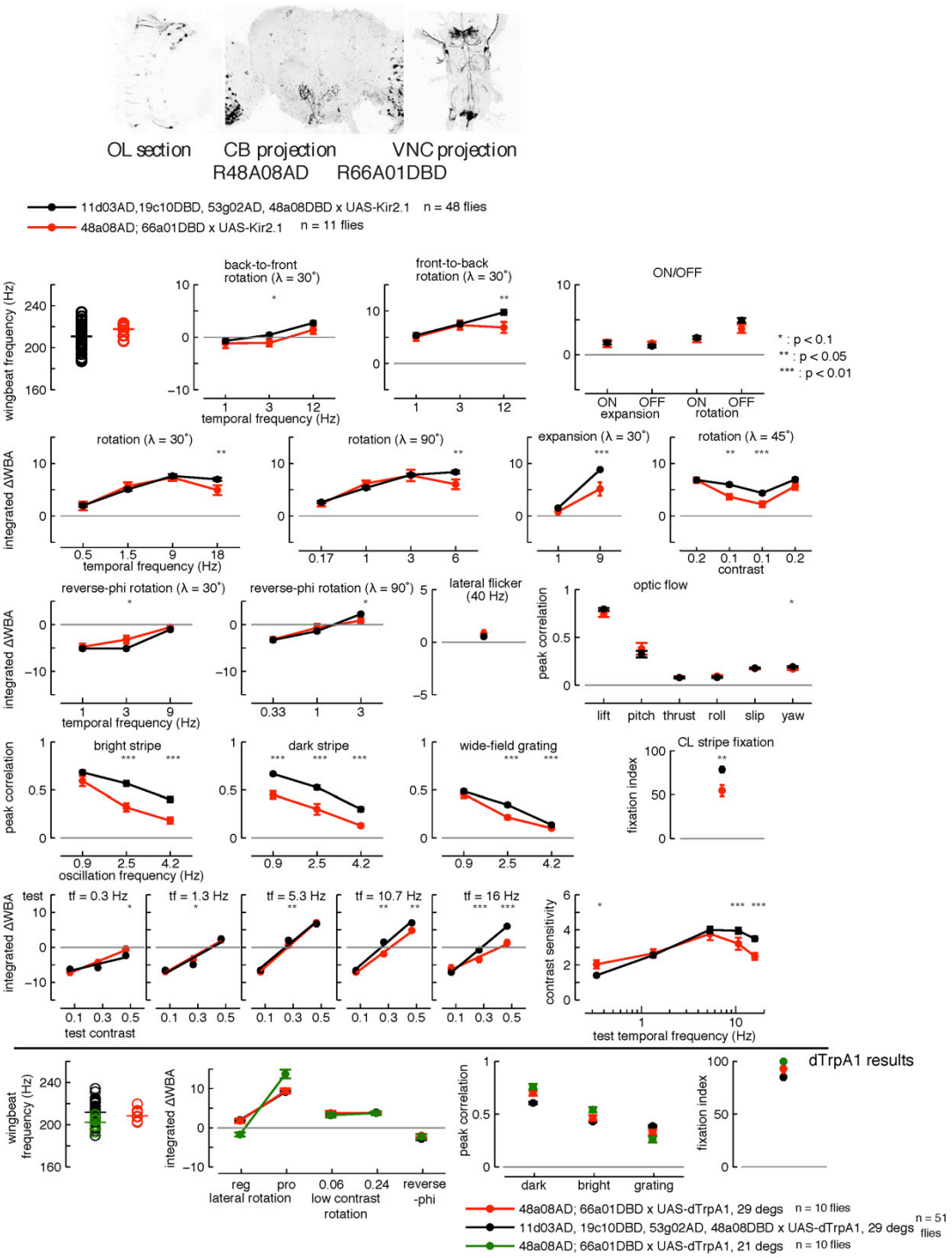

Figure S5B: Lamina Monopolar Cell 2 (L2)

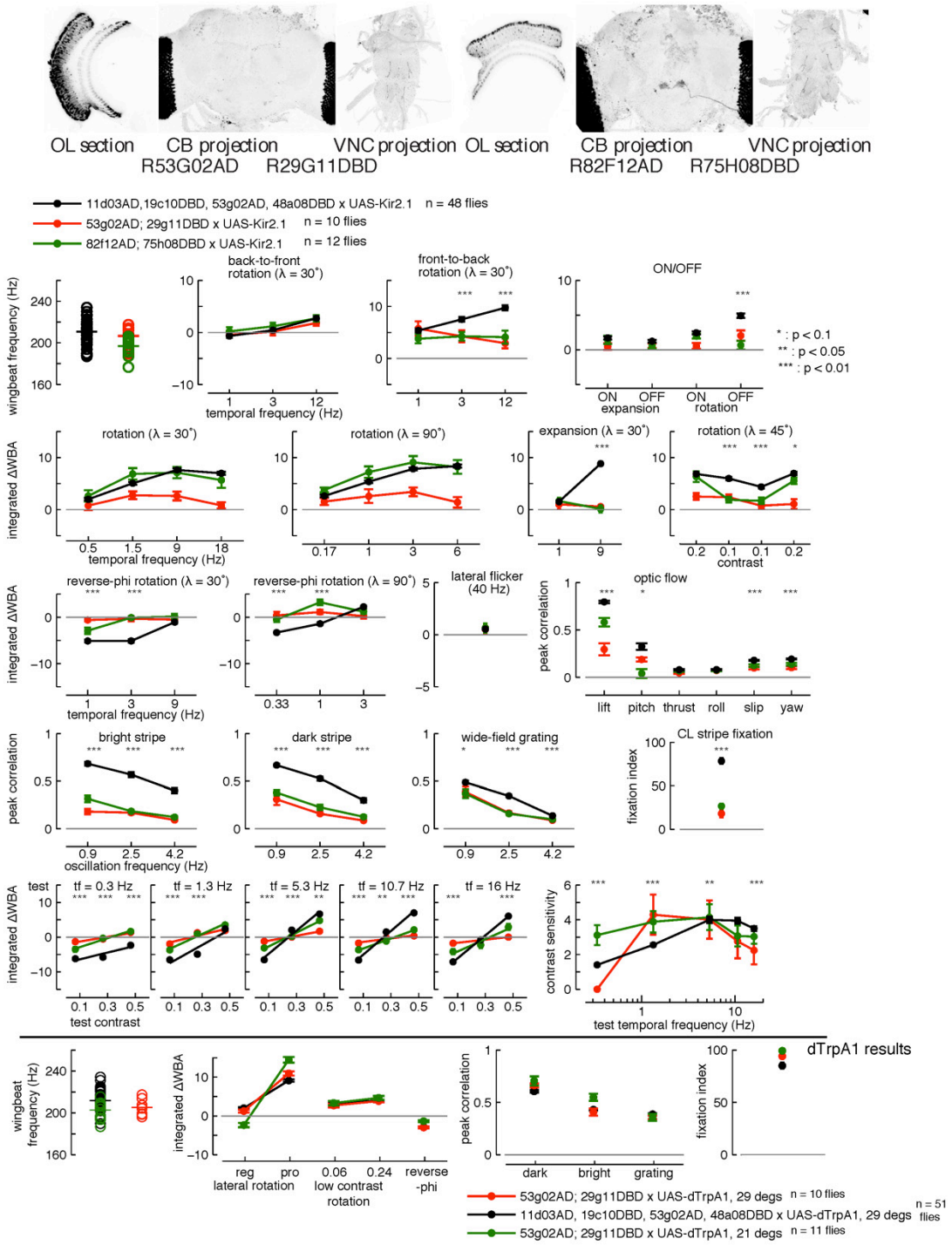

Figure S5, related to Figure 4. Summary behavioral results and Split-GAL4 line expression for L1 (A) and L2 (B). The top row of each section shows single optic lobe (OL) sections, and central brain (CB) and ventral nerve cord (VNC) projections from confocal images of each Split-GAL4 line. The middle section shows flight steering responses of flies following neuronal hyperpolarization with Kir2.1 (mean ± s.e.m., n > 10 flies for each genotype, exact number given on each figure), and the bottom section shows flight steering responses following depolarization using dTrpA1. The visual stimulus conditions for each behavior are depicted in Figure S2. The asterisks above each condition correspond to the final results of our statistical treatment, after combining p-values for cases of two driver lines used, and then applying the false discovery rate (FDR) controlling procedure (* $p < 0.1$, ** $p < 0.05$, and *** $p < 0.01$). See Supplemental Experimental Procedures for details of data treatment and statistical analysis.

Figure S6: L1 inactivation and ON stimuli

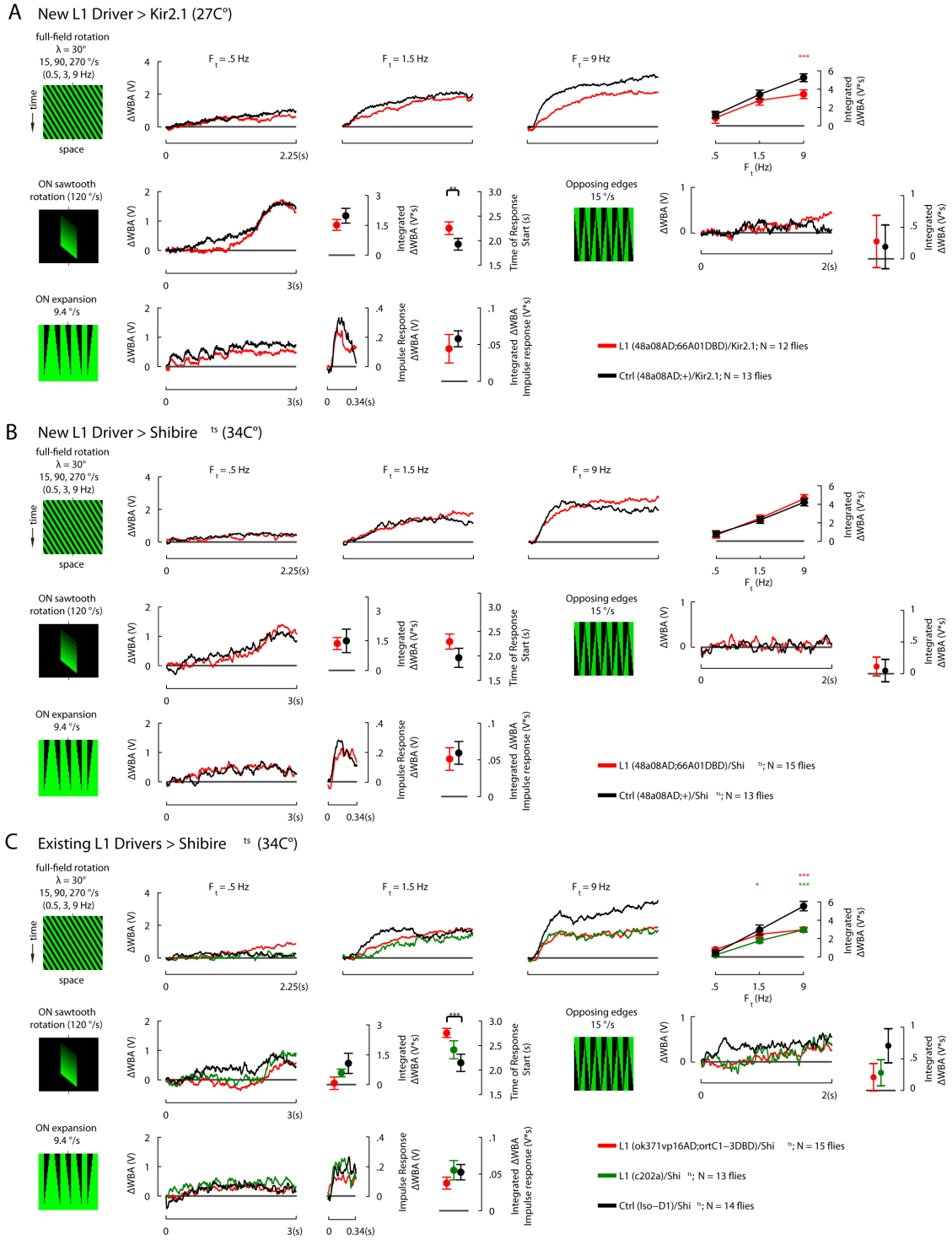

Figure S6, related to Figure 4. Summary behavioral results of new Split-GAL4 and existing drivers for L1. (A-C) Each panel shows a group of L1 drivers with either Kir2.1 or Shibire^{ts} and appropriate controls. (A) The R48A08AD;R66A01DBD driver for L1 expressing Kir2.1. In this separate set of experiments than the one summarized in Figure S5A, we find a significant reduction in the turning response to the 9Hz optomotor stimulus. The amplitude of the turning responses to ON rotation and expansion are not significantly different from control, however, the response to ON-Rotation is delayed, perhaps reflecting a reduction in contrast sensitivity. Both control and Kir2.1 expressing flies show small responses (that are not significantly different from each other) to the 'Opposing edges' stimulus, with a weak preference for the OFF (Dark) edges. (B) Same driver as in (A) expressing Shibire^{ts} at elevated temperature. The small effects to ON responses seen in (A) are diminished and not statistically significant. Both flies produce almost no measurable response to the Opposing edges stimulus. (C) Results of behavioral experiments with GAL4 drivers (expressing Shibire^{ts}) used in previous studies to investigate L1 function. The L1-inactivation deficits are similar in effect and magnitude to the results from the R48A08AD; R66A01DBD driver expressing Kir2.1 (in A). Both lines show a significant reduction in the optomotor response at the highest tested speed, a delayed response (relative to control) to the ON sawtooth rotation stimulus (but only one is significant), and a slightly reduced response to the Opposing edges stimulus (although neither is significant). Error bars show the mean ± s.e.m. for each genotype. The asterisks above each condition represent the results of un-paired, two-tailed t-tests between each genotype and the relevant control (* $p < 0.1$, ** $p < 0.05$, and *** $p < 0.01$). Asterisks for the optomotor responses are shown with each genotype's color code above the tuning curve on the right.

Figure S7A: Lamina Monopolar Cell 4 (L4)

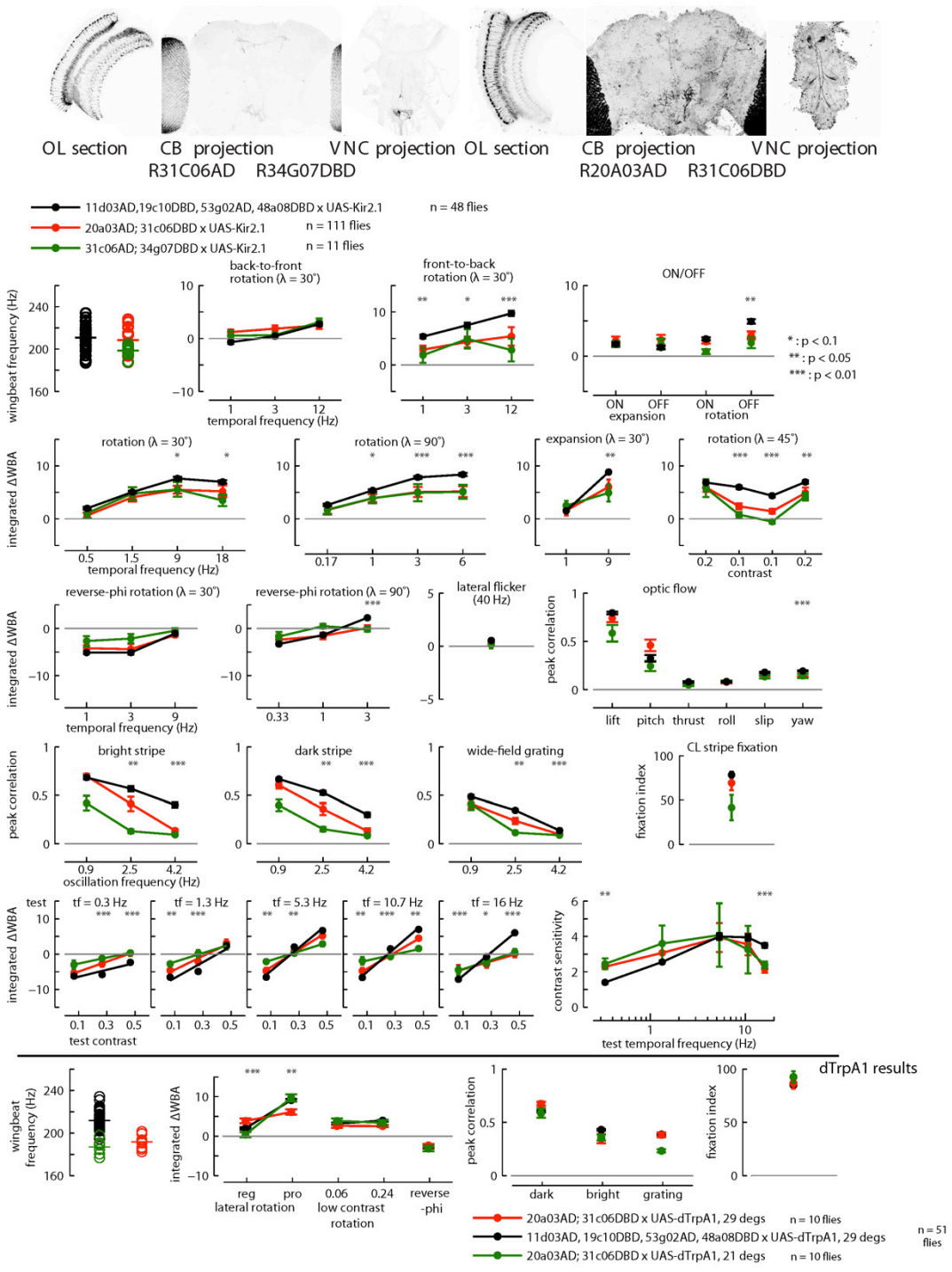

Figure S7B: Centrifugal Cell 2 (C2)

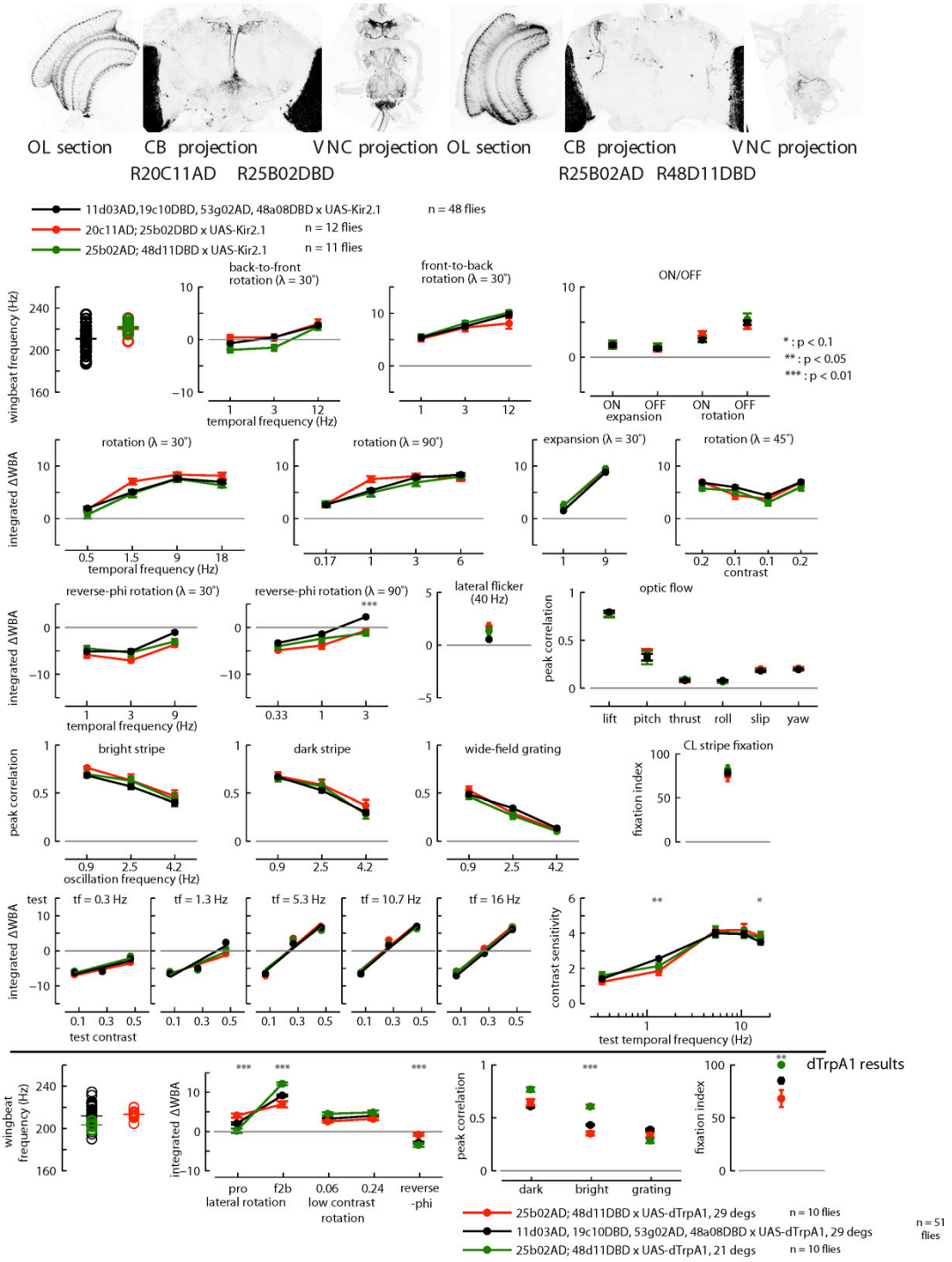

Figure S7C: Centrifugal Cell 3 (C3)

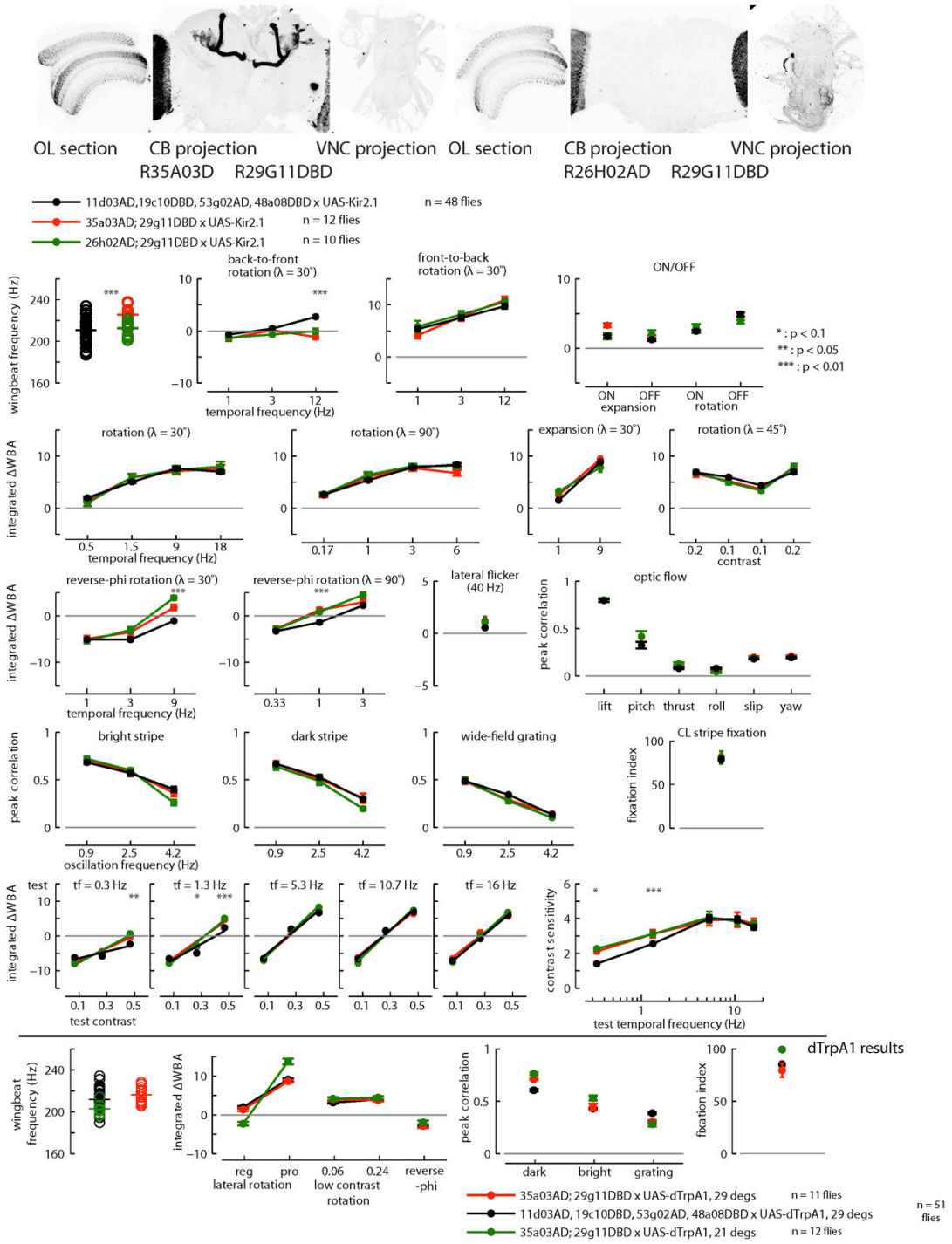

Figure S7, related to Figure 5. Summary behavioral results and Split-GAL4 line expression for L4 (A), C2 (B), and C3 (C). Data are presented identically to Figure S5.

Table S1, related to Figure 2. Summary of all Split-GAL4 lines used throughout this paper.

Cell Type	Lines	Figures with line images	Other optic lobe expression	Completeness of labeling
L1+L2	R75H09AD attP40; R29G11DBD attP2	OS**	none	gaps in both L1 and L2 patterns; kirGFP > 95%
	R48A08AD attP40; R29G11DBD attP2	S3A; OS	none	gaps in both L1 and L2 patterns; kirGFP ND
L1	R48A08AD attP40; R66A01DBD attP2	2A,A',A" ; S3A; S5A, OS	none	~ 60% ; kirGFP > 90%
L2	R53G02AD attP40; R29G11DBD attP2	2B,B',B" ; S3A; S5B, OS	none	>95%
	R82F12AD attP40; R75H08DBD attP2	S3A; S5B, OS	none	>95%
L3	R59A05AD attP40; R75H07DBD attP2	2C; S3A; OS	Lawf2 (~ 20%)	>95%
	R64B03AD attP40; R14B07DBD attP2	2C',C''; S3A; OS	T1(< 5%), Tm (< 20 cells)	>95%
L4	R20A03AD attP40; R31C06DBD su(Hw)attP2	S3A; S7A	none	>95%
	R31C06AD su(Hw)attP2; R34G07DBD attP2	2D,D',D''; 5B; S7A; OS	none	>95%
L5	R21A05AD attP40; R31H09DBD attP2	2E,E',E''; OS	accessory medulla (1 cell); L1 (~1%)	>95%
	R64B07AD attP40; R37E10DBD attP2	S3A; OS	none	>95%
C2	R20C11AD attP40; R25B02DBD attP2	2G; 5F,G,H; S3A; S7B	none	>95%
	R25B02AD attP40; R48D11DBD attP2	2G',G''; S3A,B; S7B	none	>95%
C3	R35A03AD attP40; R29G11DBD attP2	S3A; S7C	lobula plate intrinsic neurons (< 20 cells)	>95%
	R26H02AD attP40; R29G11DBD attP2	2H,H',H''; 5C,D,E; S3A,B; S7C	none	>95%
C2+C3	R20C11AD attP40; R48D11DBD attP2	S3A,B; OS	T1 (< 10%)	>95%
T1	R31F10AD attP40; R30F10DBD attP2	2F',F''; S3A; OS	none	>95%
	R31F10AD attP40; R65D07DBD attP2	2F; S3A; OS	none	>95%
Lawf1	R11G01AD attP40; R17C11DBD attP2	OS	accessory medulla (<10 cells)	>95%
	R52H01AD attP40; R17C11DBD attP2	2I,I',I''; S3A; OS	none	>95%
Lawf2	R11D03AD attP40; R19C10DBD attP2	2J,J',J''; S3A; OS	none	>90%
	R11D03AD attP40; R61H02DBD attP2	S3A; OS	none	>95%
Lai	R92A10AD attP40; R17D06DBD attP2	2K; S3A; OS	Tm with projections into central brain (< 20 cells)	>95%
	R92A10AD attP40; R66A02DBD attP2	2K',K''; S3A; OS	none	>80%
Lat	R16G04AD attP40; R55B04DBD attP2	2L,L',L''; OS	none	3-5 cells per optic lobe (same in several GAL4 lines)
controls	R11D03AD attP40			
	R53G02AD attP40			
	R48A08DBD attP2			
	R19C10DBD attP2			

**OS refers to an online supplement available at www.janelia.org/lab/reiser-lab

The table lists the cell type targeted by each combination, as well as the figure numbers (primary and supplemental) where images for the corresponding lines are displayed. The grey boxes identify the genotypes that were used in the dTrpA1 experiments. A few lines had detectable optic lobe expression in other cell types. With the exception of R11G01AD; R17C11DBD this additional labeling appeared to be incomplete and faint. Completeness of

expression in the cells of interest was estimated by examining the number of lamina cartridges without labeling (columnar cell types) or the presence or absence of areas with reduced labeling (multicolumnar cell types). Details on labeled cell types and completeness of expression are based on myrGFP labeling unless indicated otherwise. Without examining very large numbers of specimens, it is not practical to distinguish consistently 100% complete expression from nearly complete expression, and so we list all approximately complete lines as >95% complete.

Supplemental Experimental Procedures

Molecular biology and fly genetics

Flies were reared on standard cornmeal/molasses food. GAL4 drivers with apparent expression in lamina-associated neurons were identified by screening a database of GAL4-line expression patterns (Jenett et al., 2012), constructed as described (Pfeiffer et al., 2008). Further histological characterization of a subset of lines was performed by confocal imaging of overall expression patterns or single cells, as described below. Split-GAL4 transgenes corresponding to the GAL4 drivers selected from this screen were constructed using the vectors and methods described in Pfeiffer et al (2010). All activation domain (AD) constructs were p65-based (Pfeiffer et al., 2010). Transgenes were integrated into the fly genome using phiC31-integrase (injections carried out by GSI, Inc). Most AD transgenes were inserted in attP40 (chromosome 2L) and DBD constructs in attP2 (3L). For the two L4 intersections, insertions in su(Hw)attP2 (3R) were used for one Split-GAL4 half since these produced more complete L4 expression than the same AD or DBD constructs inserted in attP40 or attP2, respectively. All AD and DBD combinations were assembled in a w^{1118} background. All Split-GAL4 stocks used are summarized in Table S1. For behavior experiments, Split-GAL4 lines were crossed to effectors backcrossed into Dickinson Lab (DL) or Canton-S (CS) wild-type backgrounds, namely w+; tubP-GAL80ts; UAS-EGFP-Kir2.1(Baines et al., 2001; Ofstad et al., 2011) or w+;CS;UAS-dTrpA1(Hamada et al., 2008). tubP-GAL80ts does not suppress expression of Split-GAL4 drivers with the p65 activation domain. Individual AD and DBD transgenes, which do not drive UAS-dependent expression were used as controls for behavior experiments. Overall expression patterns were assessed using pJFRC12-10XUAS-IVS-myr::GFP/TM3 in su(Hw)attP1 (Pfeiffer et al., 2010) and w+; tubP-GAL80ts;UAS-EGFP-Kir2.1 (Baines et al., 2001; Ofstad et al., 2011) as reporters.

Histology

For characterization of Split-GAL4 line expression patterns, approximately 5-10 day old female flies raised at 25°C were dissected in S2 cell culture medium, fixed with 1% formaldehyde in PBS overnight, washed several times with PBT (PBS + 0.5% TX-100), blocked for 1 hr with PBT-NGS (PBT with 5% normal goat serum) and incubated with rabbit anti-GFP (Invitrogen, A11122, 1:1000 dilution) and Nc82 (DSHB, 1:50) overnight at 4°C. Secondary antibodies, also diluted in PBT-NGS and applied overnight at 4°C, were Alexa488 goat-anti-rabbit (Invitrogen, A11008, 1:500) and Alexa568 anti-mouse (Invitrogen, A11004, 1:300). After further washes with PBT and PBS specimens were mounted in Slow Fade Gold (Invitrogen, S36937). Samples were imaged on a Zeiss LSM710 confocal microscope with 20x 0.8 NA (for central brain and VNC patterns) or 40x 1.3 NA (for optic lobe patterns) objectives. A "flip-out"-based approach (Struhl and Basler, 1993) was used for stochastic single cell labeling with one or more colors. The detailed methodology will be described elsewhere (Nern et al, in preparation). Briefly, heat-shock induced expression of FLP recombinase was used to excise FRT-flanked interruption cassettes from UAS reporter constructs carrying HA, V5 and FLAG epitope tags, respectively. Flies were processed as above but fixed in 2% formaldehyde in PBS for 1 hr at room temperature and stained with epitope-tag specific antibodies plus Nc82. Mounting and imaging was as above with 40x 1.3 NA or 63x 1.4NA objectives. Additional C2 flip-out images used for quantification of C2 asymmetry (Figure S3D) were obtained by screening the optic lobe dataset of the Janelia Fly Light Single Neuron Project. Individual C2 neurons from the FlyLight images were segmented using NeuronSeparator (Myers et al, unpublished) and rotated views of M10 layer arbors generated using NeuronAnnotator (Janelia Fly Light Scientific Computing Team, unpublished), a modified version of V3aaD (http://www.vaa3d.org/). Images were processed using Fiji (http://fiji.sc/) and Figures assembled in Adobe InDesign and Adobe Illustrator.

Behavioral methods and fly preparation

For behavioral experiments, all flies were reared on standard cornmeal/molasses medium on a 16 h:8 h light:dark cycle. Flies expressing Kir2.1 were reared at 25° C, while dTrpA1-expressing flies were reared at 18°C. All flies were tested 0-4 hours before the onset of

their subjective night. For all experiments using Kir2.1, experimental and control flies were both tested at 21° C. For dTrpA1 experiments, each fly was first tested at 21° C, followed by a second test at 28° C. The temperature within the arena was monitored continuously using an analog temperature sensor (LM35DT, National Semiconductor).

Gravid females, 3-5 days old, were cold-anesthetized and tethered to a 0.1 mm tungsten wire with UV-activated glue. After at least 15 minutes of recovery, flies were placed within a cylindrical electronic flight simulator. Within the arena, the position of the wings was monitored using an optical wingbeat analyzer (JFI Electronics Laboratory, University of Chicago, Chicago, IL, USA), described previously (Gotz, 1987) . The wingbeat amplitudes, frequency, and signals encoding the positions of the display stimuli were sampled at 1 kHz by a DigiData 1440A (Axon Instruments). The experimental data were stored in a custom MySQL database. All data analysis was performed offline in MATLAB (Mathworks, Natick, MA). In all figures showing flight behavior, we follow a convention of plotting the turning response of flies as the left minus right wing beat amplitude (ΔWBA), a measure which is directly proportional to yaw torque (Tammero et al., 2004).

The visual arena consisted of a 32x88 array of green LEDs covering 330° in azimuth and 120° in elevation (Reiser and Dickinson, 2008). The maximum pixel size of each LED is below the inter-ommatidial distance of *Drosophila* (Heisenberg and Wolf, 1984), so single pixel jumps between consecutive frames simulate continuous motion to the fly. The arena has an intensity scale from 0 to 72 cdm^{-2}. Relative luminance values reported below are distributed linearly within this range. We made use of an updated version of the display controller (manufactured by IO Rodeo, Inc., http://www.iorodeo.com/; further details at http://flypanels.org/panels).

Flight behavior experiments used a protocol in which 3 second open-loop trials were interleaved with 3.5 seconds of closed-loop “stripe fixation”, during which the fly actively controlled the position of a 30° dark stripe against a bright background. The stripe fixation epochs ensured that the flies were actively steering at the onset of each open-loop condition. To quantify the stability of closed-loop behavior, each fly was also tested with several 10 s trials of closed-loop stripe fixation. If the fly stopped flying during any trial, a small fan automatically delivered a brief wind stimulus to encourage her to resume flight.

Trials in which the flight stopped were excluded from subsequent analysis. Within an experiment, each set of conditions was presented as random blocks repeated three times. Trials in which the fly stopped flying were repeated at the end of each block. Therefore, each fly completed each condition at least twice, and typically three times.

Visual stimuli

The standardized behavioral protocol used for the Kir2.1 (inactivation) experiments, generates 63 metrics that we subsequently test for a significant difference from the control lines. We tested twice as many conditions as appear in the summary tables (Figure 4 and Figure S4), since we averaged (with sign-conserving inversion) the results from the two directionally symmetric versions of each condition. The visual stimuli are schematized in Figure S2 with space-time diagrams and described below:

- Full-field rotation (8 conditions): Tethered flying flies readily steer in the direction of a rotating striped grating, the so-called optomotor response (Gotz, 1964). We tested 16 total conditions of rotating wide-field square wave gratings: 2 spatial wavelengths (λ = 30°, 90°), 4 angular velocities (15, 90, 270, 540 °/s), and two directions (clockwise and counter-clockwise). The relative luminance values of dark and bright bars were 0 and 1. The temporal frequency of these stimuli is defined as the ratio of the angular velocity and the spatial wavelength.
- Full-field expansion avoidance (2 conditions): Flies turn in the direction opposite a laterally-oriented focus of expansion (Tammero et al., 2004). We tested 4 total expansion conditions, constructed of square-wave gratings (λ = 30°), with the focus of expansion and focus of contraction situated on opposite sides of the arena (+/- 90°). We tested expansion at two angular velocities (15, 270 °/s), and two directions, with the focus of expansion on the right or left side of the arena. The relative luminance values of dark and bright bars were 0 and 1.
- Lateral flicker (1 condition): Flies weakly orient toward a flickering square wave grating (Duistermars et al., 2012). We tested fly steering toward a square wave grating (λ = 30°) that flickered at 40 Hz. The grating occupied either the right or left side of the arena, and half of the grating bars flickered between relative luminance

values of 0 and 6/7. The other bars and the opposite side of the arena remained at a constant luminance (3/7).

- Low contrast rotation (4 conditions): Flies respond more weakly to low contrast optomotor stimuli (Duistermars et al., 2007a). In order to test for detection of optomotor stimuli at different contrasts and luminance levels, we measured fly responses to rotating gratings (180 °/s, λ = 45°) at 4 independent luminance/contrast combinations, in two directions. In all four stimuli, the intensity of one half the bars was held constant at a luminance value of 8/15, while the luminance of the other bars varied across the four stimuli (5/15, 7/15, 9/15, 11/15). Michelson contrast was calculated as $\frac{I_{max}-I_{min}}{I_{max}+I_{min}}$, where I_{max} and I_{min} are the highest and lowest luminance intensities in the stimulus.
- Reverse-phi rotation (6 conditions): Flies turn in the direction opposite a motion stimulus that flickers as it moves, perceiving so-called reverse-phi motion (Tuthill et al., 2011). We examined flight behavior in response to rotation of reverse-phi stimuli at two spatial wavelengths (λ = 30°, 90°) and three angular velocities (30, 90, 270 °/s), in both directions. The reverse-phi stimulus was similar to a standard full-field rotation stimulus except that within each motion step alternating stripes switched between bright (6/7) and dark (1/7) intensity levels, selected to be symmetric with respect to the intensity of the intermediate intensity bars (3/7).
- Stripe oscillation (9 conditions): Flies readily track the position of oscillating stripes (Duistermars et al., 2007b). We measured the flight responses of flies to two oscillating stripes: a dark stripe (intensity 0) on a bright background (3/7), and a bright stripe (3/7) on a dark background (0). Each stripe was 15° wide. For comparison, we measured fly responses to oscillation of a full-field square-wave grating (λ = 30°, alternating bars of intensity 3/7 and 0). These three patterns started at the center of the arena and oscillated sinusoidally +/- 37.5°, at 0.9, 2.5, and 4.2 Hz. Symmetric conditions oscillated 180° out of phase.
- Regressive and progressive rotation (6 conditions): Flies respond differently to monocular optomotor stimuli moving progressively or regressively across the eye (Duistermars et al., 2012; Tammero et al., 2004). We tested flies with regressive and

progressive rotational motion stimuli (alternating bars with luminance 0 and 3/7) rotating at three angular velocities (30, 90, 270 °/s), and in two directions (clockwise and counter-clockwise). Each motion stimulus occupied one side of the arena, while the other side was held at a constant intensity (3/7).

- ON and OFF motion (4 conditions): Two studies have found that silencing L1 and L2 neurons have different effects on behavioral or physiological responses to luminance increases vs. decreases (Clark et al., 2011; Joesch et al., 2010). Because flying control flies did not respond significantly to the stimuli used in these studies, we developed two novel stimuli that contained sequential luminance increases/decreases, and elicited strong flight steering responses. The first stimulus, which we call ON/OFF expansion, started as a standard striped grating $\lambda = 30°$, followed by expansion (9.4 °/s) of either the dark (0) or bright (1) bars until the arena was uniformly illuminated. The second stimulus, called ON/OFF rotation, was a sawtooth–shaped luminance gradient (from 0→1 or 1→0) that swept across the frontal visual field of the fly at 120°/s.
- Optic flow oscillation (6 conditions): Flies exhibit robust optomotor responses to optic flow patterns about three cardinal axes (Theobald et al., 2010). We tested measured fly responses to oscillating random-dot optic flow fields. Random dot patterns appeared as a cloud of dark (0) dots on a bright (1) background, and had a uniform random distribution. Dot motion simulated translation (lift, thrust, and sideslip) and rotation stimuli (yaw, roll, and pitch). Each stimulus oscillated sinusoidally at 0.9 Hz, with a period of 45°.
- Contrast nulling (15 conditions): To study contrast sensitivity as a function of speed, we applied a psychophysical technique known as contrast or motion nulling (Cavanagh and Anstis, 1991; Smear et al., 2007), in which two optomotor stimuli (striped gratings) are superimposed— a reference grating moving in one direction, and a test grating moving in the opposite direction. Both gratings had a spatial wavelength of $\lambda = 45°$. The angular velocity of the reference grating was constant (180°/s, for a temporal frequency of 4 Hz), as was its contrast (grating intensity values of 7/15 and 4/15, for a relative contrast of 0.27). The contrast of the test

stimulus was varied between trials (0.09, 0.27, 0.45), while the mean luminance was constant (0.41). The angular velocity was also varied between trials (15, 60, 240, 480, 720 °/s).

- Stripe fixation (1 condition): When given closed-loop control of a small-field object, flies will actively fixate the object within their frontal visual field (Reichardt and Wenking, 1969). We tested for closed-loop stripe fixation by using the fly's ΔWBA to control the position of a dark stripe (intensity 0, 30° wide) on a bright background (intensity 1). Each trial lasted for 10 s. The closed-loop gain was fixed at a value previously found to maximize stripe fixation behavior.
- Wing beat frequency (1 condition): The wing-beat frequency was averaged over all the trials described above, as a metric for flight vigor.

Since flies will not fly for nearly as long at elevated temperatures, our dTrpA1 (activation) experiments employed a reduced behavioral protocol that consisted of 10 of the conditions described above:

- Regressive and progressive motion at one angular frequency (360 °/s).
- Wide-field rotation at two contrast/luminance values (grating contrast 0.23 and 0.06) and one speed (180 °/s).
- Reverse-phi rotation at 180 °/s, $\lambda = 30°$.
- Dark stripe, bright stripe, and wide-field grating oscillating at 2.5 Hz.
- Closed-loop stripe fixation for 10 s.
- Wing-beat frequency.

Data treatment

For each open-loop trial, the mean response during the 50 ms previous to stimulus onset was subtracted from the subsequent turning response. To correct for errors in fly alignment, the ΔWBA signals were normalized to the mean cumulative steering behavior of each fly. In other words, the ΔWBA of each trial was divided by: (the mean absolute value of each fly's ΔWBA across all trials) / (the grand mean of the absolute value of the ΔWBA of all flies). These normalization values were normally distributed ($\mu = 1.0$, $\sigma = 0.3$), and the mean normalization value of each genotype fell within 1 s.d. of the mean. Half of the

conditions (e.g., CCW rotation) were inverted and averaged with the corresponding symmetric conditions (e.g., CW rotation). These data were then averaged on a per-fly basis to produce a mean turning response for each pair of symmetric conditions. Time series data are plotted throughout the paper as the mean ± s.e.m. across flies. The convention in all behavior figures is that rotation is CW.

Mean response amplitudes were calculated by integrating the area under the ΔWBA time-series for each trial, and averaging these values on a per-fly basis. For small-field and optic flow stimuli, in which the fly tracked an oscillating pattern, the maximum correlation coefficient was calculated for each trial from the cross-correlation of the visual stimulus position and the wingbeat modulations of the fly, either ΔWBA or ΣWBA (for optic flow lift, pitch, and thrust). These maximum correlation coefficient values were then averaged on a per-fly basis.

We quantified the quality of closed-loop stripe fixation by computing the percentage of time that each fly maintained the 30° dark stripe within a 90° window directly in front of the fly, a quantity defined as the "fixation index" (Reiser and Dickinson, 2010).

For motion nulling conditions, we quantified contrast sensitivity as a function of stimulus temporal frequency by computing the "null contrast" at each test speed (Cavanagh and Anstis, 1991; Chichilnisky et al., 1993; Smear et al., 2007). The null contrast is the contrast of the test stimulus needed to perceptually cancel, or null, the constant reference stimulus. The null contrast was determined by fitting a line through the mean response to three test contrasts at each test velocity (Figure 7A). The zero-crossing of this line corresponds to the point at which the test and reference stimuli are perceptually equivalent. An important advantage of using this null contrast metric is that it does not depend on absolute turning amplitudes. In other words, the nulling technique distinguishes between flies with general motor deficits vs. flies with altered visual sensitivity, and enables an analysis of the contrast sensitivity of animals whose motion vision is significantly compromised (e.g. L2-inactivated).

The contrast sensitivity (1/null contrast) was measured from the mean integrated turning response across all flies of each genotype. Because this fitting procedure does not provide

an appropriate measure of variance, we estimated the null contrast error by determining the zero crossing of lines fit through mean steering responses ± 1 s.e.m. This error estimation procedure was used to generate error bars for Figure 7, and the null contrast tuning curves in Figures S5 and S7. However, statistical tests were performed directly on each of the 15 motion nulling conditions, and separately on the mean contrast sensitivity of each individual fly (see below). The complete dataset for all lamina cell types is available at the authors' website (http://www.janelia.org/lab/reiser-lab)

Statistical Analysis

To determine statistical significance, un-paired, two-tailed t-tests were performed on the mean turning amplitudes, mean correlation values, or mean fixation indices for each genotype. For the 11 (out of 14) cases where we generated two independent driver lines expressing in a cell type (or combination), we employed a stringent method for combining p values—that is for each experimental condition we take the maximum of the two p values (Lazar et al., 2002; Loughin, 2004). The quantity resulting from this conjunction method is a valid p value, for which we then perform multiple comparisons correction (against all 63 p values for each cell type) by using the false discovery rate (FDR) controlling procedure of Benjamini and Hochberg (1995). For the 3 cases where we only have a single driver line, we directly employ the FDR procedure on the 63 p-values. The complete map of p-values, before the FDR controlling procedure is provided in Figure S4, and gives an indication of the phenotypes which were present within a single line, but did not find support in both lines, or were rejected during multiple comparisons correction. This conservative procedure allowed us to focus on the most robust behavioral phenotypes, but likely underestimated the phenotypic effects of our manipulations. For example, there were several instances in which two lines of a given cell type were both individually different from controls (e.g., Lai; Figure S4), but together they did not satisfy our statistical criterion.

In the summarized data we report, we control for the FDR with 3 levels, q=0.1, 0.05, and 0.01, and report the significant results at each level with a color map, where red (and blue) indicates a numerical decrease (increase) in the test metric as determined by the signed difference between the mean of the test metric for each line\cell type and the mean of the control set. In the behavioral data of Figures 3-7 we present the mean turning response and

correlation value of the two genotypes expressing in each individual cell-type (or just the mean of the single genotype for the 3 cell-types that are only targeted by one driver line). The mean values for each condition and each genotype are available for L1, L2, L4, C2, and C3 in Figures S5 and S7, and equivalent data for all cell types is available on the authors' website (http://www.janelia.org/lab/reiser-lab). In these figures, the significance level indicated by the asterisks corresponds to the final determination after the conjunction and FDR controlling-procedures. For the contrast nulling results (Figure 7), we computed the statistical significance of the contrast sensitivity at each temporal frequency using un-paired, two-tailed t-tests of the mean sensitivity (1/null contrast) for each genotype. This resulted in 5 p-values per line. For cell types where 2 different driver lines were used we then used the maximum p-value of both lines, at each temporal frequency to assign the final significance score. For Figure 7, we list all individual cell types (excluding the combinations of L1+L2 and C2+C3) for which the null contrast for at least 2 temporal frequencies is significant at the $p < 0.1$ level or lower. For experiments in which we activated neurons using UAS-dTrpA1, one driver line was tested for each genotype at both the permissive (21 C°) and restrictive (28 C°) temperatures. Behavioral responses under restrictive conditions were compared to fly behavior at the permissive temperature and control lines at the restrictive temperature using the same statistical procedure described above (FDR correction).

Model and Simulation

We modeled a single HR-EMD with elaborated lamina preprocessing as a series of linear filters beneath simple compound eye optics. For the point-spread function of an ommatidial lens we used Gaussian sampling:

$$L(\theta) = k\ exp\left[\frac{4 \ln 2}{\Delta p^2}\theta^2\right]$$

where k is a standardization constant, Δp is the acceptance angle of the photoreceptor (5°; Heisenberg and Wolf, 1984) and θ is the vector of discrete positions through a pair of ommatidia with increments of 0.375° used an interommatidial angle ($\Delta\varphi$) of 4.5° (Snyder, 1979). The image was formed by the convolution of an intensity signal, $I(\theta,n)$, a function of angular position (θ) and the discrete sample time (n), with the acceptance angle of the

ommatidia. We then used ray tracing to simulate the view of two neighboring ommatidia in front of our standard cylindrical LED display. This resulting retinal image was the input to the model.

For simplicity, the temporal properties of the photoreceptors, LMCs, and perhaps subsequent processing stages were modeled as single first-order low-pass filters with time constant of $\tau = 4$ ms for L1 and L2/L4 pathways, and $\tau = 80$ ms for the L3 pathway. We found good agreement between the temporal tuning from this simulation and previously measured 'optomotor response' tuning curves, by using an HR-EMD time constant of 18 ms (in a previous study we used $\tau = 20$ ms (Tuthill et al., 2011)). The simulation was implemented in Simulink (Mathworks, Natick, MA). The simulation is completely deterministic, and so single presentations of each stimulus condition were run. Each simulated trial consists of a 0.2 second epoch where the visual system is presented with an intermediate gray level, and then is followed by 2 seconds of the presented motion stimulus. Time was discretized at 1 kHz. The stimuli we used were the identical 15 conditions of the composite stimulus (combined reference and test pattern) that were used in the motion nulling behavioral experiments. The result of each simulation is taken as the mean response during the 2 seconds of pattern motion. The contrast sensitivity was determined as it was for the behavioral results (by fitting a line through the mean response to three test contrasts at each test frequency to find the zero-crossing; the inverse of this point is the contrast sensitivity). For the intact visual system condition (black line in Figure 7G) the 3 input pathways were summed and then fed into the HR-EMD. For the silencing simulations the corresponding filter's output (either L1 or L2/L4, for the orange trace, or L3 for the purple trace of Figure 7G) was set to zero, while the other 2 pathways were added and supplied to the HR-EMD. The essential feature of the model that produces the results of Figure 7G is that the L1 and L2/L4 pathways are tuned differently than the L3 pathway. Indeed, the behavioral results are well accounted for by making L1 and L2 identical and significantly faster than the L3 pathway. We note that this simulation result was robust to many variants of the models, and could also be implemented with a set of parallel high-pass filters at the front-end, so long as the L3 pathway was configured to be much slower than the L1 and L2 pathways. By 'slower' we mean that the L3 pathway is

expected to be insensitive to the faster speeds that the L1 and L2/L4 pathways pass along to the HR-EMD.

Evaluation of L1 function (reported in Figure S6)

We performed an additional set of behavioral experiments to address the discrepancy between our results (no specific effect for L1 inactivation to "ON" edges) and those previously reported for L1 inactivation (Clark et al., 2011; Joesch et al., 2010). There are 4 potential sources for the difference between our experimental results and these previous studies: 1) visual stimuli used, 2) GAL4 driver lines, 3) different effectors (we used Kir2.1, whereas the two previous studies used Shibire^{ts}) and 4) potential differences between visual reactions in flight, in walking, or in the non-behavioral state. We systematically explored the first 3 potential contributions by testing our L1 GAL4 line, as well as the previously used GAL4 lines, through a range of ON-type and OFF-type edge stimuli. In addition, we tested these flies with both Kir2.1 and Shibire^{ts}. We note that adapting our flight experiment to Shibire^{ts} conditions was very challenging, since flies will not fly for very long at the required elevated temperatures. We were not able to test the two previously used L1 lines with Kir2.1 since in these flies were not viable (even with GAL80ts for temporal control).

<u>Drivers / Control lines used:</u>

+;ok371VP16AD; ortC1−3DBD (backcrossed into ISO-D1 background)

+;P{GAL4}c202a;+ (backcrossed into the ISO-D1 background)

+;R48A08AD; R66A01DBD

ISO-D1 (isogenized background)

+;R48A08AD ;+

<u>Effector Lines:</u>

+;tubP-gal80ts;P{UAS-EGFP-Kir2.1} (backcrossed into DL background)

+;;UAS-Shibire^{ts1}

For all Kir2.1 experiments, the flies were crossed and raised as described above. For all Shibire^{ts} experiments, Shibire^{ts} virgin females were crossed to male GAL4 driver or control lines. These flies were raised at 21.5°C. For Shibire^{ts} experiments, we used flies that were between 5 and 8 days old.

For all experiments in Figure S6, we placed a flight arena within a temperature and humidity controlled incubator (PH09, Darwin Chambers, St. Louis, MO). Flies were tethered under cold anesthesia and allowed to recover for at least 45 minutes. For Shibire^{ts} experiments, flies that showed acceptable wing beat profiles were "pre-incubated" within the incubator housing the flight arena for at least 6 minutes prior to starting experiments (incubator set for 32°C and 60% RH, levels measured at the location of the fly within the flight arena were ~34°C and 60% RH; in this same incubator all flies expressing Shibire^{ts} pan-neuronally would paralyze within at most 4 minutes). All of the experiments were conducted during the last 4 hours of the flies' subjective day (as determined by the light cycle of their rearing incubator). Since flies are reluctant to fly at 34°, we used a shortened protocol with only two repetitions of each stimulus, as opposed to the rest of the experiments in this paper, which used 3 repetitions. For the Kir2.1 experiments, we used the arena with the incubator turned off and the door open, so that the conditions were identical to those for the flies in the remainder of the paper (temperature near the fly was ~27°C).

Visual Stimuli

We tested the identical ON rotation and ON expansion stimuli that were used in the main experiments of this paper. The first stimulus, ON expansion, started as a standard striped grating $\lambda = 30°$, followed by expansion (9.4°/s) of bright (maximum intensity) bars until the arena was uniformly illuminated. The second stimulus, ON rotation, was a sawtooth–shaped luminance gradient (from 0→1) that swept across the frontal visual field of the fly at 120°/s. In addition to these stimuli, we also included optomotor stimuli and other stimuli designed to elicit specific responses to luminance increments and decrements. One of these other stimuli is the so-called 'opposing edges' condition of Clark et al. (2011), which we've implemented as 15°/s rotation of the bright edges in the e.g. counter-clockwise direction while the dark edges rotate clockwise (as in the space-time diagram on

Figure S6, the mirror-symmetric condition was also included in the protocol). We note that despite repeated efforts (we attempted 6 different protocols), all tested variants of the previously employed stimulus (the 2-bar minimal motion stimuli (Clark et al., 2011; Joesch et al., 2010)) did not yield consistently large turning reaction in tethered flight with wild-type animals, and did not produce any consistent differences upon L1 manipulation, and so are not included in the supplemental figure. In order to shorten this experimental protocol, the trial lengths for each stimulus type were not identical (but were between 2-3 seconds, and are indicated in Figure S6).

Analysis

As with all behavioral responses presented in this study, the turning responses for each stimulus condition are averaged across the repeated trials that include sign-inverted responses to mirror symmetric stimulus presentations. The time series data shown in Figure S6 were smoothed with a second-order Butterworth low-pass filter (cutoff frequency of 35 Hz) before averaging.

To determine the time of response to the ON-rotation stimulus, we quantified the time at which the integrated turning response crosses a threshold. We computed the time (after the first 500 ms of each trial) at which the integrated turning response of each fly reached 1/3 of the average integrated turning response of all flies of that genotype. A small number of flies that did not reach this threshold were counted as having the maximum delay to response of 3s. This provides a reduced metric (for statistical analysis) that agrees well with the averaged turning response across flies.

To determine an 'impulse response' to the ON-expansion stimulus, we averaged (on a per-fly basis) the responses to the first three discrete motion steps after subtracting the response mean of the preceding 20 ms. For statistical analysis, un-paired, two-tailed t-tests were used to compare groups of per-fly average metrics across genotypes. Significance asterisks are used as in other supplemental figures.

Supplemental References

Baines, R.A., Uhler, J.P., Thompson, A., Sweeney, S.T., and Bate, M. (2001). Altered electrical properties in Drosophila neurons developing without synaptic transmission. J Neurosci *21*, 1523-1531.

Benjamini, Y., and Hochberg, Y. (1995). Controlling the False Discovery Rate: A Practical and Powerful Approach to Multiple Testing. J R Stat Soc Ser B-Methodol *57*, 289-300.

Cavanagh, P., and Anstis, S. (1991). The contribution of color to motion in normal and color-deficient observers. Vision Res *31*, 2109-2148.

Chichilnisky, E.J., Heeger, D., and Wandell, B.A. (1993). Functional segregation of color and motion perception examined in motion nulling. Vision Res *33*, 2113-2125.

Clark, D.A., Bursztyn, L., Horowitz, M.A., Schnitzer, M.J., and Clandinin, T.R. (2011). Defining the computational structure of the motion detector in Drosophila. Neuron *70*, 1165-1177.

Duistermars, B.J., Care, R.A., and Frye, M.A. (2012). Binocular interactions underlying the classic optomotor responses of flying flies. Frontiers in behavioral neuroscience *6*, 6.

Duistermars, B.J., Chow, D.M., Condro, M., and Frye, M.A. (2007a). The spatial, temporal and contrast properties of expansion and rotation flight optomotor responses in Drosophila. J Exp Biol *210*, 3218-3227.

Duistermars, B.J., Reiser, M.B., Zhu, Y., and Frye, M.A. (2007b). Dynamic properties of large-field and small-field optomotor flight responses in Drosophila. J Comp Physiol A Neuroethol Sens Neural Behav Physiol *193*, 787-799.

Gotz, K.G. (1964). Optomoter studies of the visual system of several eye mutants of the fruit fly Drosophila. Kybernetik *2*, 77-92.

Gotz, K.G. (1987). Course-Control, Metabolism and Wing Interference During Ultralong Tethered Flight in Drosophila Melanogaster. J Exp Biol *128*, 35-46.

Hamada, F.N., Rosenzweig, M., Kang, K., Pulver, S.R., Ghezzi, A., Jegla, T.J., and Garrity, P.A. (2008). An internal thermal sensor controlling temperature preference in Drosophila. Nature *454*, 217-220.

Heisenberg, M., and Wolf, R. (1984). Vision in Drosophila: Genetics of Microbehavior (Berlin: Springer-Verlag).

Jenett, A., Rubin, G.M., Ngo, T.T., Shepherd, D., Murphy, C., Dionne, H., Pfeiffer, B.D., Cavallaro, A., Hall, D., Jeter, J.*, et al.* (2012). A GAL4-Driver Line Resource for Drosophila Neurobiology. Cell reports *2*, 991-1001.

Joesch, M., Schnell, B., Raghu, S.V., Reiff, D.F., and Borst, A. (2010). ON and OFF pathways in Drosophila motion vision. Nature *468*, 300-304.

Lazar, N.A., Luna, B., Sweeney, J.A., and Eddy, W.F. (2002). Combining brains: A survey of methods for statistical pooling of information. Neuroimage *16*, 538-550.

Loughin, T.M. (2004). A systematic comparison of methods for combining p-values from independent tests. Comput Stat Data An *47*, 467-485.

Ofstad, T.A., Zuker, C.S., and Reiser, M.B. (2011). Visual place learning in Drosophila melanogaster. Nature *474*, 204-207.

Pfeiffer, B.D., Jenett, A., Hammonds, A.S., Ngo, T.T., Misra, S., Murphy, C., Scully, A., Carlson, J.W., Wan, K.H., Laverty, T.R*., et al.* (2008). Tools for neuroanatomy and neurogenetics in Drosophila. Proceedings of the National Academy of Sciences of the United States of America *105*, 9715-9720.

Pfeiffer, B.D., Ngo, T.T., Hibbard, K.L., Murphy, C., Jenett, A., Truman, J.W., and Rubin, G.M. (2010). Refinement of tools for targeted gene expression in Drosophila. Genetics *186*, 735-755.

Reichardt, W., and Wenking, H. (1969). Optical detection and fixation of objects by fixed flying flies. Naturwissenschaften *56*, 424-425.

Reiser, M.B., and Dickinson, M.H. (2008). A modular display system for insect behavioral neuroscience. Journal of neuroscience methods *167*, 127-139.

Reiser, M.B., and Dickinson, M.H. (2010). Drosophila fly straight by fixating objects in the face of expanding optic flow. The Journal of experimental biology *213*, 1771-1781.

Smear, M.C., Tao, H.W., Staub, W., Orger, M.B., Gosse, N.J., Liu, Y., Takahashi, K., Poo, M.M., and Baier, H. (2007). Vesicular glutamate transport at a central synapse limits the acuity of visual perception in zebrafish. Neuron *53*, 65-77.

Snyder, A.W. (1979). Physics of vision in compound eyes. In Handbook of Sensory Physiology, H. Autrum, ed. (Berlin: Springer), pp. 225-313.

Struhl, G., and Basler, K. (1993). Organizing activity of wingless protein in Drosophila. Cell *72*, 527-540.

Tammero, L.F., Frye, M.A., and Dickinson, M.H. (2004). Spatial organization of visuomotor reflexes in Drosophila. J Exp Biol *207*, 113-122.

Theobald, J.C., Ringach, D.L., and Frye, M.A. (2010). Dynamics of optomotor responses in Drosophila to perturbations in optic flow. J Exp Biol *213*, 1366-1375.

Tuthill, J.C., Chiappe, M.E., and Reiser, M.B. (2011). Neural correlates of illusory motion perception in Drosophila. Proc Natl Acad Sci U S A *108*, 9685-9690.

Tuthill, J.C., Nern, A., ,Rubin, G.M., and Reiser, M.B. (2013). Wide-field feedback neurons dynamically tune early visual processing. (In review).

Lamina Monopolar Cell 1 (L1)

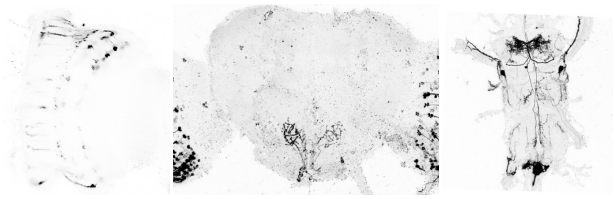

OL section CB projection VNC projection

R48A08AD R66A01DBD

11d03AD,19c10DBD, 53g02AD, 48a08DBD x UAS-Kir2.1 n = 48 flies

48a08AD; 66a01DBD x UAS-Kir2.1 n = 11 flies

wingbeat frequency (Hz)

back-to-front rotation (λ = 30˚)

front-to-back rotation (λ = 30˚)

ON/OFF

temporal frequency (Hz)

expansion rotation

* : p < 0.1
** : p < 0.05
*** : p < 0.01

integrated ΔWBA

rotation (λ = 30˚)

rotation (λ = 90˚)

expansion (λ = 30˚)

rotation (λ = 45˚)

contrast

reverse-phi rotation (λ = 30˚)

reverse-phi rotation (λ = 90˚)

lateral flicker (40 Hz)

optic flow

peak correlation

lift pitch thrust roll slip yaw

bright stripe

dark stripe

wide-field grating

CL stripe fixation

fixation index

oscillation frequency (Hz)

test

tf = 0.3 Hz

tf = 1.3 Hz

tf = 5.3 Hz

tf = 10.7 Hz

tf = 16 Hz

test contrast

contrast sensitivity

test temporal frequency (Hz)

dTrpA1 results

reg pro lateral rotation

0.06 0.24 low contrast rotation

reverse -phi

dark bright grating

48a08AD; 66a01DBD x UAS-dTrpA1, 29 degs n = 10 flies

11d03AD, 19c10DBD, 53g02AD, 48a08DBD x UAS-dTrpA1, 29 degs n = 51 flies

48a08AD; 66a01DBD x UAS-dTrpA1, 21 degs n = 10 flies

Lamina Monopolar Cell 2 (L2)

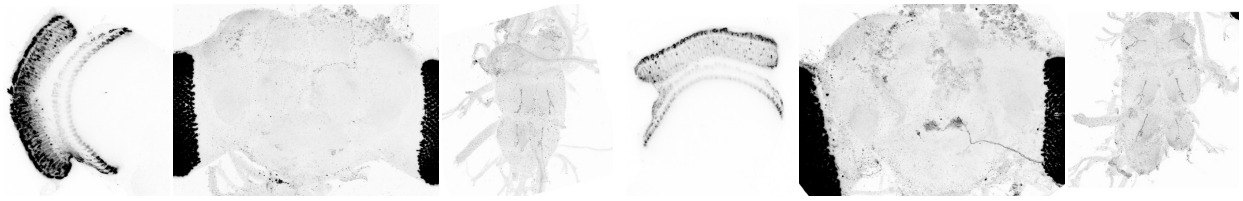

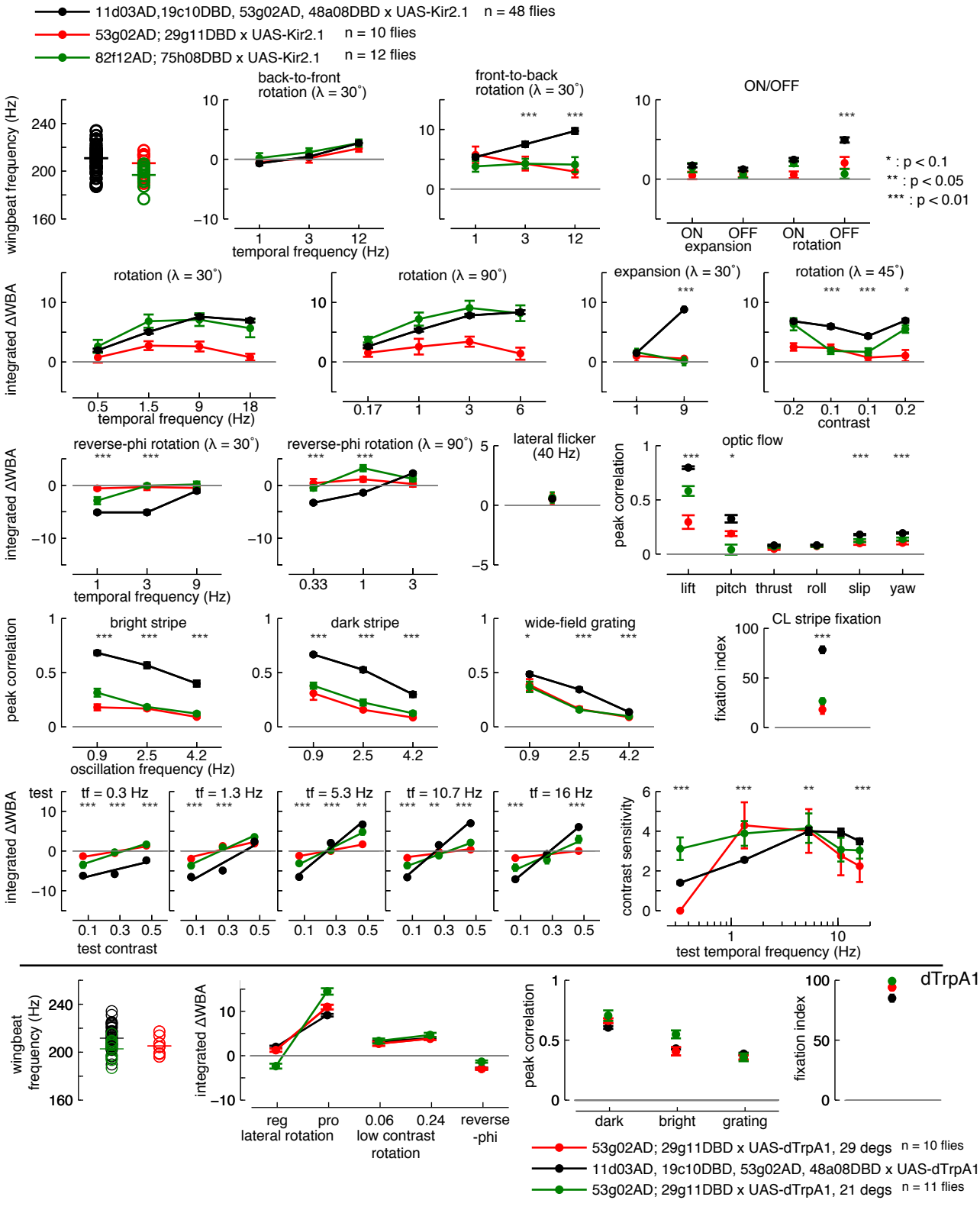

Lamina Monopolar Cells 1 and 2 (L1 +L2)

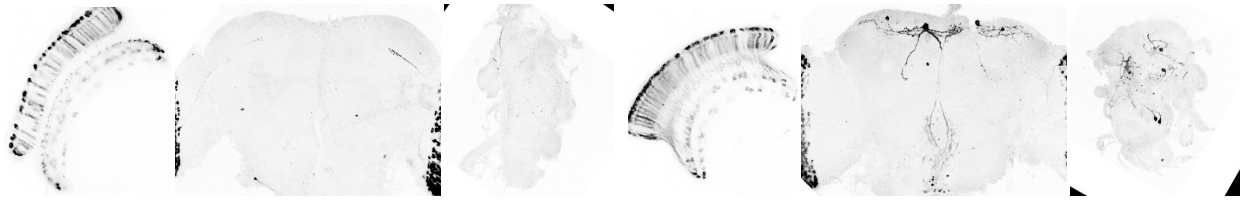

R75H09AD R29G11DBD R48A08AD R29G11DBD

11d03AD,19c10DBD, 53g02AD, 48a08DBD x UAS-Kir2.1 n = 48 flies
75h09AD; 29g11DBD x UAS-Kir2.1 n = 10 flies
48a08AD; 29g11DBD x UAS-Kir2.1 n = 14 flies

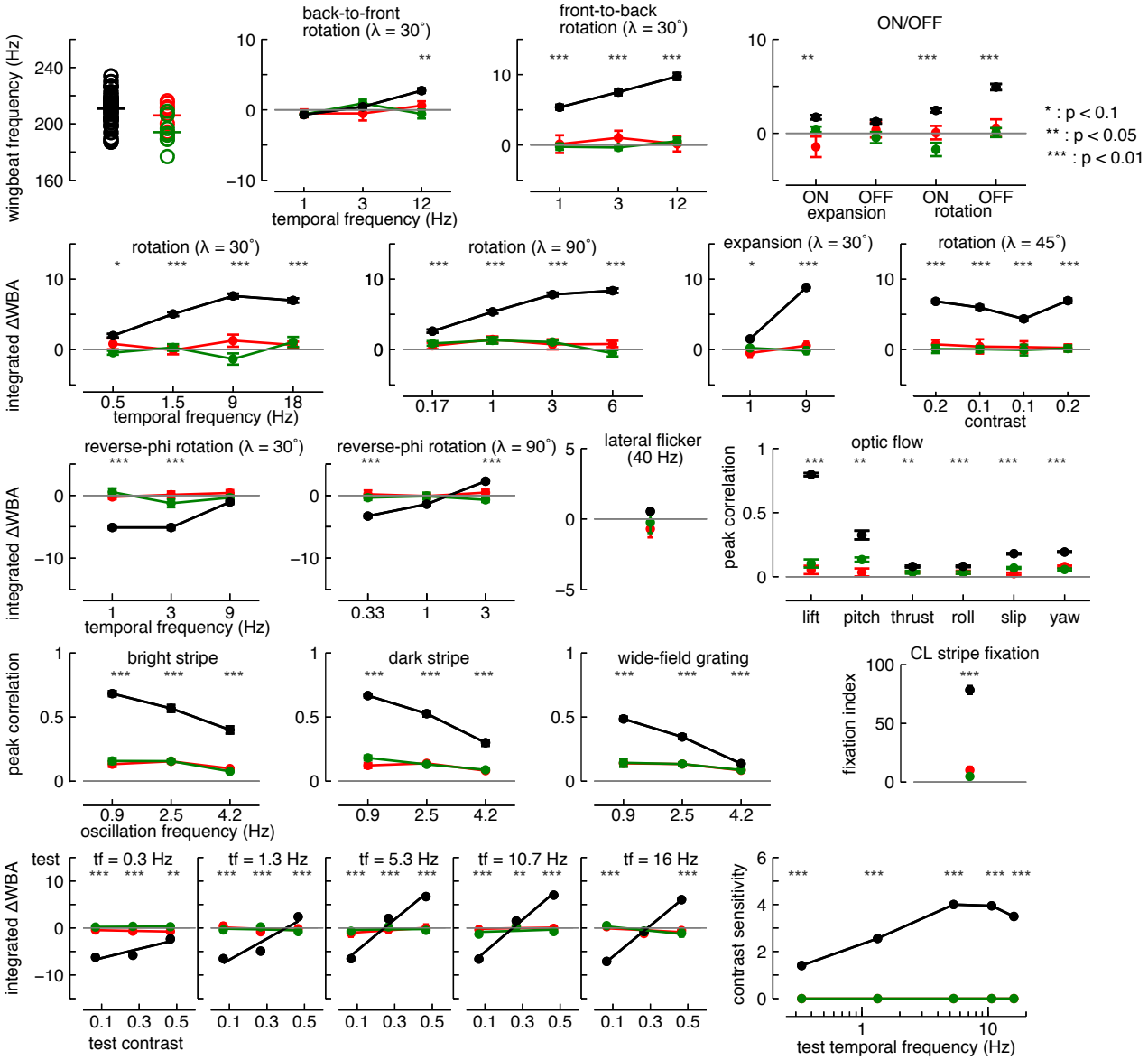

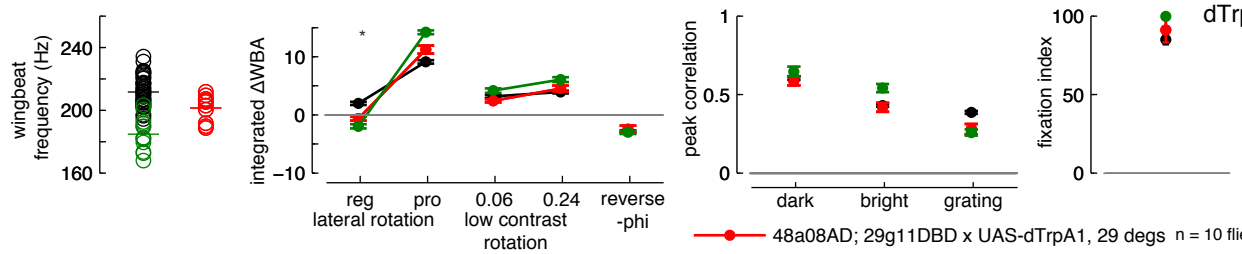

48a08AD; 29g11DBD x UAS-dTrpA1, 29 degs n = 10 flies
11d03AD, 19c10DBD, 53g02AD, 48a08DBD x UAS-dTrpA1, 29 degs n = 51 flies
48a08AD; 29g11DBD x UAS-dTrpA1, 21 degs n = 13 flies

Lamina Monopolar Cell 3 (L3)

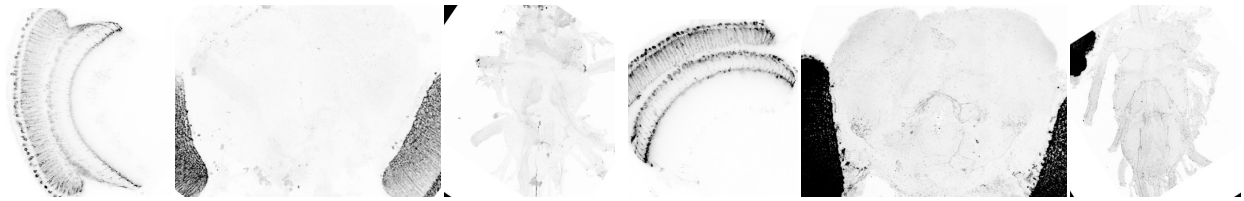

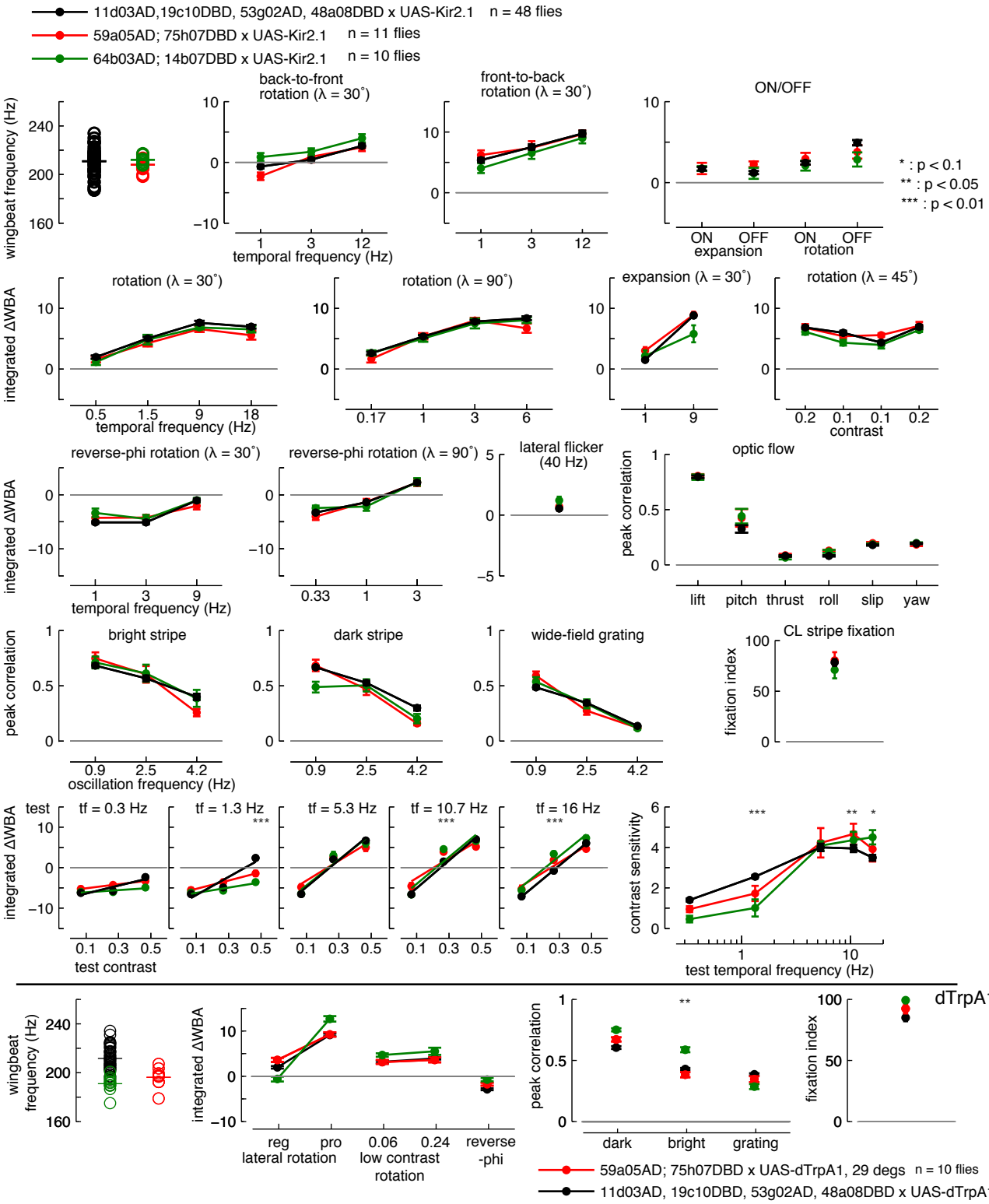

Lamina Monopolar Cell 4 (L4)

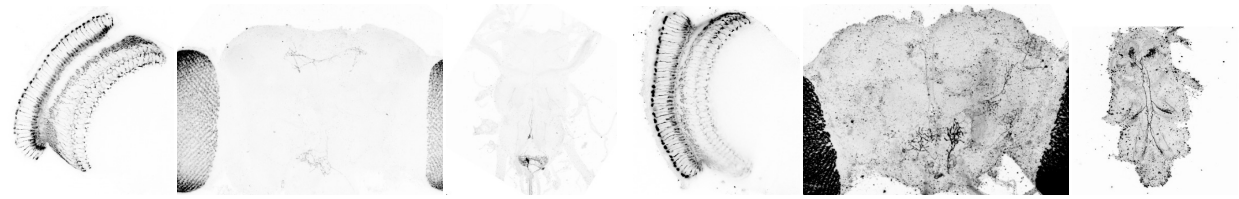

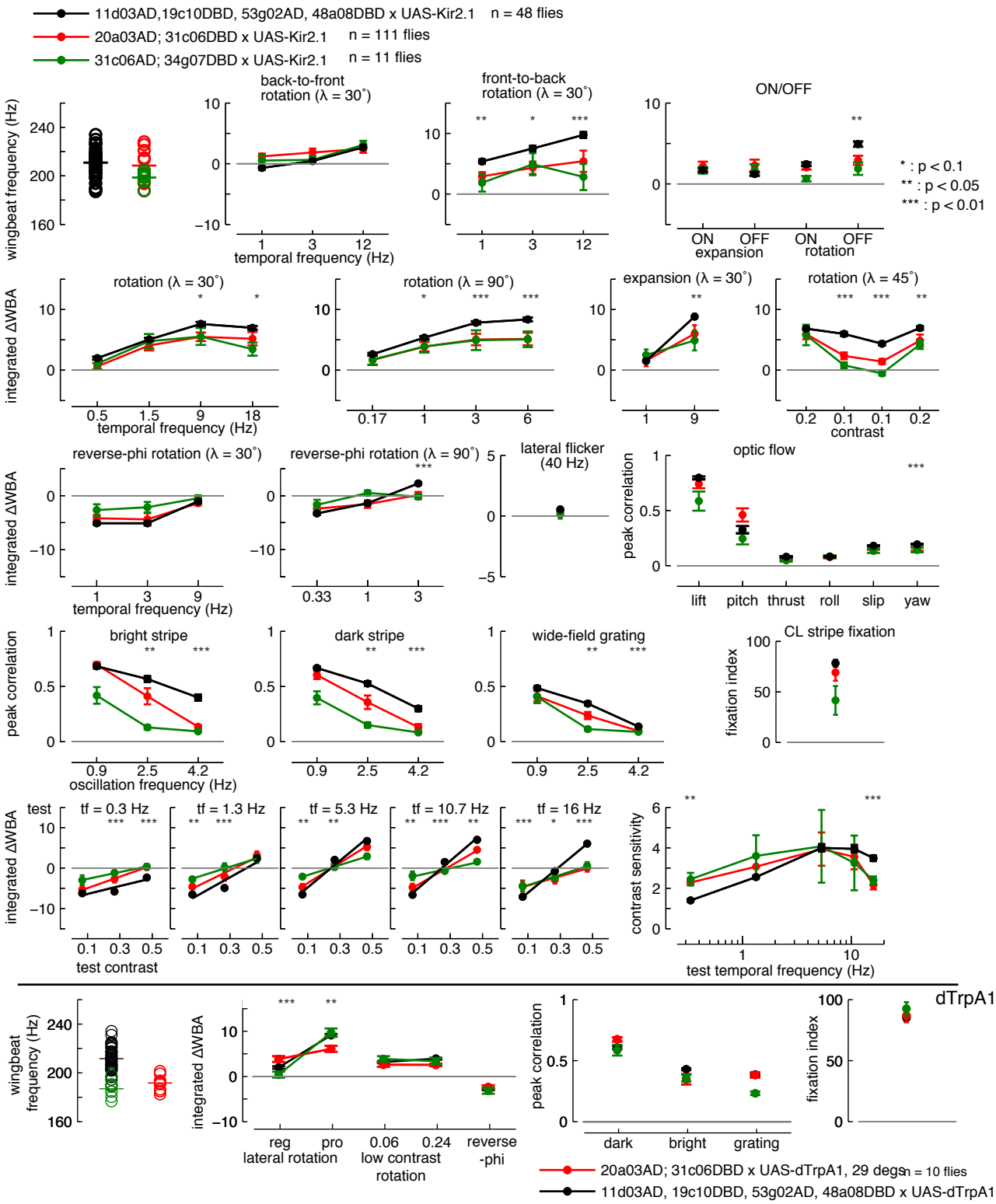

Lamina Monopolar Cell 5 (L5)

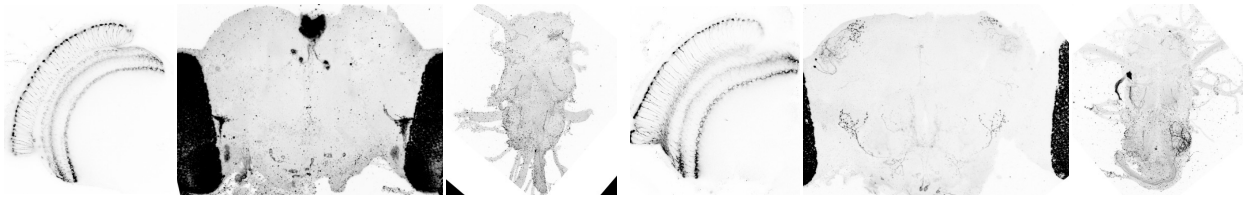

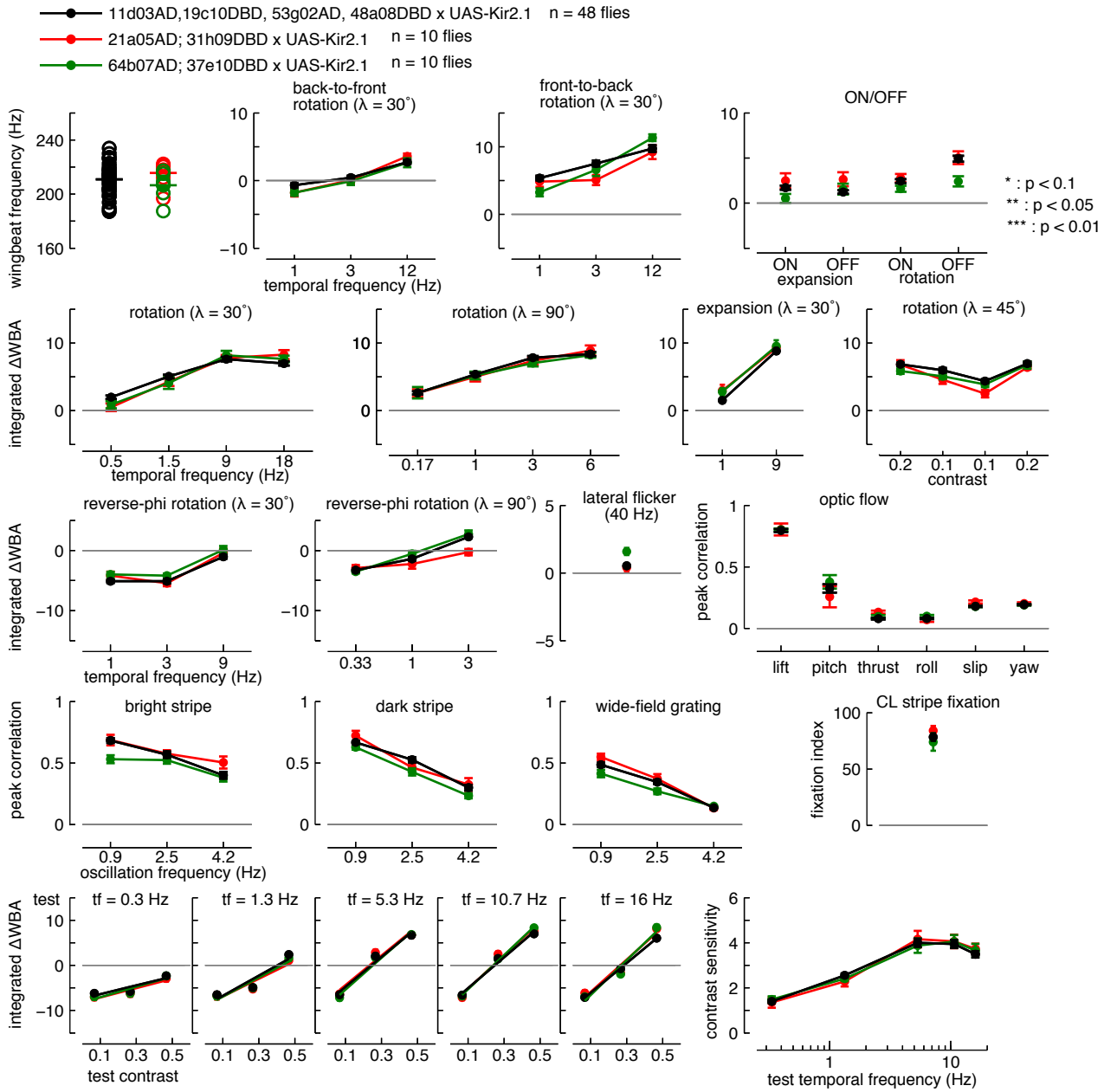

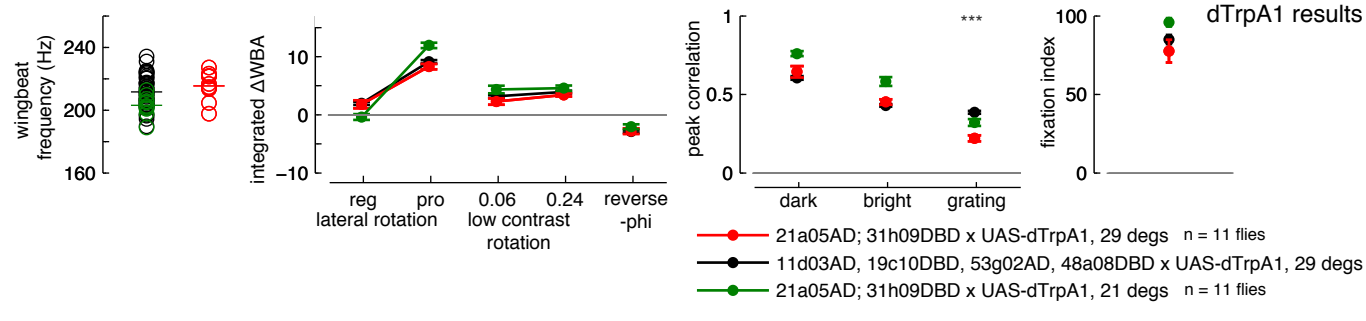

Centrifugal Cell 2 (C2)

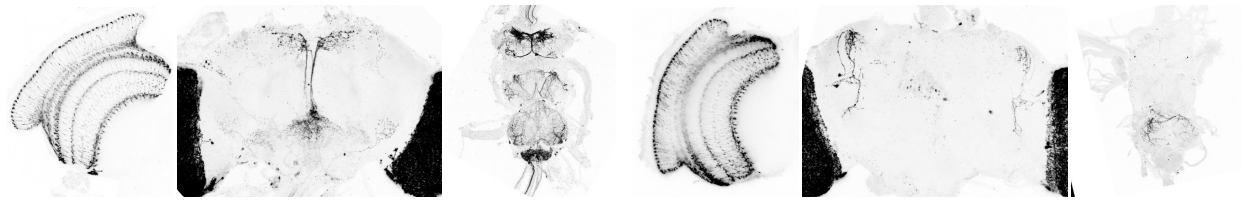

R20C11AD R25B02DBD R25B02AD R48D11DBD

11d03AD,19c10DBD, 53g02AD, 48a08DBD x UAS-Kir2.1 n = 48 flies
20c11AD; 25b02DBD x UAS-Kir2.1 n = 12 flies
25b02AD; 48d11DBD x UAS-Kir2.1 n = 11 flies

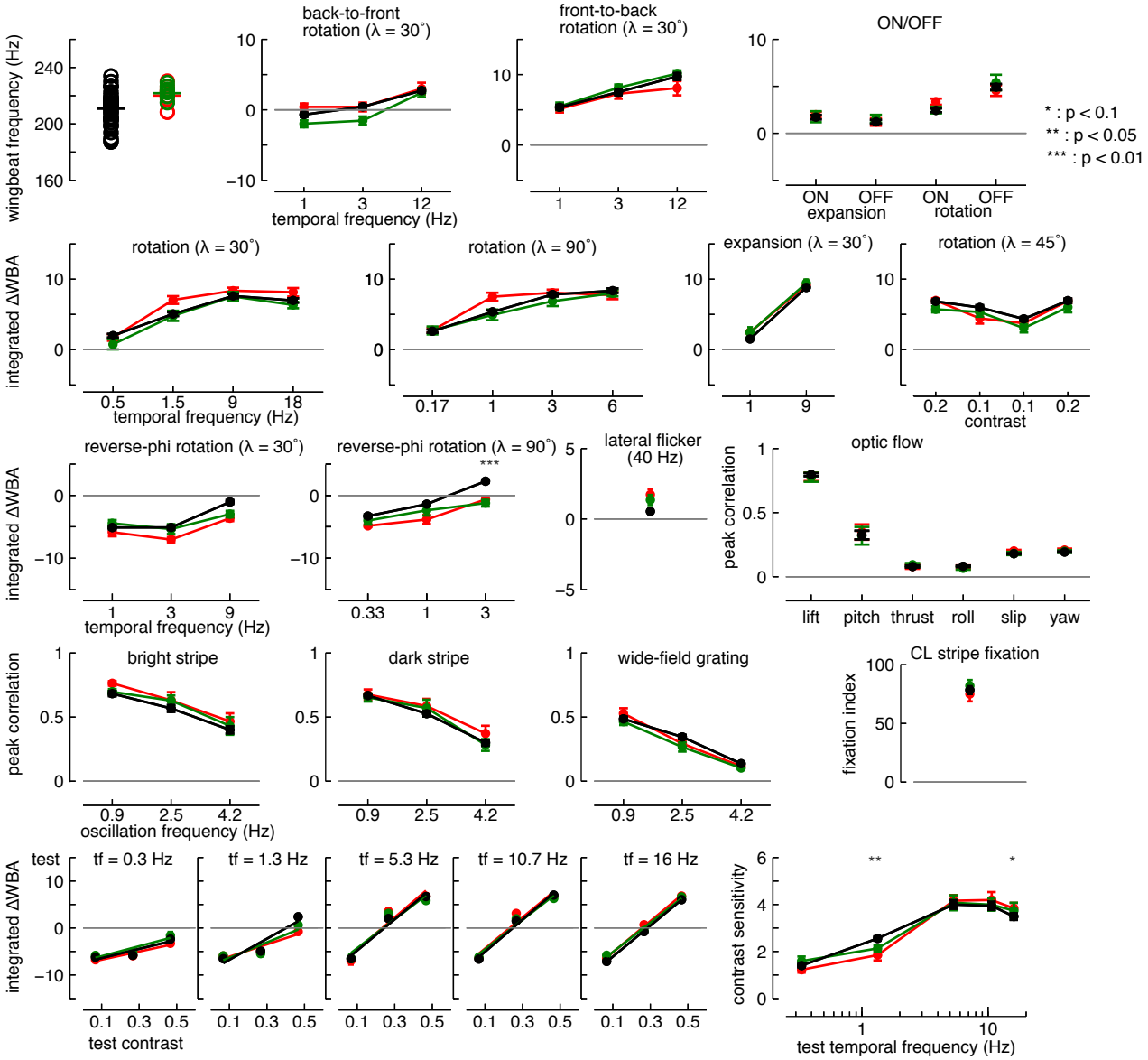

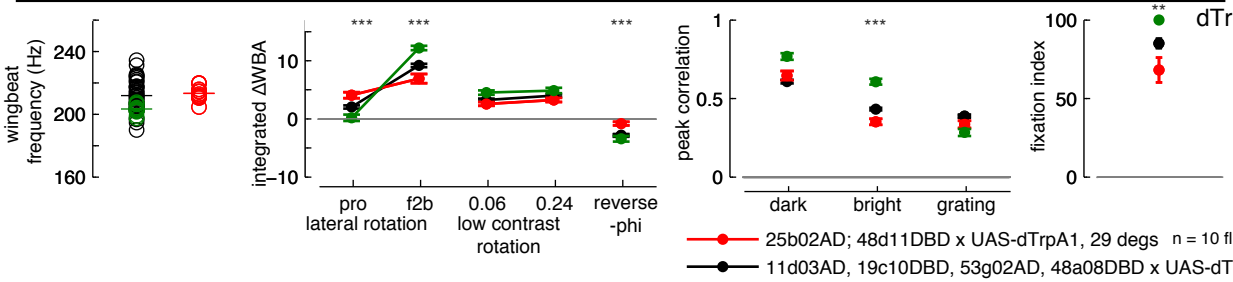

Centrifugal Cell 3 (C3)

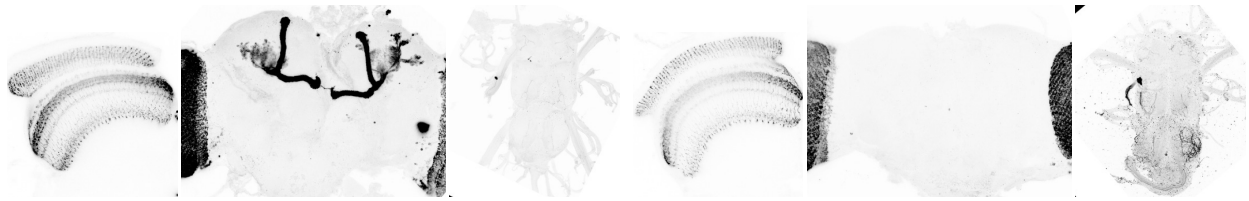

OL section | CB projection R35A03D R29G11DBD | VNC projection | OL section | CB projection R26H02AD | VNC projection R29G11DBD

11d03AD,19c10DBD, 53g02AD, 48a08DBD x UAS-Kir2.1 n = 48 flies
35a03AD; 29g11DBD x UAS-Kir2.1 n = 12 flies
26h02AD; 29g11DBD x UAS-Kir2.1 n = 10 flies

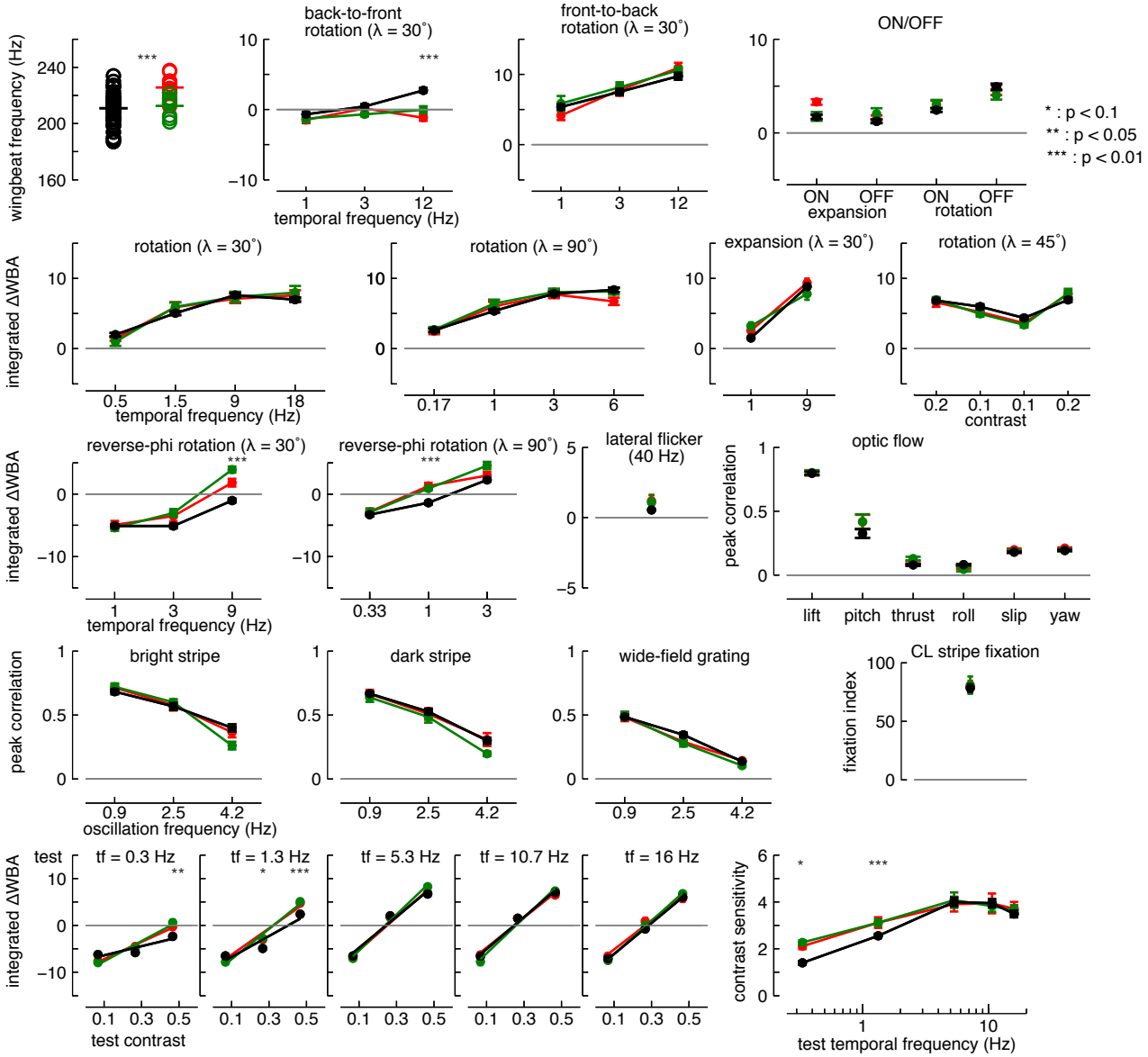

dTrpA1 results

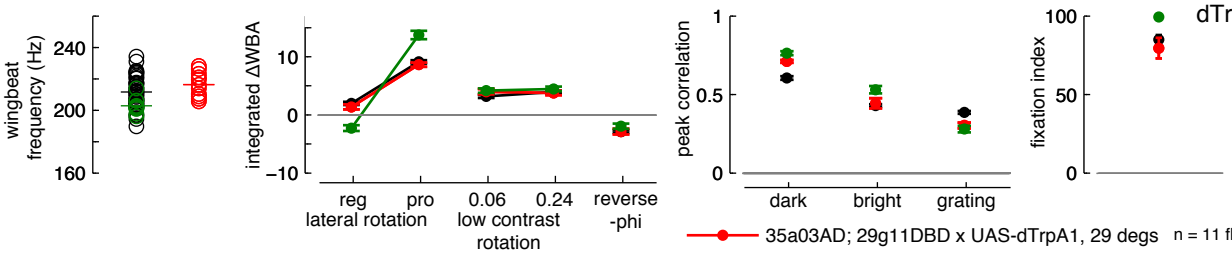

35a03AD; 29g11DBD x UAS-dTrpA1, 29 degs n = 11 flies
11d03AD, 19c10DBD, 53g02AD, 48a08DBD x UAS-dTrpA1, 29 degs n = 51 flies
35a03AD; 29g11DBD x UAS-dTrpA1, 21 degs n = 12 flies

Centrigual Cells 2 and 3 (C2+C3)

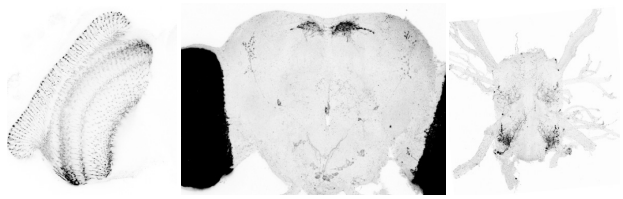

11d03AD,19c10DBD, 53g02AD, 48a08DBD x UAS-Kir2.1 n = 48 flies

20c11AD; 48d11DBD x UAS-Kir2.1 n = 10 flies

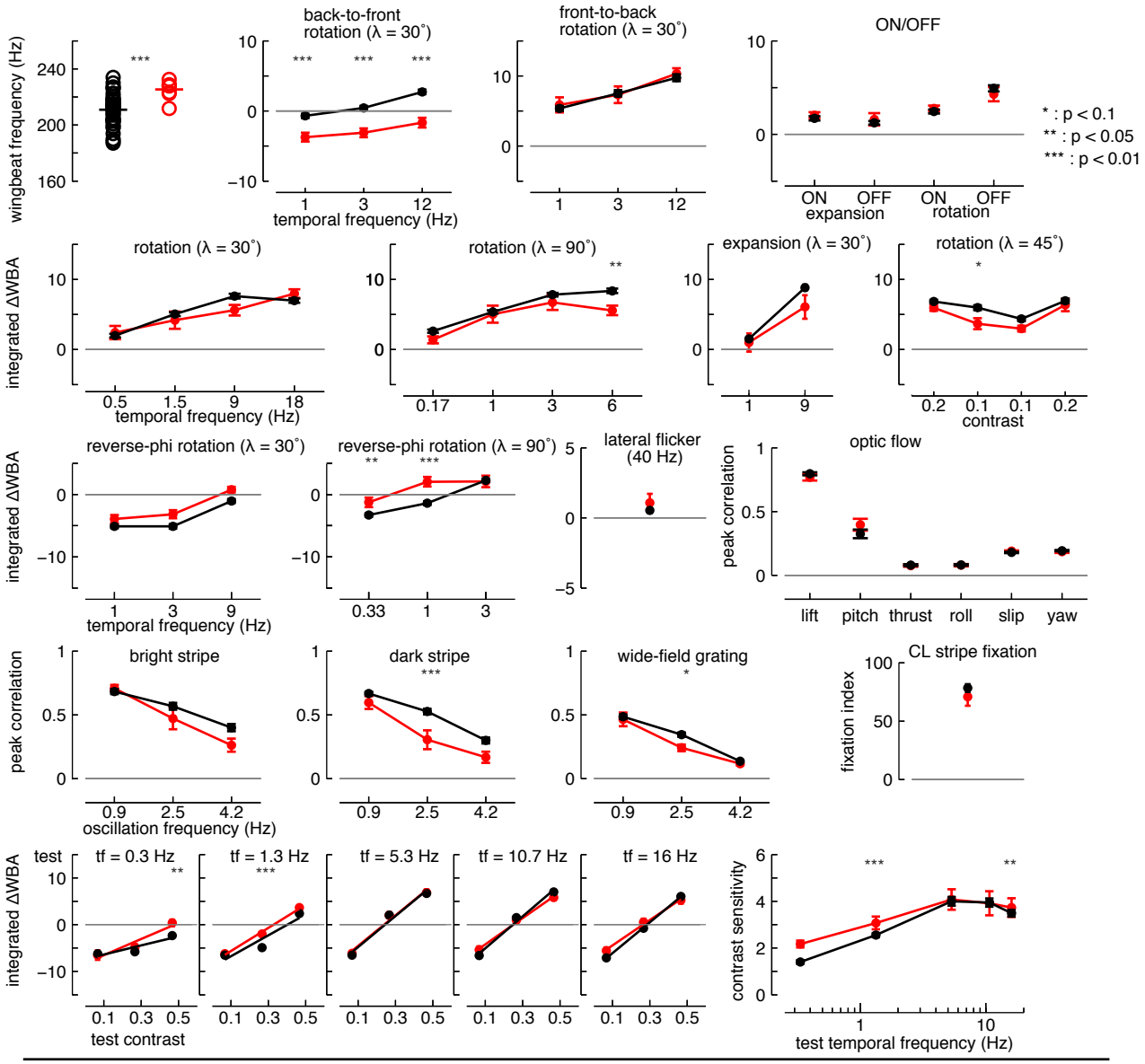

dTrpA1 results

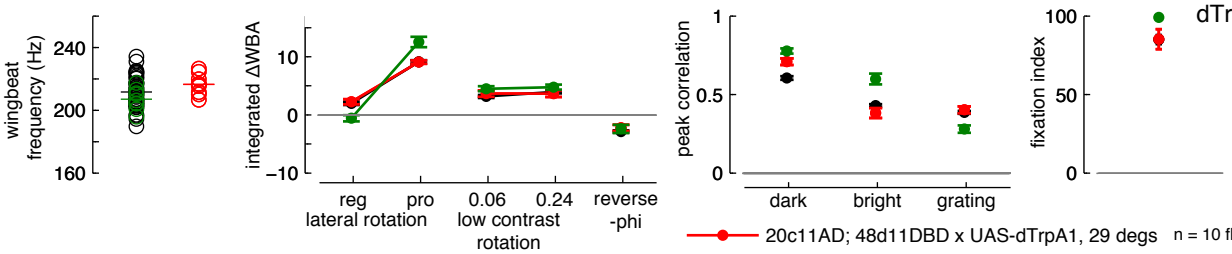

20c11AD; 48d11DBD x UAS-dTrpA1, 29 degs n = 10 flies

11d03AD, 19c10DBD, 53g02AD, 48a08DBD x UAS-dTrpA1, 29 degs n = 51 flies

20c11AD; 48d11DBD x UAS-dTrpA1, 21 degs n = 10 flies

T1 Cell

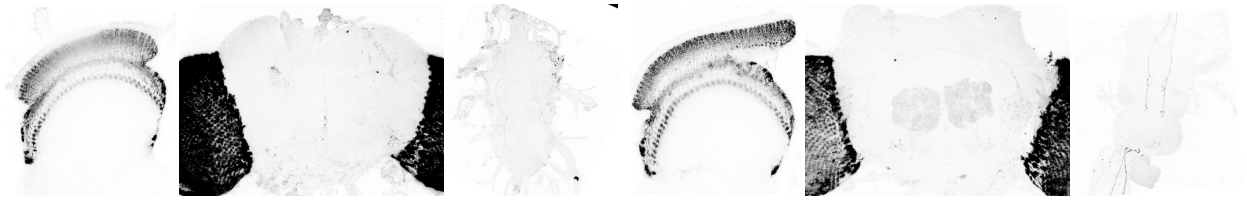

11d03AD,19c10DBD, 53g02AD, 48a08DBD x UAS-Kir2.1 n = 48 flies
31f10AD; 30f10DBD x UAS-Kir2.1 n = 10 flies
31f10AD; 65d07DBD x UAS-Kir2.1 n = 12 flies

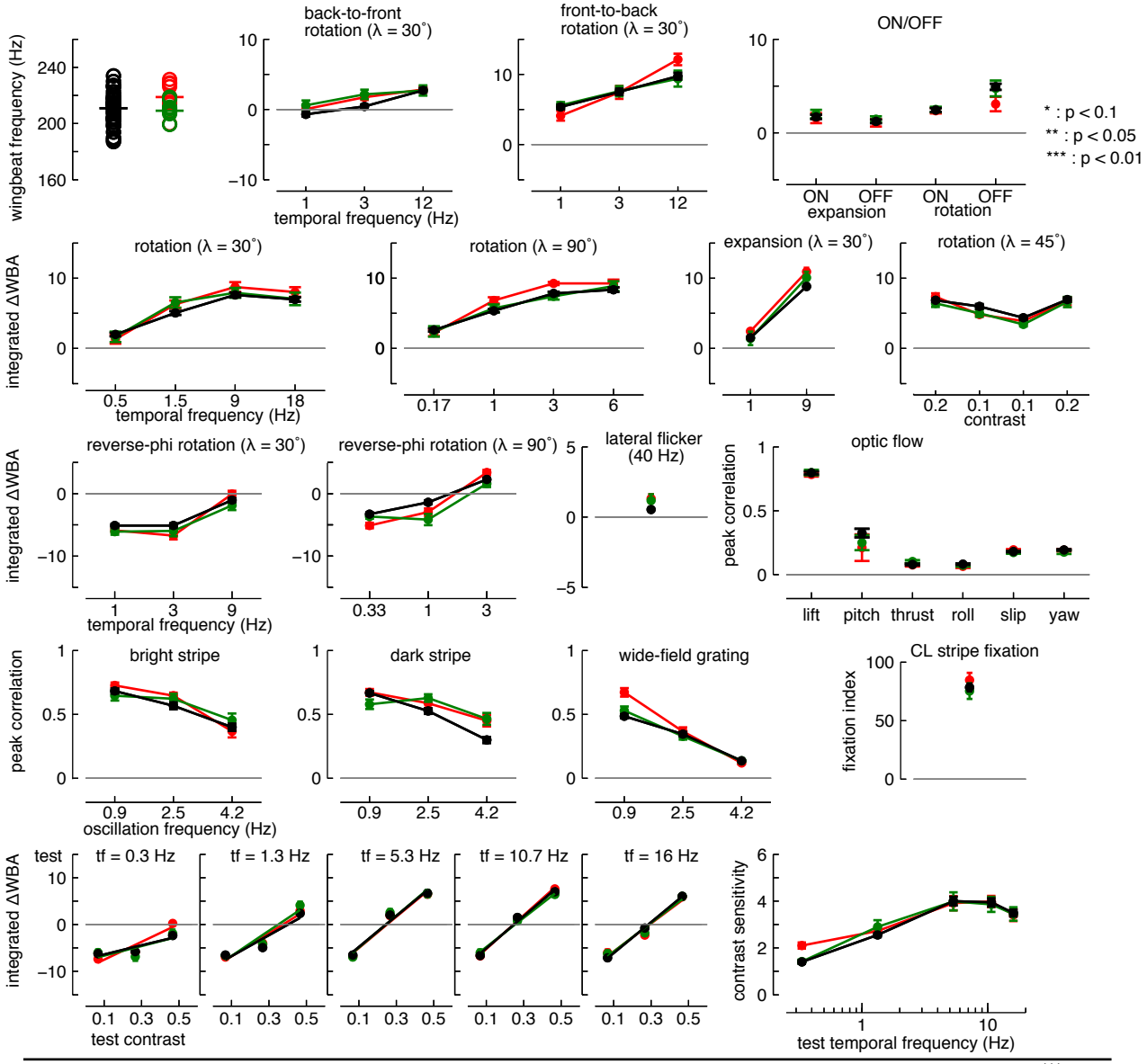

dTrpA1 results

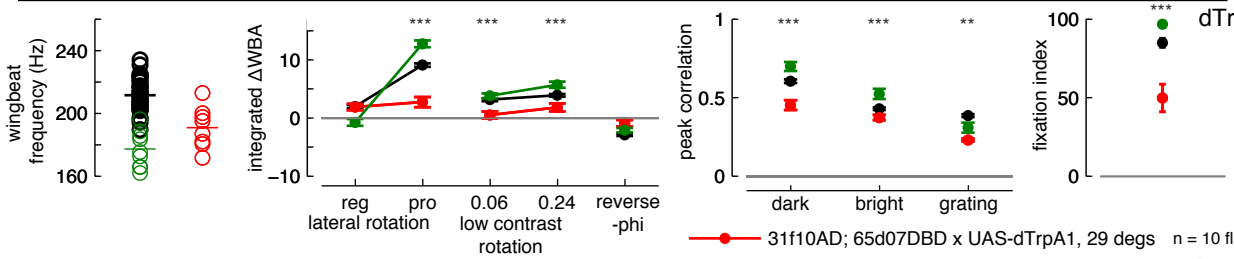

31f10AD; 65d07DBD x UAS-dTrpA1, 29 degs n = 10 flies
11d03AD, 19c10DBD, 53g02AD, 48a08DBD x UAS-dTrpA1, 29 degs n = 51 flies
31f10AD; 65d07DBD x UAS-dTrpA1, 21 degs n = 10 flies

Lamina Intrinsic (Lai)

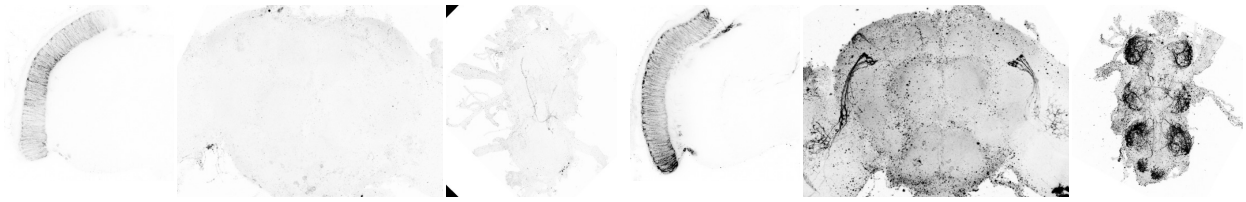

OL section CB projection VNC projection OL section CB projection VNC projection
R92A10AD R66A02DBD R92A10AD R17D06DBD

11d03AD,19c10DBD, 53g02AD, 48a08DBD x UAS-Kir2.1 n = 48 flies
92a10AD; 17d06DBD x UAS-Kir2.1 n = 12 flies
92a10AD; 66a02DBD x UAS-Kir2.1 n = 10 flies

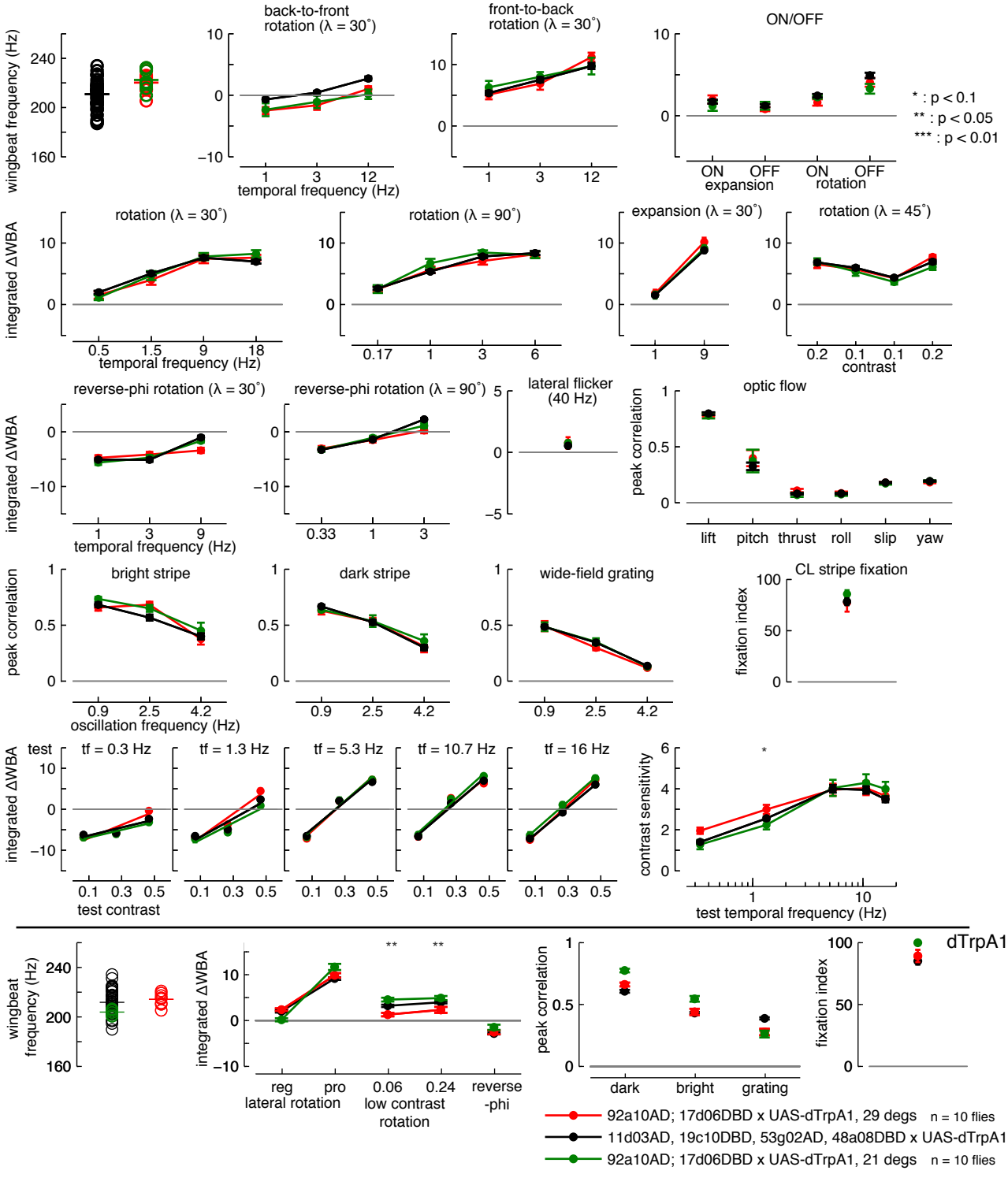

dTrpA1 results

92a10AD; 17d06DBD x UAS-dTrpA1, 29 degs n = 10 flies
11d03AD, 19c10DBD, 53g02AD, 48a08DBD x UAS-dTrpA1, 29 degs n = 51 flies
92a10AD; 17d06DBD x UAS-dTrpA1, 21 degs n = 10 flies

Lamina Wide-Field 1 (Lawf1)

OL section CB projection VNC projection OL section CB projection VNC projection
R52H01AD R17C11DBD R11G01AD R17C11DBD

11d03AD,19c10DBD, 53g02AD, 48a08DBD x UAS-Kir2.1 n = 48 flies
11g01AD; 17c11DBD x UAS-Kir2.1 n = 12 flies
52h01AD; 17c11DBD x UAS-Kir2.1 n = 11 flies

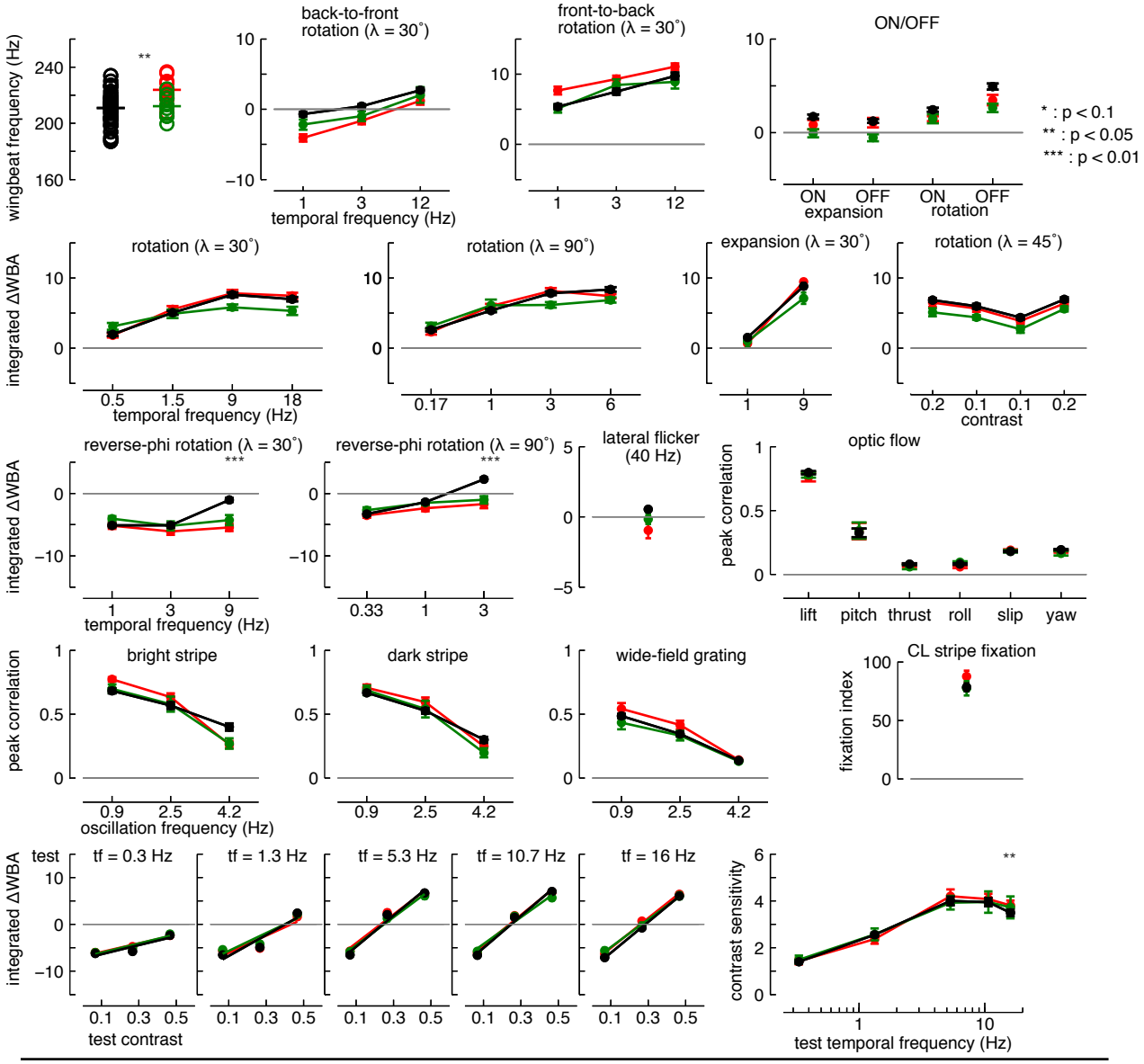

dTrpA1 results

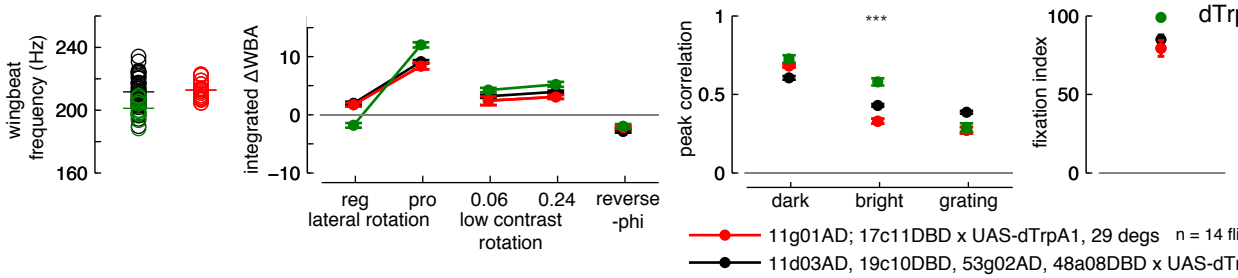

11g01AD; 17c11DBD x UAS-dTrpA1, 29 degs n = 14 flies
11d03AD, 19c10DBD, 53g02AD, 48a08DBD x UAS-dTrpA1, 29 degs n = 51 flies
11g01AD; 17c11DBD x UAS-dTrpA1, 21 degs n = 16 flies

Lamina Wide-Field 2 (Lawf2)

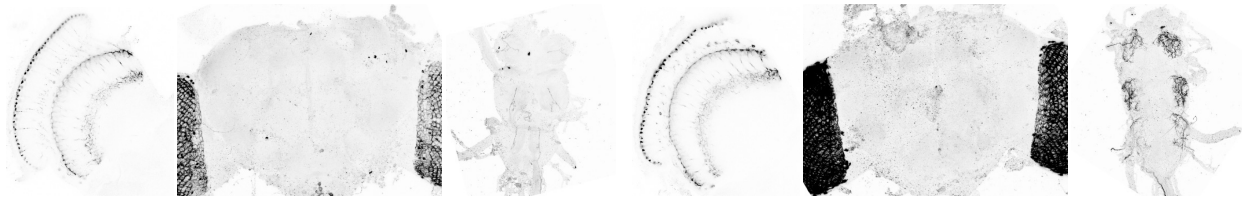

11d03AD,19c10DBD, 53g02AD, 48a08DBD x UAS-Kir2.1 n = 48 flies
11d03AD; 61h02DBD x UAS-Kir2.1 n = 11 flies
11d03AD; 19c10DBD x UAS-Kir2.1 n = 14 flies

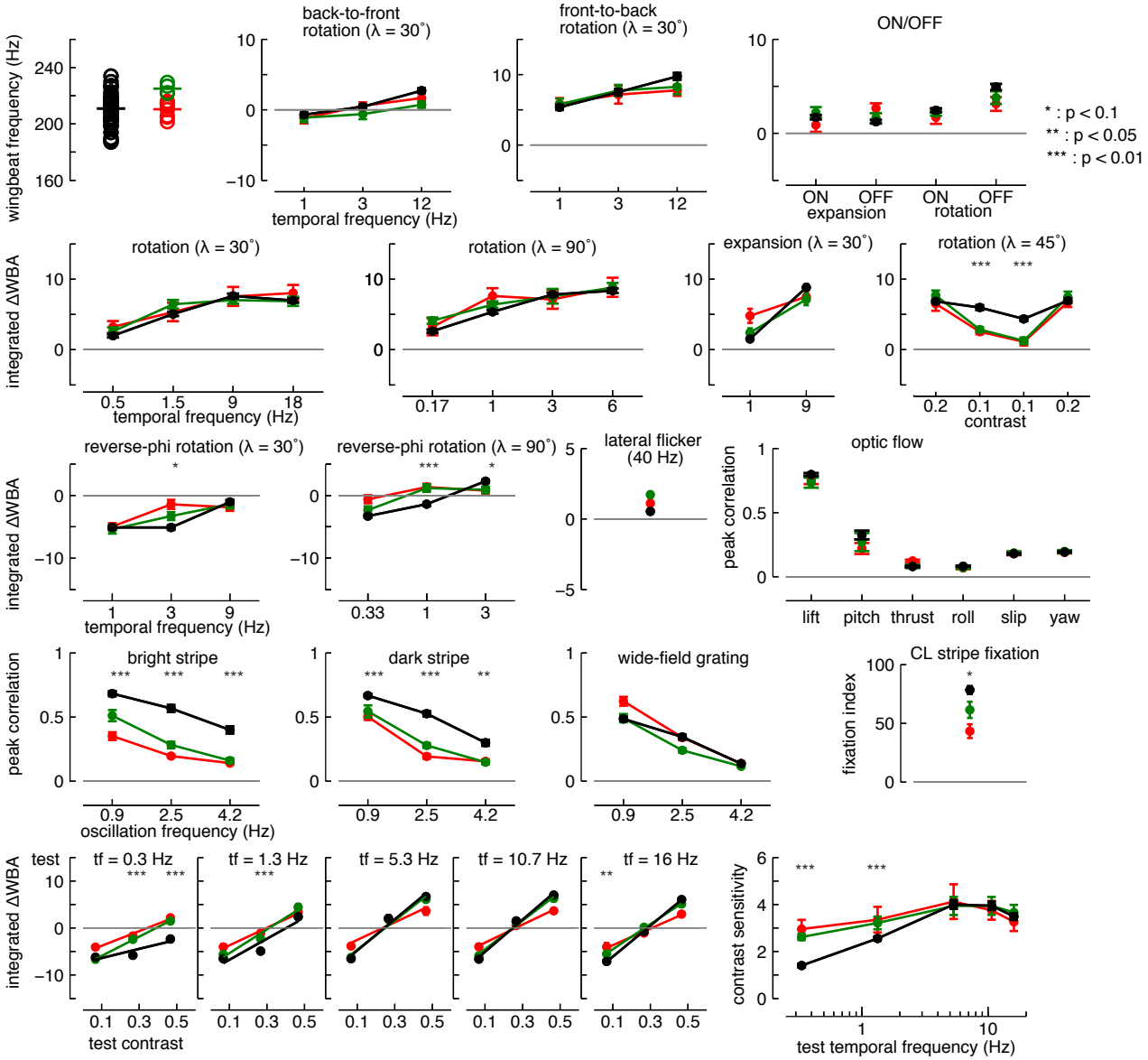

dTrpA1 results

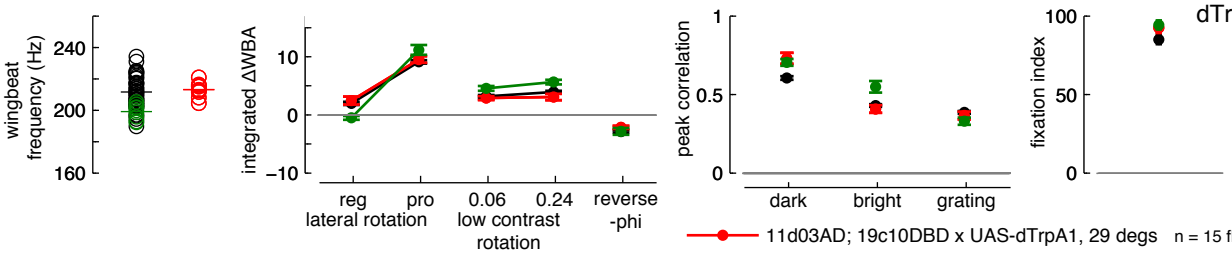

11d03AD; 19c10DBD x UAS-dTrpA1, 29 degs n = 15 flies
11d03AD, 19c10DBD, 53g02AD, 48a08DBD x UAS-dTrpA1, 29 degs n = 51 flies
11d03AD; 19c10DBD x UAS-dTrpA1, 21 degs n = 10 flies

Lamina Tangential (Lat)

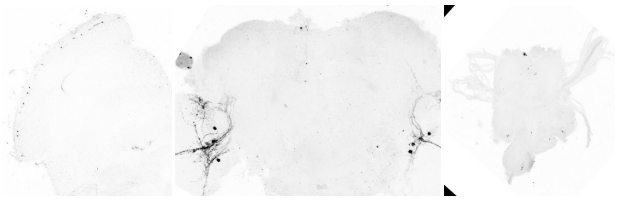

OL section CB projection VNC projection

R16G04AD R55B04DBD

11d03AD,19c10DBD, 53g02AD, 48a08DBD x UAS-kir2.1 n = 48 flies

16g04AD; 55b04DBD x UAS-kir2.1 n = 13 flies

wingbeat frequency (Hz)

back-to-front rotation (λ = 30˚)

temporal frequency (Hz)

front-to-back rotation (λ = 30˚)

ON/OFF

ON OFF ON OFF

expansion rotation

* : p < 0.1

** : p < 0.05

*** : p < 0.01

integrated ΔWBA

rotation (λ = 30˚)

temporal frequency (Hz)

rotation (λ = 90˚)

expansion (λ = 30˚)

rotation (λ = 45˚)

contrast

reverse-phi rotation (λ = 30˚)

temporal frequency (Hz)

reverse-phi rotation (λ = 90˚)

lateral flicker (40 Hz)

peak correlation

optic flow

lift pitch thrust roll slip yaw

bright stripe

dark stripe

wide-field grating

oscillation frequency (Hz)

fixation index

CL stripe fixation

test

tf = 0.3 Hz

tf = 1.3 Hz

tf = 5.3 Hz

tf = 10.7 Hz

tf = 16 Hz

test contrast

contrast sensitivity

test temporal frequency (Hz)

dTrpA1 results

reg pro 0.06 0.24 reverse

lateral rotation low contrast rotation -phi

dark bright grating

16g04AD; 55b04DBD x UAS-dTrpA1, 29 degs n = 14 flies

11d03AD, 19c10DBD, 53g02AD, 48a08DBD x UAS-dTrpA1, 29 degs n = 51 flies

16g04AD; 55b04DBD x UAS-dTrpA1, 21 degs n = 13 flies